ANNUAL REPORT 2019-2020

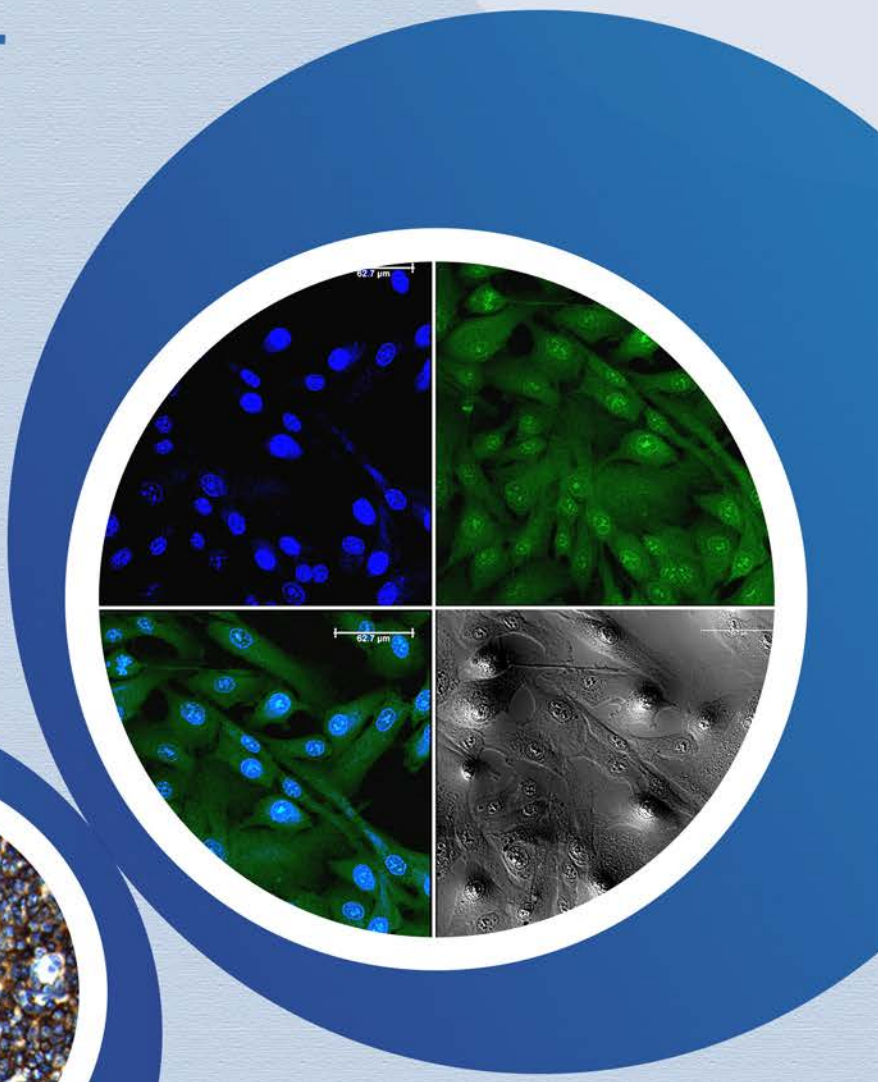

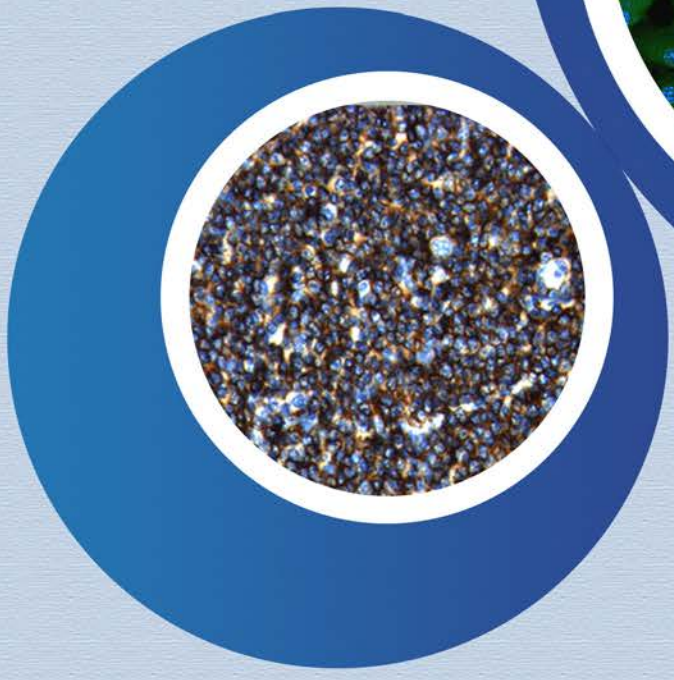

RESEARCH IN OPHTHALMIC SCIENCES

Aravind Medical Research Foundation

Aravind Medical Research Foundation

Aravind Medical Research Foundation is recognised as Scientific and Industrial Research Organization (SIRO) by the Department of Scientific and Industrial Research (DSIR), Government of India

MISSION

To eliminate needless blindness by providing evidence through research and evolving methods to translate existing evidence and knowledge into effective action.

RESEARCH IN OPHTHALMIC SCIENCES

Dr. G. Venkataswamy Eye Research Institute

Annual Report 2019 - 2020

ARAVIND MEDICAL RESEARCH FOUNDATION

BOARD OF MANAGEMENT

Dr. P. Namperumalsamy, MS, FAMS

Dr. G. Natchiar, MS, DO

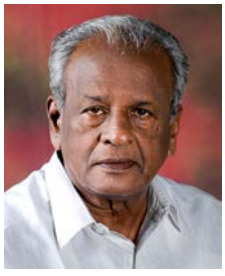

Er. G. Srinivasan, BE, MS

Mr. R.D. Thulasiraj, MBA

Dr. S.R. Krishnadas, DO., DNB

Dr. R. Kim, DO., DNB

Dr.N.Venkatesh Prajna DO., DNB., FRCophth

Dr. S. Aravind, MS, MBA

FACULTY

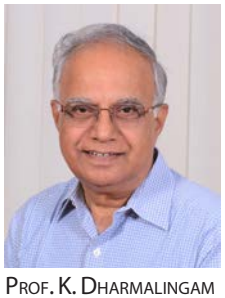

Prof. K. Dharmalingam
Director - Research

Prof. VR. Muthukkaruppan
Advisor-Research

Dr. P. Sundaresan
Senior Scientist
Molecular Genetics

Dr. C. Gowri Priya
Scientist, Immunology &
Stem Cell Biology

Dr. S. Senthilkumari
Scientist, Ocular Pharmacology

Dr. A. Vanniarajan
Scientist, Molecular Genetics

Dr. J. Jeya Maheshwari
Scientist, Proteomics

Dr. D. Bharanidharan
Scientist, Bioinformatics

Dr.O.G.Ramprasad
Scientist, Proteomics

ARAVIND MEDICAL RESEARCH FOUNDATION

CLINICIAN-SCIENTISTS

Dr. P. Vijayalakshmi, MS
Professor of Paediatric Ophthalmology

Dr. S.R. Krishnadas, DO., DNB
Professor of Ophthalmology

Dr. SR. Rathinam, MNAMS, PH.D
Professor of Ophthalmology & HOD - Uvea Services

Dr. Haripriya Aravind, MS
HOD - IOL & Cataract Services

Dr. R. Kim, DO., DNB
Professor of Ophthalmology & Chief Medical Officer

Dr. N. Venkatesh Prajna DO., DNB., FRCOphth
Professor of Ophthalmology & HOD - Cornea Services

Dr. Usha Kim, DO, DNB
Professor of Ophthalmology & HOD - Orbit, Oculoplasty & Ocular Oncology Services

Dr. Lalitha Prajna, MD., DNB
HOD - Microbiology

Dr. R. Shanthi, MD (Pathology)
Pathologist

Dr. R. Sharmila, DNB
Medical Consultant Glaucoma Services

Dr. Madhu Shekar, DNB
Chief - Cataract Services

RESEARCH ADVISORY COMMITTEE MEMBERS

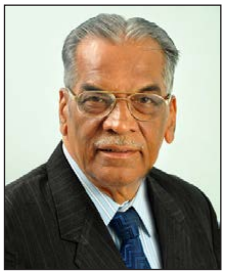

Dr. P. Namperumalsamy
Chairman

Dr. Ch. Mohan Rao
Member

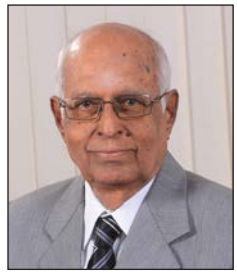

Prof.VR. Muthukkaruppan
Member

Prof. Anuranjan Anand
Member

Prof. S. Murty Srinivasula
Member

Prof. S.Karuthapandian
Member

Dr. N. Venkatesh Prajna
Member

Dr. R. Kim
Member

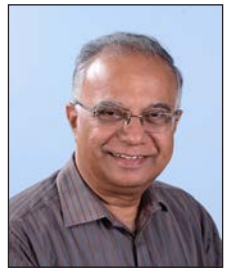

Prof. K. Dharmalingam
Member Secretary

INSTITUTIONAL ETHICS COMMITTEE (IEC)

Chairman

Prof. R. Venkataratnam m.a., ph.d

Senior Prof.of Sociology (Retired)
Madurai Kamaraj University, Madurai

Member-Secretary

Dr. R. Sharmila, dnb

Medical Officer, Glaucoma Clinic,
Aravind Eye Hospital, Madurai

Members

Dr. C. Srinivasan m.sc.,ph.d

UGC Emeritus Professor
New No. 2/249 (Old No 2/172), 7th Street, Kalvinagar,
Rajambadi, Madurai - 625021

Dr. T.S. Chandrasekaran ms, do

Ophthalmologist,
No.6, N.M.R.Subbaraman Road,Chokkikulam North,
Madurai

Mr. M. Senthilkumar m.a., b.l

Advocate
Plot No.32, Sindanayalar Nagar
Senthamil Nagar, Karuppayoorani East, Madurai

Mr. R. Raja Govindasamy m.a., m.a (usa)

Former Principal, Thiagarajar College
169-1, 2nd Cross Street, I Main Road, Gomathipuram,
Madurai - 625020

Dr. S. Sabhesan dpm, mnams, ph.d

Consultant – Psychiatrist, Apollo Specialty Hospitals
Lake view Road, K.K.Nagar, Madurai

Dr. A. Amirtha Mekhala bds, mph, mfdsrcps

Private Practice - Dental Services
208 Karpaga Nagar 8th Street, K.Pudur, Madurai - 625007

Mrs. Premalatha Panneerselvam m.a., m.ed

Secretary, Mahatma Montessori Matriculation Hr.Sec.
School, Madurai

Dr.J.R.Vijayalakshmi md (Pharmacology)

Professor of Pharmacology
CSI college of Dental Sciences, Madurai

Mr. ARM. Ganesh b.com., llb

Advocate, D-3/4, First Cross Street
K.K.Nagar west, Madurai - 625020

Dr. Lalitha Prajna dnb

Chief - Microbiology, Aravind Eye Hospital, Madurai

CONTENTS

FOREWORD

With the help from our supporters from industry we have launched several projects, which have direct bearing on clinical practice. One of the areas we explore is focused exploration of diseases where presymptomatic prediction of clinical outcome of a disease is feasible. More such translational projects including the ongoing discovery and validation of serum, tear and vitreous biomarkers for Diabetic Retinopathy, Fungal Keratitis and Glaucoma respectively will be pursued vigorously in the coming years.

Two more scientists, Dr. Daipayan Banerjee and Dr. Swagata Ghosh will be joining the AMRF team this year. Dr. Daipayan Banerjee will be working on Age Related Macular Degeneration. Dr. Swagata Ghosh will be focusing on microbial systems and their role in ocular disorders.

With the expanding close collaboration from our clinicians, I hope the research contributions of AMRF will be more substantial in the near future.

Dr. P. Namperumalsamy
President, AMRF

INTRODUCTION

More than 260 gene are responsible for retinal functions and defect in any of them will lead to sight threatening disease. Defects in RPE65 gene leads to Retinitis Pigmentosa an early onset retinal disease. Recent gene augmentation therapy using LUXTURNA, approved by US food and Drug Administration, for Retinitis Pigmentosa treatment is a landmark achievement. This opens up immense possibilities for gene editing for therapeutic purposes. Patients carrying the mutation in RPE65, fail to produce the enzyme retinol isomerohydrolase responsible for converting the all-trans retinyl ester in to 11-cis- retinol. This step is crucial to keep the visual cycle continue uninterrupted. Luxturna can augment the production of this protein and thereby the treated patients carrying the autosomal recessive RP mutations gain sight more or less permanently. This treatment, however, is a boon only for early onset RP patients with biallelic mutation in RPE65.

This achievement, which resulted from a close collaboration of multiple investigators from clinical and basic sciences as well as industry, illustrates how far we have to go in order to achieve such translational capability in India.

Our research groups now increasingly attempt to take their lab work to clinical practice. In this context it is important to acknowledge the role of some of our industrial collaborators including Sunpharma and Cognizant.

In this report the activities highlighting the various projects, their progress and their potential for clinical utility are presented.

Prof. K. Dharmalingam
Director - Research

Molecular genetics of *ABCA4* gene in stargardt disease

Investigators : Dr. Pankaja Dhoble,
Dr. Rupa Anjanamurthy and
Dr. P. Sundaresan
Research Scholar : R.Kadarkarai Raj
Funding : Aravind Medical Research Foundation

Introduction

Stargardt disease-1 (STGD-1, OMIM-248200) is one of the most common macular degenerative disorder observed with the clinical features including macular atrophy, impaired central vision, decreased visual acuity and color vision (especially red, green) defect. Globally prevalence of STGD is 1 in 10,000. The onset of STGD-1 disease is usually in the first two decades of life and less frequently in adulthood. Mostly it follows an autosomal recessive mode of inheritance. Mutations in ATP-binding cassette transporter 4 (*ABCA4*) are responsible for 95% of cases of STGD-1. *ABCA4* located in chromosome 1p13, contains 50 exons and involved in the hydrolyzing of N-retinylidene-phosphatidylethanolamine to all-trans-retinal and phosphatidylethanolamine in visual cycle pathway. To our knowledge, only study showed the phenotype and genotype of STGD1 disease in five families belongs to Indian origin. The current study utilized a combinatorial approach including conventional Sanger sequencing and Targeted exome sequencing (TES) to identify the frequency of disease-causing variants associated with Stargardt disease in South Indian patients.

Results and Conclusion

Twenty eight patients presented with Stargardt disease-like phenotype were recruited from south India. All the probands had complaints of defective vision or central vision loss in both eyes. Approximately 5 ml of peripheral blood was collected from probands and DNA was extracted. Twenty four individuals were screened for *ABCA4* through Sanger sequencing and remaining 4 probands were subjected to TES to identify the disease causing mutations. Identified mutations were classified based on the American College of Medical Genetics and Genomics (ACMG) guidelines. Using this strategy, we identified 75% (21/28) of disease causing mutations in *ABCA4* gene (Table 1), 7% (2/28) exhibited benign variants and 18% (5/28) were negative for the disease-causing mutations. Two novel missense, frameshift mutations (in/del, single base pair deletion) and a splice variant were identified in *ABCA4* (Table 1). In addition, the frequency of *ABCA4* is poorly understood in our cohort. Therefore, this preliminary study contributes to the allelic diversity and mutation rate of *ABCA4* in a South Indian population.

ID	Exon	c.DNA change	Amino acid change	Variant Class	Zygosity	Method	dbSNP
2	30	c.C4506A	C1502Ter	Stop Codon	Homozygous	Sanger	rs61750149
4	14	c.C1995A	Y665Ter	Stop Codon	Homozygous	Sanger	rs757302286
8	13	c.G1819A	G607R	Missense	Homozygous	Sanger	rs61749412
9	9	c.G1188A	G396C	Missense	Homozygous	Sanger	rs866219294
10	12	c.G1556T	C519F	Missense	Homozygous	Sanger	Novel
11	35	c.T4956G	Y1652Ter	Stop Codon	Homozygous	Sanger	rs61750561
13	42	c.G5882A	G1961E	Missense	Homozygous	Sanger	rs1800553
17	48	c.C6658T	Q2220Ter	Stop Codon	Homozygous	Sanger	rs61753046
18	48	c.C6658T	Q2220Ter	Stop Codon	Homozygous	Sanger	rs61753046
22	44	c.A6095G	H2032R	Missense	Homozygous	Sanger	rs1242866408
24	19	c.C2900T	A967V	Missense	Homozygous	Sanger	rs1291080436
26	19	c.C2912A	T971A	Missense	Homozygous	NGS	rs61749450
27	22	c.G3323A	A1108H	Missense	Homozygous	NGS	rs61750121
28	19	c.C2912A	T971A	Missense	Homozygous	NGS	rs61749450
19	14,19,42	c.C1995A/ c.C2912A/ c.G5882A	Y665Ter, T971A, G1961E	Stop codon/ Missense	Compound Heterozygous	Sanger	rs757302286/ rs1800553
20	46,48	c.6355DelC/ c.C6658T	Q2220Ter	Del / Missense	Compound Heterozygous	Sanger	rs61753046
21	26,33	c.C3830T/ (c.4774-2A>G)	T1277M	Missense/ Splice variant	Compound Heterozygous	Sanger	rs374565343 / Novel
25	3,42	c.A217T/ c. G5882A	I73F, G1961E	Missense / Missense	Compound Heterozygous	NGS	Novel / rs1800553
5	14	c.C1995A	Y665Ter	Stop Codon	Heterozygous	Sanger	rs757302286
6	26	c.C3830T	T1277M	Missense	Heterozygous	Sanger	rs374565343
14	40	c.5710delCAATGinsA	-	Ins/Del	Heterozygous	Sanger	-

Table: 1 List of pathogenic mutations identified across ABCA4 gene exons in STGD1 patients

Macular corneal dystrophy: Comparison of structural data and genetic variations using confocal microscopy

Investigators : Dr. P. Sundaresan,
Dr. N. V. Prajna
Research Scholar : M.Durga

Funding Agency : Aravind Eye Care System,
DST-INSPIRE, New Delhi

Introduction

Macular corneal dystrophy (MCD) is an autosomal recessive disorder caused by carbohydrate sulfotransferase 6 gene (*CHST6*) which is essential for the sulfation of keratan sulfate. Mutations in *CHST6* results in abnormal accumulation of keratan (unsulfated) extracellularly in corneal stroma, Descemet's membrane and intracellularly in keratocytes and endothelium leading to vision loss. MCD is subdivided into three immunophenotypes, including type I, IA and II. MCD type I is reported as a predominant immunophenotype in Indian population, associated with missense mutations in the coding region of *CHST6*. In early stages, Photo Therapeutic Keratectomy (PTK) can be done, whereas at advanced disease stage requires Penetrating Keratoplasty (PKP). The recurrence rate of corneal opacities is more than 40% in MCD corneal grafts even after 10 years of PKP. Therefore, understanding the intricacies of MCD disease mechanism and its progression, detailed studies for *CHST6* mutations spectrum and their correlations with respect to corneal micro-structural changes will be helpful to address the gaps in knowledge. Imaging techniques such as slit lamp biomicroscope and in vivo confocal microscope (IVCM) provides the way to enhance our understanding of the corneal structural changes in the patients harbouring *CHST6* mutations.

Understanding the genetic aspects, structural changes and pathophysiological mechanism of MCD

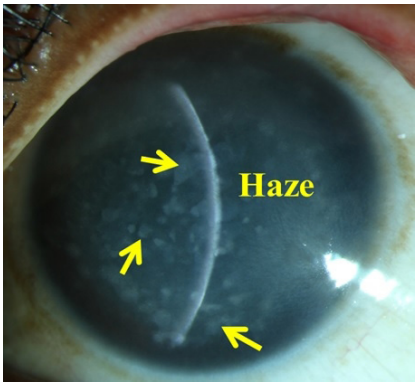

Figure 1: Slit lamp image of MCD patient (family 81) showing the multiple, irregular grey-white opacities with intervening stromal haze

is essential for the earlier accurate diagnosis, better treatments and preventive therapy. So far, there are limited genetic studies of *CHST6* mutations and their effects on micro-structural changes associated with MCD patients. Therefore, this study aimed to determine the micro-structural changes in MCD cornea due to corresponding *CHST6* mutations. To achieve this, we have recruited 100 MCD families, 30 unaffected relatives and 100 healthy volunteers (control) without any corneal dystrophies for PCR and Sanger sequencing analysis. For IVCM analysis, 15 MCD patients and 5 controls were recruited. Additionally, 27 MCD corneal buttons during penetrating keratoplasty (PKP) along with 10 cadaver corneal buttons (control) were also collected for further light and confocal analysis.

Results and Conclusion

The team identified 7 novel mutations (S53X, S81X, L129V, V172M, R202H, S248K, E274Q) and 16 previously reported mutations in 100 different MCD families. Patients with frameshift mutations (deletion, deletion-insertion) and deletion of open reading frame (ORF) mutation shown to have a

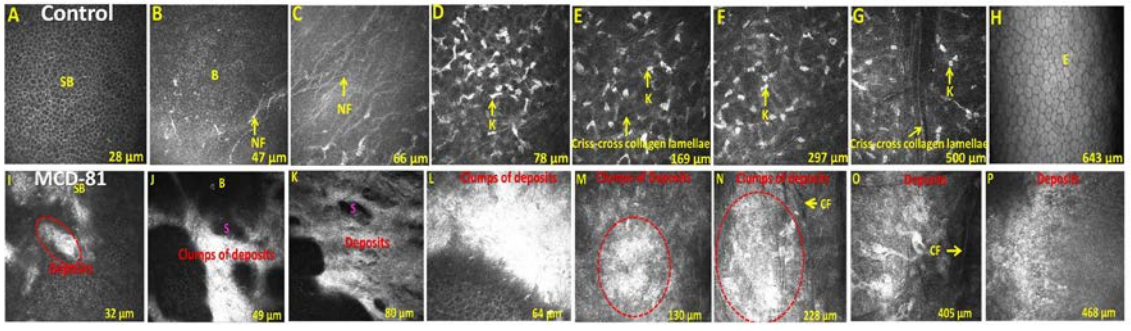

Figure 2: IVCM images of a normal human cornea (A-H) in comparison to MCD patient (family 81) cornea (I-P). The cornea was scanned from epithelium (SB) to endothelium. I-supra basal epithelium (SB) showing a scattered deposit. J-basal epithelium (B) showing a confluent, clumps of deposits with high edema or scar (S). K- bowman's layer showing a clump of highly reflective deposit with the rupture of basement membrane and loss of bowman's layer. L, M-anterior stroma showing a uniform confluent deposit. N, O-middle, posterior stroma showing a clump of highly reflective deposits. L, M, N, O- loss of keratocyte cell (K) & disrupted collagen fibrils (CF) P-endothelium showing a uniform, scattered deposits.

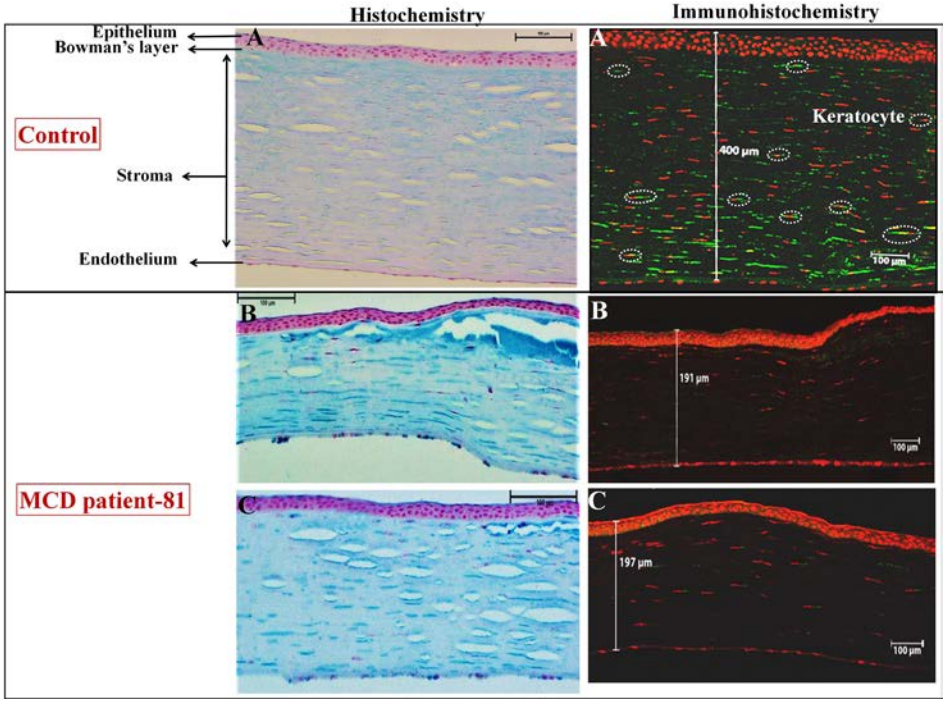

Figure 3: Light and confocal microscopic images. Representative cornea showing immunophenotype IA of MCD patient (B, C) compared to the control (A). B, C- In histochemistry, blue colour showing a positive alcian blue stain representing inter, intra lamellar deposition of amorphous, finely granulated material (GAG's) associated with the loss of bowman's layer (20X). B, C- In immunohistochemistry, FITC showing green colour (positive KS expression) and PI showing red colour (nucleus). Due to ORF mutation MCD cornea shows the KS expression only in stromal keratocytes with the reduced corneal thickness and reduced keratocyte cell count along with the loss of bowman's layer (20X).

severe corneal structural change as compared to the controls. For instance, MCD patient from family 81 (Figure1&2) with ORF mutation had the clumps of highly reflective, diffuse deposits with irregular edges that leads to the focal rupture of Bowman's layer with the complete loss of nerve fibres.
High stromal edema (honey-comb appearances) associated with confluent, clumps of deposits with large intervening spaces was observed in the anterior stroma (immediately after the bowman's layer). Additionally, we observed a drastically reduced keratocyte cell count along with altered collagen fibrils throughout the stroma. This study also revealed, MCD immunophenotype IA is predominantly present in Indian population associated with frameshift mutations and ORF mutation (Figure 3).

Clinical and molecular diagnosis of retinal dystrophies

Investigators : Dr. Pankaja Dhoble,
Dr. Rupa Anjanamurthy
Dr. P. Sundaresan
Research Scholar : R.Kadarkarai Raj
Funding Agency : Subroto Bagchi Grant

Introduction

Retinal Dystrophies (RDs) are group of heterogeneous disorder, characterized by degeneration of photoreceptors (rods and cones) and retinal pigment epithelium (RPE) cells. Even though more than 250 genes are involved in retinal degenerations, large number of genes associated with RDs is unknown. Around 50-60% of RDs are inherited through autosomal recessive manner followed by 30-40% through autosomal dominant form and 2-20% is inherited by X-linked or mitochondrial mode of inheritance. RDs are categorized into (i) non-syndromic such as retinitis pigmentosa (RP), cone-rod dystrophy (CRD), Leber congenital amaurosis (LCA), and Stargardt disease (STGD). (ii) syndromic are Usher Syndrome (USH) and Bardet-Biedl Syndrome (BBS). Since patient exhibits phenotypic heterogeneity, identification of disease causing gene in RDs is still challenging. Next-generation sequencing technology is an efficient tool to identify the disease causing genes involved in RDs. In this report, clinical exome sequencing method was employed for genetic analysis of 9 individuals who were clinically diagnosed or suspected with RDs (Best disease, USH, BBS).

S.No	Age/ Sex	Gene	cDNA change	AA change	Variant class	Zygosity	Clinical Phenotype
1	8/F	*BEST1*	c.523G>T	p.V175L	Missense	Heterozygous	Best disease
2	17/M	*BEST1*	c.133C>A	p.R45S	Missense	Homozygous	Best disease
3	34/M	*BEST1*	c.133C>A	p.R45S	Missense	Homozygous	Best disease
4	60/M	*BEST1*	c.133C>A	p.R45S	Missense	Homozygous	Best disease
5	30/M	*USH1C*	c.308G>A	p.R103H	Missense	Homozygous	Usher syndrome type 1C
6	18/M	*MYO7A*	c.4485G>A	p.W1495Ter	Nonsense	Homozygous	Usher syndrome type 1
7	30/M	*PDZD7*	c.82C>T	p.R28 Ter	Nonsense	Homozygous	Usher syndrome type 1
8	11/F	*CLRN1*	c.461_467dup	p.Q157P rofsTer17	Frameshift-Ins	Heterozygous	Usher syndrome type 3
9	35/M	*BBS5*	c.413G>A	p.R138H	Missense	Homozygous	Bardet-Biedl syndrome

Table: 1 List of pathogenic mutations identified in RDs patients through CES method

Results and Conclusion

The team recruited 9 unrelated individuals for this pilot study and keenly observed the clinical diagnosis like fundus changes, optical coherence tomography (OCT) imaging, full-field electroretinography (ERG), visual acuity, visual fields along with the family history. Among nine patients, four had Best disease, other four patients associated with Usher syndrome and one patient with Bardet-Biedl syndrome. USH and 1 had BBS. A pre-designed panel covering more than 250 genes associated with RDs was used to identify the disease causing mutations in RDs patients. Approximately 5 ml of peripheral blood was collected from probands followed by DNA extraction. Target genes were enriched with the Agilent Sure Select kit (V3) panel and the sequencing was performed on Illumina HiSeq4000 (Illumina, San Diego, CA, USA). Once sequence was completed, quality of raw FASTQ files was checked by using open-source fastq-mcf command line tool. Further, FASTQ files trimmed and reads were compared to a human genome reference sequence (hg19/GRCh37). Finally, tertiary analysis was done using the in-house pipeline to annotate variants through VariMAT - Variation and Mutation Annotation Toolkit. Disease variants were prioritized based on the American College of Medical Genetics and Genomics (ACMG) guidelines (Table 1).

To summarize, NGS was found to be a powerful clinical utility tool to identify the potential causal variants in nine individuals affected with various retinal disorders which helped provide an accurate clinical diagnosis and genetic counseling for their family members.

Genetics of Ocular Tumors

Eye cancer is a relatively uncommon, but debilitating disease. It can cause loss of sight, eye and even life, if it is not diagnosed early and treated appropriately. It can be intraocular or extraocular anatomically and can affect individuals across all ages. The most common childhood cancer, retinoblastoma affects about 1500 children each year in India. Among adults, lymphoma and carcinoma are common eye cancers in India. The symptoms of these cancers are innocuous, often ignored and hence presented at late stages. The disease prognosis becomes further complex with the poor response to chemotherapeutic drugs and varied disease course in many patients. Newer methods are adopted in our AMRF to understand the disease process and improve the diagnosis and prognosis of ocular tumors.

Genetic testing of retinoblastoma

Investigators : Dr. A. Vanniarajan
Dr. Usha Kim
Prof. VR.Muthukkaruppan
Project Fellow : S. Ulaganathan
Funding Agency : Aravind Eye Care System
Madurai

Retinoblastoma (RB) is primarily caused by mutational inactivation of *RB1* gene. Depending on the mutational pattern, it can be classified as somatic if it is present in only tumor and germline if it is present in constitutional cells. The risk of inheritance will be higher in germline mutations, whereas it will be the same as that of general population in case of somatic mutations. During the last year, the team done genetic analysis of 35 RB patients and also examined the genetic data for the last 3 years to check the disease penetrance.

Results

Among the 35 patients analysed this year, 11 are bilateral and 24 are unilateral. Four of them had positive family history. Germline mutations were identified in all the 11 bilateral patients with 100% sensitivity. Among the unilateral patients, the detection of somatic mutation was possible in all the 16 patients where the tumor tissues were analysed. In addition, three of the unilateral patients had constitutional mutations. The genetic counselling was provided with the predicted risk of retinoblastoma based on the inheritance pattern of the mutation.

Analysis of 3 years genetic data showed variable penetrance and expressivity in terms of laterality and disease presentation in five families. Genetic analysis of *RB1* gene in these families revealed

Family No	Mutation description	No. of family members	Affected members (Grouping)	No. of asymptomatic carriers	Un affected
F1	c.920 C>T p.T307I	3	1 (Unilateral)	1	1
F2	c.2069 A>G p.N690S	5	3 (2-bilateral 1-Unilateral)	1	1
F3	c.1981C>T p.R661W	4	1 (Unilateral)	2	1
F4	c.1981C>T p.R661W	3	1 (Unilateral)	1	1
F5	c.1888A>G p.T630A	3	1 (Unilateral)	1	1

Table 1: Retinoblastoma families with variable disease penetrance having missense germline mutations

the inheritance of germline missense mutations (Table 1). In two families, a missense mutation at c.1981C>T (p.Arg661Trp) were identified. Other missense mutations identified include c.920C>T (p.Thr307Ile), c.1888A>G (p.Thr630Ala), c.2069A>G (p.Asn690Ser). The reduced penetrance in *RB1* gene mutations was often associated with either reduction of normal pRB or production of defective pRB. Genetic analysis of complete family is recommended for predicting the risk clearly and understanding the penetrance and expressivity.

Genomic characterization of kinome related genes in Retinoblastoma

Investigators : Dr. A. Vanniarajan
Dr. Usha Kim
Prof. V.R. Muthukkaruppan
Research Scholar : K. Jeyaprakash
Funding Agency : Department of Biotechnology

Introduction

Retinoblastoma tumor progression requires additional genetic alterations other than the biallelic

Sample ID	Genes	Mutation	AA change	dbSNP	Poly phen2	CADD	GERP++	Domain - Interpro
RB1	*EPHA3*	c.G1775A	p.G592D	rs534679111	D	27.2	5.95	Ephrin receptor\x2c transmembrane domain
	CSF1R	c.T68C	p.I23T	rs749946644	D	28.3	5.76	Immunoglobulin-like domain
RB2	*TEK*	c.A309C	p.E103D	rs572527340	P	24.3	5.92	Tyrosine-protein kinase
RB3	*MAP3K15*	c.A1099C	p.I367L	rs771844821	.	31	5.16	Domain of unknown function
	CDC42BPA	c.G3593A	p.R1198H	rs961490	D	24.9	5.71	Pleckstrin homology domain
	YES1	c.C566A	p.T189K	rs774998072	D	32	5.7	SH2 domain|SH3 domain
RB4	*SYK*	c.G259A	p.D87N	rs201177148	P	23.8	4.79	SH2 domain
RB5	*EPHA8*	c.C2827T	p.R943C	rs199559772	D	35	4.25	Sterile alpha motif/pointed domain
RB6	*LIMK2*	c.T1601C	p.I534T	-	D	29.1	5.53	Protein kinase domain
	PDGFRB	c.C1610A	p.A537D	.-	D	29.2	4.92	Linker region

Table 1: Mutation details of kinase genes.

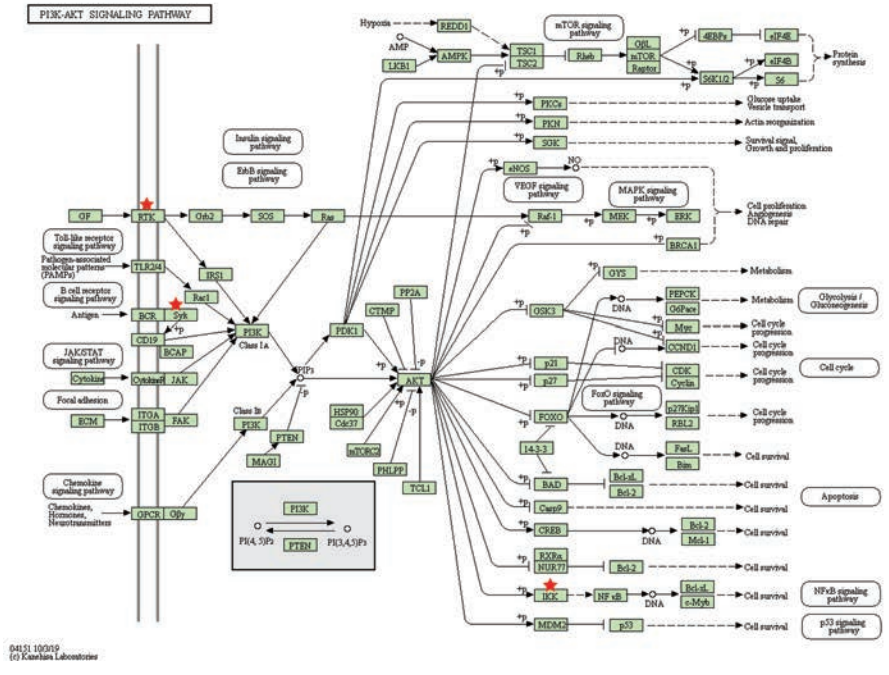

Figure 1: Gene enrichment by KEGG showing PI3K-AKT pathways. Red star indicates the receptor tyrosine kinase (RTK) family genes that are frequently mutated in retinoblastoma.

inactivation of *RB1* gene. Kinases and phosphatases are key modulators of signalling pathways regulating differentiation, transcription, cell cycle progression, apoptosis, motility and invasion. Genetic alterations of these genes have been widely documented in association with development and progression of human cancers including neuroblastoma. However, the status of kinase gene mutations in retinoblastoma is not fully known. Therefore, the team performed whole exome sequencing of six RB tumors and segregated the kinase gene variants.

Result

Segregated analysis of 518 kinase genes in six RB tumors showed frequent mutations in receptor tyrosine kinase family genes including *CSF1R, PDGFRB, TEK* and *MET* (Table1). Pathway analysis of these pathogenic genes using gene enrichment tools unravelled that these genes are involved in the regulation of *RAS, PI3K* and axon guidance pathways (Figure1). In addition, > 50% of tumors showed mutations in *TTN* and *OBSCN*.

Conclusion

The team's analysis showed the alterations in key genes of RAS and PI3K pathways in retinoblastoma. Detailed investigation of these genes will help in identifying suitable drug targets and develop personalized therapies.

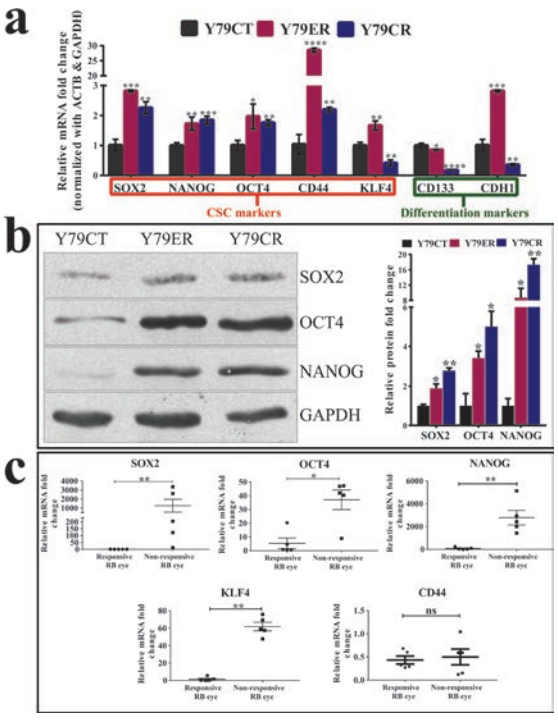

Figure 1: Increased expression of neuronal/CSC markers in RB chemoresistance.

Understanding the Molecular Mechanisms of Chemoresistance in Retinoblastoma

PhD Scholar : T.S. Balaji
Investigators : Dr. A. Vanniarajan, Dr. Usha Kim, Dr. R. Shanthi, Prof. V.R. Muthukkaruppan

Funding Agency : Council of Scientific & Industrial Research (Fellowship)

Introduction

Retinoblastoma (RB) can be curable if diagnosed in early stages and treated appropriately. However, most of RB in India is presented at late stages. In bilateral RB, oncologist will try to preserve at least one of the eyes by reducing the tumor burden with chemotherapy. In such cases, chemoresistance is a main hindrance for the success of therapy. Various mechanisms were reported for chemoresistance including drug efflux pump (ABC transporters), cancer stem cells (CSC) and defective apoptotic pathway. Recent studies have reported that all these mechanisms may be interconnected. In this study, the team have examined primarily the expression of stem cell markers as a molecular factor for chemoresistance. In addition, we also addressed the problem of pseudo house-keeping genes in normalisation of gene expression.

Results

The team developed etoposide and carboplatin resistant retinoblastoma (Y79) cell lines by stepwise drug increment treatment and validated with MTT. Presence of cancer stem cells was confirmed by quantitative real time PCR with upregulation of CSC markers such as, SOX2, OCT4, NANOG, CD44 and KLF4 and downregulation of CD133 in both Y79ER & Y79CR (Figure 1a). Western blot analysis also showed the upregulation of neuronal stem cell markers such as SOX2, OCT4 and NANOG in resistant cell lines (Figure 1b). In non-responsive RB tumors also, we have observed overexpression of neuronal/CSC markers (Figure 1c).

The general problem with many expression studies is the co-amplification of pseudogenes. *In silico* analysis revealed that among commonly used 6 reference genes (*ACTB, GAPDH, HPRT1, TUBB,* 18S rRNA and *B2M*), only *B2M* was found with no pseudogenes. Remaining genes were having significant number of pseudogenes as listed in Table 1.

Gene	Function	No of pseudogenes*
β-actin (ACTB)	Cytoskeleton structural protein	10
Glyceraldehyde-3-phosphate dehydrogenase (GAPDH)	Glucose metabolism	47
Hypoxanthine- guanine phosphoribo syltransferase (HPRT1)	Nucleotide metabolism	2
-tubulin (TUBB)	Cytoskeleton structural protein	6
18S ribosomal RNA (RNA18SN1)	Non-coding RNA, forms ribosomal complex during translation	5
β-2-Microglobuln (B2M)	MHC I Antigen processing	0

Table 1: Pseudogenes of commonly used reference genes for normalization of RT-qPCR data.

In order to prove *B2M* as pseudogene less reference gene, we performed PCR of both cDNA (synthesized from mRNA) and gDNA isolated from human peripheral blood, in which cDNA specific *B2M* primer amplify only the cDNA. The primers from *ACTB* and *GAPDH* amplify cDNA along with gDNA and mRNA from no RT control (Figure 2).

Using valid primer assay (VPA), the fluorescence signal from pseudogene amplification was neutralized along with gDNA amplification signal during qPCR data analysis. cDNA specific primers (*GAPDH, ACTB* and *B2M*, represented as GOI) and gDNA specific primer (represented as VPA) targeting intron of *GAPDH* gene were used to amplify cDNA converted from total RNA and gDNA isolated from peripheral blood. cDNA is represented as nucleic acid (NA) as it is believed to be contaminated with gDNA. Ct values were normalized to nullify gDNA amplification signal using following equations.

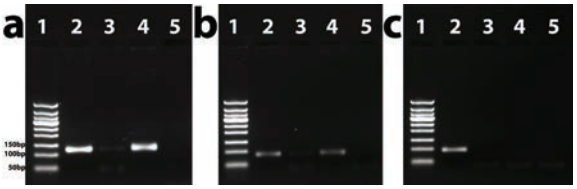

Figure 2: PCR amplification of a) ACTB and b) GAPDH, showing pseudogene amplification in lane 4 compared to c) B2M. Lane 1, 50bp ladder; Lane2, cDNA; Lane3, NRT (No Reverse Transcriptase control); Lane4, gDNA; Lane5, NTC (No template control).

CtDNA=Ct of VPA from cDNA + Ct of GOI from gDNA – Ct of VPA from gDNA - Eq 1

Ct¬RNA=-log2(2^[-CtNA] – 2^[-CtDNA]) - Eq 2

%DNA=(2^[-CtDNA]/2^[-CtNA]) - Eq 3

Ct from ACTB cDNA amplification using GOI primers was 24.670, which we represented as Ct of nucleic acid (cDNA + gDNA or pseudogene). In order to derive Ct only from gDNA amplification, VPA primers specific for gDNA and ACTB cDNA specific primers were used for amplification parallel. Using the Eq 1, we derived 23.852 as Ct from gDNA, which is fed into Eq 2 (Table 2). The Ct obtained from Eq 2 is signal only from mRNA amplification that can further be utilized for usual normalizing method of 2-ddCt to calculate fold change difference of GOI.

Conclusion

Elevated level of neuronal/cancer stem cell markers facilitate chemoresistance in RB. Developing therapies targeting these neuronal factors may improve the overall treatment efficacy in RB chemoresistant patients. The team has also developed a newer method for normalisation that can be used for any gene expression studies.

GOI	Ct of VPA in NA (cDNA +gDNA)	Ct of GOI in gDNA	Ct of VPA in gDNA	Ct of gDNA (Eq 1)	Ct of GOI in NA (cDNA +gDNA)	Ct of cDNA (NA-gDNA) (Eq 2)	Difference in Ct of cDNA from CT of gDNA	% of Nullified amplification signal from pseudogenes of GOI (Eq 3)
(1)	(2)	(3)	(4)	(5)=(2) +(3)-(4)	(6)	(7)=-log2 (2-(6)-2-(5))	(8)=(7)-(6)	(9)=(2-(5)/2-(6))*100
ACTB	24.670	24.828	25.646	23.852	21.799	22.197	0.398	24.1
GAPDH	24.670	25.092	25.646	24.116	20.139	20.233	0.094	6.35
B2M	24.670	33.023	25.646	32.047	24.355	24.362	0.007	0.5

Table 2: RT-qPCR normalization using VPA assay method. GAPDH primers covers intronic region used as VPA primer for gDNA normalization. Ct- Threshold cycle.

Microsatellite instability analysis in retinoblastoma tumors

Investigators : Dr. A.Vanniarajan, Dr. Usha Kim, Prof. VR. Muthukkaruppan
Research Scholar : A. Aloysius Abraham
Funding Agency : Department of Biotechnology

Introduction

Microsatellites are short tandem repeats (STRs) that contain a repeat sequence of 2–7 nucleotides across the genome and microsatellite instability is commonly seen in many tumors. The team has examined the microsatellites found in the regions of copy number gain and losses, covered in the customized targeted NGS panel. MISA microsatellite finder is a tool for finding microsatellites in nucleotide sequences obtained from Sanger or high-throughput sequencing data. MISA-web (http://misaweb.ipk-gatersleben.de/) was used to detect the microsatellites located in the region of copy number gains and losses.

Results

Four microsatellites in the *RB1* gene [(CA)23 in Intron 2 – *RB1*-i2; (CTTT)15 in Intron 20 – *RB1*-i20; (TG)20 in Intron 4 – *RB1*-i4; (AAAC)5 in Intron 17 – *RB1*-i17] were chosen for the analysis. In two tumors with homozygous and heterozygous deletion, the CA repeat count compared to the blood sample for *RB1*_i2 were found to be 13/22 and 22/30. Validation

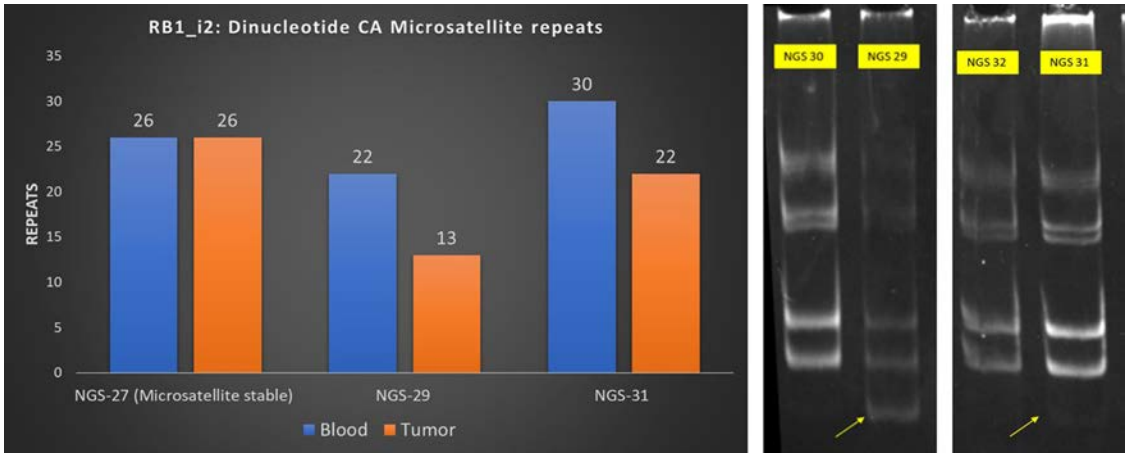

Figure 1: Microsatellite instability found in two tumor samples (NGS-29, NGS-31). Gel shift denoting the variable length of microsatellites for marker RB1_i2 (CA) repeats

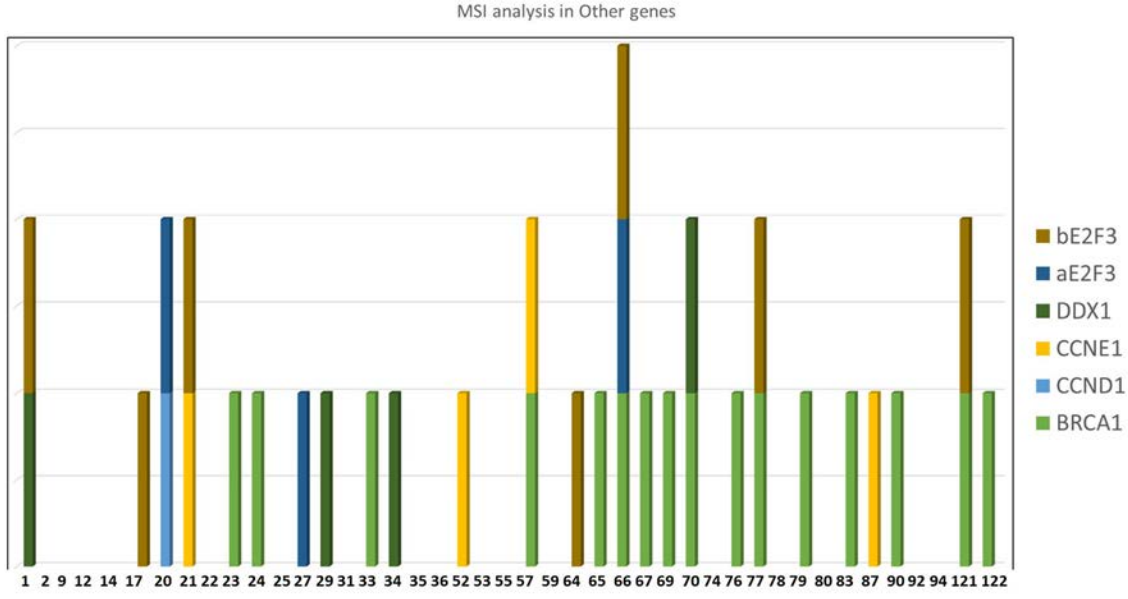

Figure 2: Microsatellite instability analysis of genes whose loci are covered in Targeted NGS

of a result is performed by amplifying the region and checking it in 15% polyacrylamide gel, that showed a clear shift in the band pattern showing microsatellite instability in that loci (figure 1).

Similarly, other microsatellite regions covered in the targeted panel [BRCA1- (GAA)6; CCND1- (GAG)5; CCNE1- (GGACG)5; DDX1 - (TC)7; E2F3 -(CGC)6 & (GCG)5] were analysed (Figure 2). Tumors with microsatellite instability in *BRCA1* gene had no copy number alteration in that gene except one sample. Similar trend was seen in genes *CCNE1* and *DDX1*. In E2F3, irrespective of microsatellite instability, there were copy number gains observed. Further analysis is required to check the possible association of CNVs and MSI.

Conclusion

Microsatellite instability analysis is a good technique for identifying the loss of heterozygosity in samples with whole gene deletions or segmental chromosomal deletions. These alterations could act as a breakpoint region for chromosomal abnormalities. These instabilities also suggest that there is a defective function of DNA mismatch repair genes that adds further mutational burden in tumor cells.

Molecular characterization of tumor progression in retinoblastoma

Investigators : Dr. A.Vanniarajan, Dr. Usha Kim
Prof. VR. Muthukkaruppan
Research Scholar : T.Shanthini
Funding Agency : DST-INSPIRE Fellowship

Introduction

The *RB1* is a tumor suppressor gene located on chromosome 13q14.2 and its inactivation includes mutations such as point mutations, indels, large deletion/duplications, phosphorylation and *RB1* promoter methylation. The co-existence of various disease and abnormalities due to the loss of chromosome 13q14 were collectively called as 13q deletion syndrome. In addition to detecting *RB1* deletion, we demonstrated Multiplex Ligation dependent Probe Amplification (MLPA) technique could also be used to identify the 13q deletion syndrome with extended deletion.

Results

Among the patients with *RB1* deletions over the past 3 years, thirteen patients had extended deletion of *RB1* gene and other flanking regions. Five patients had additional symptoms and other systemic illness related to the deletions. In one patient, 6-month-old girl, born to the non-consanguineous parents via caesarean section, was diagnosed with Waardernburg Syndrome (WS) along with RB. The proband had heterochromia iridis, telecanthus, high arch palate, low set ears along with white forelock which is the characteristic feature of WS (Figure 1). Based on the phenotype and earlier genetic studies of WS4 and RB, we narrowed down our analysis to *RB1* gene and EDNRB both located in the chromosome 13q.

MLPA analysis in patient's blood showed ratios of 0.5 indicating monoallelic deletion in the whole *RB1* gene along with the extended flanking genes (Figure 2). Additionally, the SNP microarray with Affymetrix Cytoscan 750K was done to identify the extent of the deletion in 13q. This microarray data clearly showed extended loss of 35 Mb on the long arm of chromosome 13 at band 14.11 to 31.1 (Figure 3).

Conclusion

The team reports a unique case of Waardenburg syndrome Type 4 and Retinoblastoma. This serves as

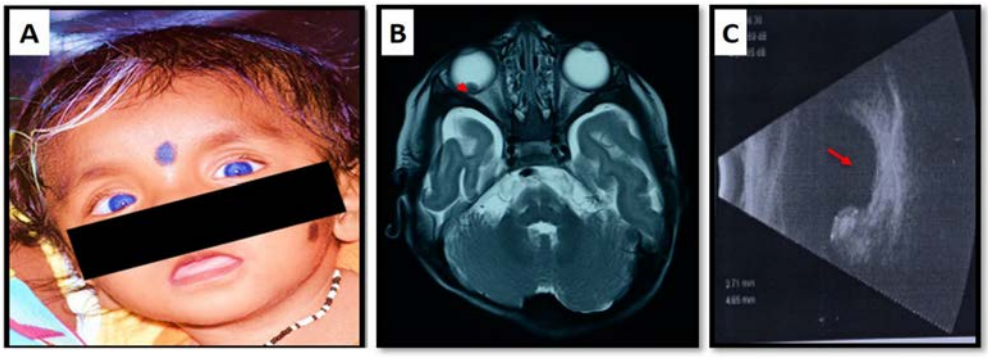

Figure 1: Retinoblastoma patient with Waardenburg syndrome A. Clinical picture showing heterochromia iridis, telecanthus, high arch palate, low set ears and white forelock. B. MRI examination showing calcification in right eye in vitreous chamber pointed by arrow. C. USB- Scan showing mass in the inferior retina of right eye with hyperechoic internal structure shows calcification with no orbital extension, confirming retinoblastoma

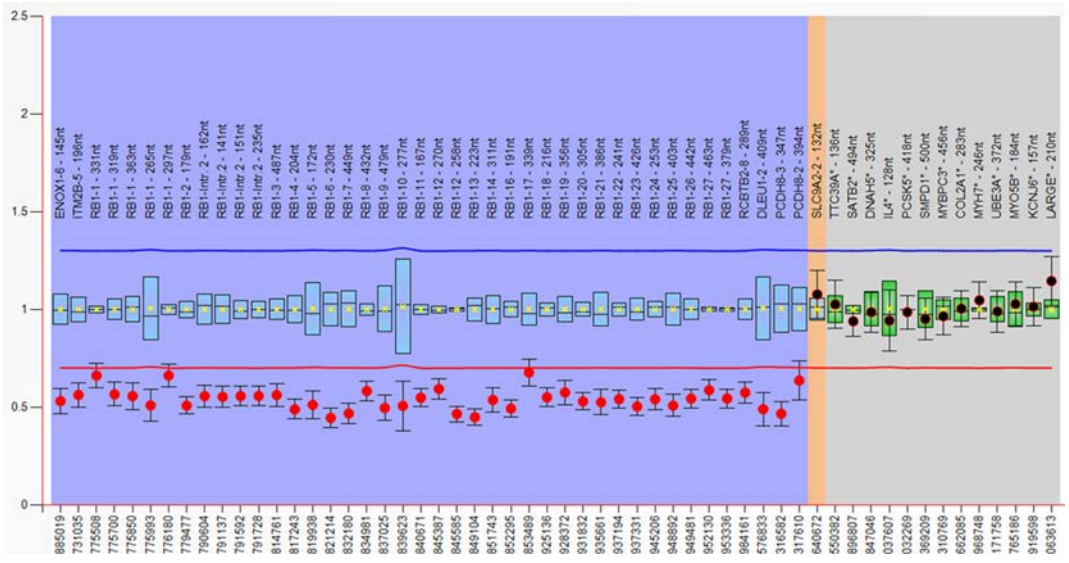

Figure.2: MLPA analysis showing heterozygous deletion from ENOX1 to PCDH8 along with the RB1 denoted by the reduced ratio in red lying below the cutoff range (<0.7).

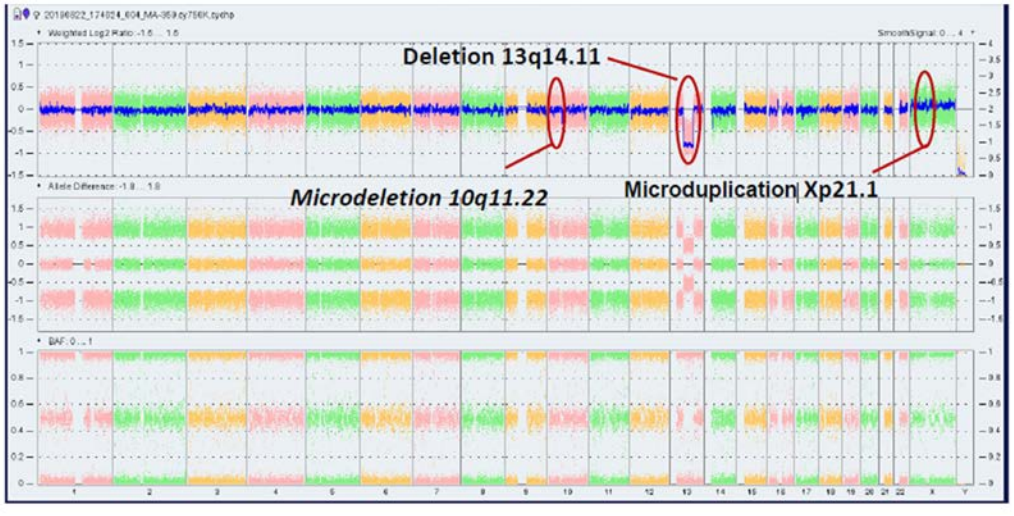

Figure 3: Microarray showing extended loss of 35 Mb on the long arm of chromosome 13 at band 14.11 to 31.1 and other microdeletions at Chromosome 10 and X.

an additional phenotype to the existing syndromes of 13q interstitial deletion. Additionally, MLPA proves to be an effective method of screening retinoblastoma and also provides clues to detect additional genetic changes apart from *RB1*.

Identification and validation of deregulated pathways in retinoblastoma

Investigators : Dr. A.Vanniarajan, Dr. Usha Kim
Dr. D. Bharanidharan
Prof. VR. Muthukkaruppan
Project Fellow : Anindita Rao
Funding Agency : DST-SERB

Introduction

Gene expression studies have proven to be valuable tools for identification of genes and their associated molecular pathways involved in cancers. There are other transcriptional events that have pronounced effects on RB tumor development, invasion, metastasis and conferring chemoresistance. Analysis of expression data of RB tumors has showed dysregulation of genes belonging to functional classes like apoptosis, phosphorylation, cell cycle, DNA damage, oncogenesis and tumorigenesis. Further studies suggested the involvement of signalling pathways like insulin, aryl hydrocarbon receptor (AHR), polo-like kinase and mitosis, purine metabolism, p53 inactivation, etc.

Upregulated genes	Pathway/Function	Fold change
MKI67 - Antigen identified by monoclonal antibody Ki-67	Cellcycle/Ki-67 proliferation marker	1000-fold
PGF - Placental growth factor	Angiogenesis/Growth factor active in endothelial cell growth, stimulating their proliferation and migration	100-fold
WEE1 - Checkpoint kinase	Cell cycle/Catalyzes the inhibitory tyrosine phosphorylation of CDC2/cyclin B kinase	80-fold
MCM2 - Minichromosome maintenance complex component 2	Cell cycle/initiation of eukaryotic genome replication	50-fold
CDC20 - Cell division cycle protein 20 homolog	Cell cycle/Nuclear movement prior to anaphase and chromosome separation.	40-fold

Table 1. List of commonly upregulated genes in RB tumor tissues

It is therefore necessary to investigate the key mechanisms through which the disease progresses towards its malignant form.For transcriptional level analysis, RNA was isolated from 13 samples including RB tumors and cell lines. cDNA synthesis was performed using Qiagen First Strand Kit with a starting template RNA concentration of 1µg. Real-time PCR was carried out using RT^2 PCR Human CancerPathwayFinder™ Arrays.

Results

Gene expression profiling was to analyze the expression of 84 genes associated with cancer specific pathways like cell cycle, apoptosis, angiogenesis, epithelial-to-mesenchymal transition, hypoxia, metabolism and telomerase activity. Preliminary analysis of relative fold-change data from the real-time PCR revealed deregulation of genes in tumor tissues as compared to normal neural retina in 5 genes. Among the top 5 genes expressed in high magnitudes (shown in Table1) 4 were cell cycle associated and 1 is angiogenesis-related thus suggesting activation of pathways aiding tumor growth and proliferation. Clinical findings of samples would give an insight into which transcriptional events define certain tumorigenic properties.

Conclusion

Further analysis of these genes in larger set of samples would confirm their role in tumorigenesis. This transcription-level assessment of cancer specific genes would pave way for better understanding the cascade of events that lead to uncontrolled tumor proliferation and progression.

Translational genomics of ocular cancers

Investigators : Dr. A.Vanniarajan,
Dr. Usha Kim, Dr. R. Shanthi
Dr. D. Bharanidharan
Prof. VR. Muthukkaruppan
Project fellow : K. Saraswathi
Funding Agency : Aravind Eye Foundation, USA

Introduction

Ocular lymphoma (OL) is the common orbital malignancy affecting actively working group and elders. OL is not only sight threatening but is also life threatening if not diagnosed on time and treated appropriately. OL may be intraocular or localized in ocular adnexal structures. Similar to systemic lymphoma , Non-Hodgkin's B cell type is most predominant in OL. Lymphoma histologically segregated into indolent and aggressive types based on the clinical outcome. Indolent B cell lymphoma includes Follicular Lymphoma and Extranodal Marginal Zone Lymphoma that shows better survival than aggressive subtypes like Diffuse Large B-Cell Lymphoma and Mantle Cell Lymphoma.

Generally ocular lymphoma are genetically characterized by immunoglobulin rearrangement(IGH) and chromosomal translocations associated with specific subclass of lymphoma, for example; t(14;18)(q32;q21) in Follicular Lymphoma, t(3;14)(q27,q32) in Diffuse Large B-cell Lymphoma (DLBCL) and t(11;14)(q13;q32) in Mantle Cell Lymphoma (MCL). Other than fusion genes many recurrent genetic alterations in NHL are associated with better or worse prognosis. As a preliminary study, genetic screening of *RB1* in ocular lymphoma were carried out in 4 tumor samples

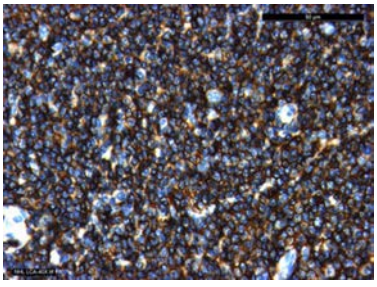

Fig1: LCA- leukocyte common antigen a major membrane glycoprotein stains all the leukocytes.Immunostaining shows diffuse positive reactivity for numerous lymphocytes.

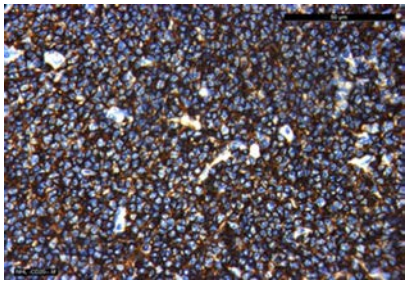

Fig 2 : CD 20 is a cell surface marker for B-cells. Immunostaining represents diffuse and strong positivity for CD20

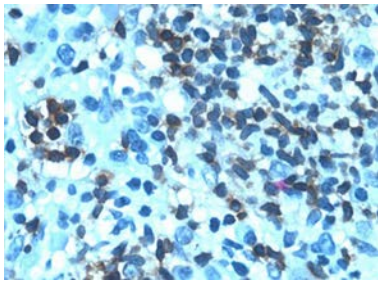

Fig 3: CD 3 is a cell surface marker for T-cells. Immunostaining shows scattered positivity for CD3

as *RB1* dysregulation is frequently associated with poor disease prognosis. Thus, *RB1* alterations were analyzed by multistep approach that includes MLPA, MS-MLPA and Sanger sequencing.

Results

Clinical data of ocular lymphoma patients indicated male predominance with mostly unilateral presentations. Proptosis was the most common clinical sign followed by swelling. Their mean age of presentation was 50 years. Histopathology and immuno-histochemistry markers (LCA, CD20, CD3- Fig 1,2&3) revealed that all the lymphomas were of B-cell origin and were further classified based on their shape, size and pattern of the cell types as small, medium and large. Chemotherapy regimen of COP/ CHOP (cyclophosphamide- vincristine-doxorubicin-prednisolone) was given based on the patient's clinical features and treated successfully with complete regression. Genetic analysis of *RB1* gene revealed that no inactivating mutation or deletions of pRB in 4 tumors studied here.

Conclusion

Further investigations on subtyping and chromosomal rearrangement would complement these investigations of clinical and histopathological findings. These findings will be useful in segregating the patient and providing appropriate treatment of tumor aggressiveness.

Translational genomics of paediatric eye diseases

Investigators : Dr. P. Sundaresan
Dr. A. Vanniarajan
Dr. D. Bharanidharan
Dr. VR. Muthukkaruppan
Dr. P. Vijayalakshmi
Dr. R. Kim, Dr. Usha Kim

Project Fellows : R.C. Vignesh, D. Nancy, Gowri Poigaialwar, A.S.Sriee Viswarubhiny, Susmita Chowdhury, A. Aloysius Abraham, K. Jeyaprakash, A. Mohamed Hameed Aslam, C. Prakash, K. Manoj Kumar

Funding Agency : Department of Biotechnology

Introduction

Major causes of childhood blindness in India include congenital anomalies and retinal dystrophies together contributing to 40%. Childhood blindness not only affects vision but also their learning and cognitive abilities. Diagnosis of genetic eye diseases in children is really challenging due to phenotypic heterogeneity with overlapping symptoms. Retina being the most affected site of blindness contributes about 29% of abnormalities in children. Our work on paediatric eye diseases has shed light on specific eye diseases such as Leber's Congenital Amaurosis (LCA), Leber's Hereditary Optic Neuropathy (LHON), Retinoblastoma (RB) and Juvenile X-linked Retinoschisis (JXLR). The major focus of this project is to understand the allied molecular mechanisms underlying these pediatric eye diseases for early detection and possible treatment.

Exome sequencing and data analysis

A composite panel with a total of 124 genes (RB: 74 genes, LCA: 48 genes, JXLR: 2 genes & LHON: mitochonodrial genome targeting known ocular disease genes was made with an updated list of novel candidates. Exome sequencing (whole exome and clinical exome sequencing) was performed for 20 samples (12 LCA, 6 RB and 2 LHON) using Illumina HiSEQ4000 platform. An indigenous pipeline for the exome sequencing has been established for the analysis. From the annotated variant data obtained, the pathogenic variants were filtered using an algorithm as described (Figure 1). For Nonsense, indels and frameshift mutation - segregation was

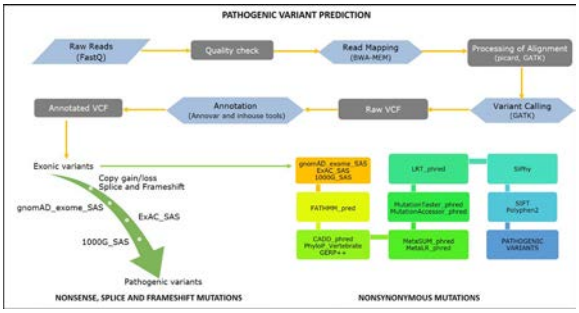

Figure 1: Algorithm for identification of pathogenic variants from WES data

done based on population frequencies and the functional annotation of nonsynoymous mutations was made using the optimal tools.

Diverse genetic pattern of Leber's Congenital Amaurosis

LCA is often reported as an autosomal recessive disorder with a rare incidence of autosomal dominant inheritance. Twelve LCA probands were analysed by whole exome (2) and clinical exome sequencing (10). The candidate LCA genes were identified in 75% of the patients. By whole exome sequencing, we identified pathogenic mutations in two families. Out of ten probands analysed by clinical exome sequencing, causative variants were identified in seven probands (Table 1). Of these, two variants in *LCA5* (c.1823del) and *CRX* (c.848del) genes were not reported so far (Figure 2). The unique heterozygous frameshift deletion in *CRX* gene was identified both in proband and mother with autosomal dominant LCA (Figure 2). In addition, our results are promising for patients with *RPE65* mutations, who are eligible for gene therapy and may recover the useful vision.

Alterations of cell proliferation and apoptosis genes in retinoblastoma

Apart from *RB1* gene, there are multiple genes involved in retinoblastoma tumor progression. The mutations along with copy number changes identified by the whole exome analysis of six tumors are listed in the Table 2. Mutations in *RSU1* were identified at canonical splice sites, thereby altering Ras signal transduction pathway, growth inhibition, and nerve-growth factor induced differentiation processes. Prominent nonsense mutations were identified in genes such as *FLG* (Filaggrin, a filament-associated

S.No.	Gene	Variant Type	c.DNA Change	Amino acid change	Zygosity
1	*PRPH2*	Missense	c.629C>T	P. Pro210Leu	Homozygous
2	*LCA5*	Frameshift_del	c.1062_1068del	P. Tyr354Ter	Homozygous
3	*ALMS1*	Frameshift_del	c.11310_11313del	p. Glu3771TrpfsTer18	Homozygous
4	*LCA5*	Frameshift_del	c.1823del	p. Leu608TyrfsTer30	Homozygous
5	*CRX*	Frameshift_del	c.848del	p. Met283ArgfsTer88	Heterozygous
6	*CEP290*	Missense	c.2483G>T	p. Ser828Ile	Homozygous
7	*RPE65*	Frameshift_ins	c.361dup	p. Ser121PhefsTer10	Homozygous

Table 1: Pathogenic variants identified in LCA patients by Clinical Exome Sequencing

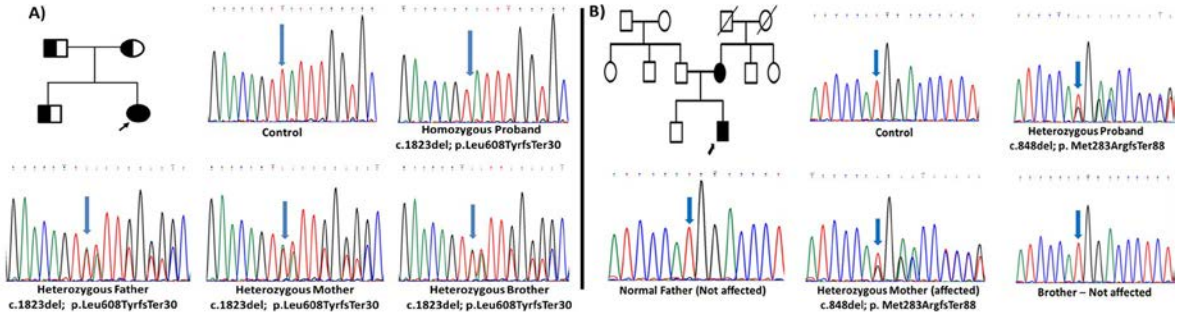

Figure 2: Distinct Inheritance pattern of LCA. The pedigree and electropherogram depicting A) Autosomal Recessive LCA with homozygous LCA5 gene mutation and B) Autosomal Dominant LCA with heterozygous CRX gene mutation in both proband and mother

Sample ID	RB1 Mutation	Copy number gain	Copy number loss	Other Pathogenic variants
WES_AMRF_BR1 (Unilateral)	No Mutation	KIF14, MDM4, DEK,E2F3	TP73, SYK, CHFR, BAZ1A, OTX2, CDH11,CDH13	ARSD:c.G992A:p.W331X RSU1:c.599-2->C AQP7:c.406+2T>C FHIT: c.C301T:p.P101S POTEG:c.A226G:p.S76G
WES_AMRF_BR2 (Unilateral)	exon15:c.C1399T :p.R467X (homozygous)	-	-	FLG:c.G8281T:p.G2761X AQP7:c.406+2T>C NBPF1:c.2666+2T>C ABCA10:c.2012-2A>G PSPH:c.275+1 del G DGUOK:c.A218G:p.Q73R FHIT:c.C301T:p.P101S POTEG:c.A226G:p.S76G
WES_AMRF_BR3 (Unilateral)	No Mutation	KIF14, MDM4, DDX1, MYCN, DEK, E2F3	ATM	FLG:c.G8281T:p.G2761X ARSD:c.G992A:p.W331X RSU1:c.599-2->C AQP7:c.406+2T>C PSPH:c.275+1 del G CHEK2:c.G937A:p.V313M BCOR:c.4340delG:p.R1447Pfs*36
WES_AMRF_BR4 (Bilateral)	Heterozygous deletion of RB1 exon20:c.A2069 G:p.N690S (homozygous)	TP73, KIF14, MDM4, DEK, E2F3, CHFR, OTX2, TP53, GATA5, E2F2, CCNE1, E2F1	CDH11, CDH13, BRCA2, CHEK2	ZNF717:c.G107A:p.W36X ARSD:c.G992A:p.W331X AQP7:c.406+2T>C SYK:c.G259A:p.D87N POTEG:c.A226G:p.S76G
WES_AMRF_BR5 (Bilateral)	exon3:c.G297A:p .W99X (homozygous)	MDM4, DDX1, MYCN, DEK, E2F3	TP73, CDH11, CDH13, TP53, GATA5, E2F2	AQP7:c.406+2T>C NBPF1:c.2666+2T>C PSPH:c.275+1 del G DGUOK:c.A218G:p.Q73R
WES_AMRF_BR6 (Bilateral)	exon11:c.1079del G:p.S360lfs*6 (heterozygous) exon17:c.G1597 T:p.E533X (heterozygous)	KIF14, MDM4, DDX1, MYCN, E2F3	TP53, ATM	ZNF717:c.G107A:p.W36X AQP7:c.406+2T>C ABCA10:c.2012-2A>G PSPH:c.275+1 del G POTEG:c.A226G:p.S76G

Table 2: WES mutation analysis and copy number details of Retinoblastoma six tumors

protein that binds to keratin fibers in epithelial cells), *ZNF717* (Zinc finger protein 717 involved in cell proliferation, differentiation and apoptosis) and *ARSD* (Arylsulfatase D - a member of the sulfatase family required for correct composition of bone and cartilage matrix). Copy number gain and loss were identified in the genes largely involved in cell proliferation and apoptosis.

Besides, the team has also resolved a mysterious case of JXLR with mutation in *BEST1* but not with candidate *RS1* gene for the first time in India.

Molecular analysis of mitochondrial disease with ophthalmic manifestations

LHON patients were recruited based on well-defined clinical criteria for further molecular analysis. Representative images for Fundus and Optical Coherence Tomography (OCT) examinations for LHON and control subjects are shown in Figure 3.

Whole mitochondrial genome sequencing

Sanger sequencing using 24sets of primers for targeting whole mitochondrial sequence and amplicon based Next Generation Sequencing was used for 60 LHON probands. Mutations were found to be prevalent in the *MT-ND1* gene (13%), followed by *MT-ND5* (11%), *MT-RNR1* (9%) and *MT-TT* (9%) (Figure 4).

Determining the haplogroup (HG) for identification of group at risk of mitochondrial disease

Identification of haplogroup was done for the 60 LHON probands using the HaploGrep tool with

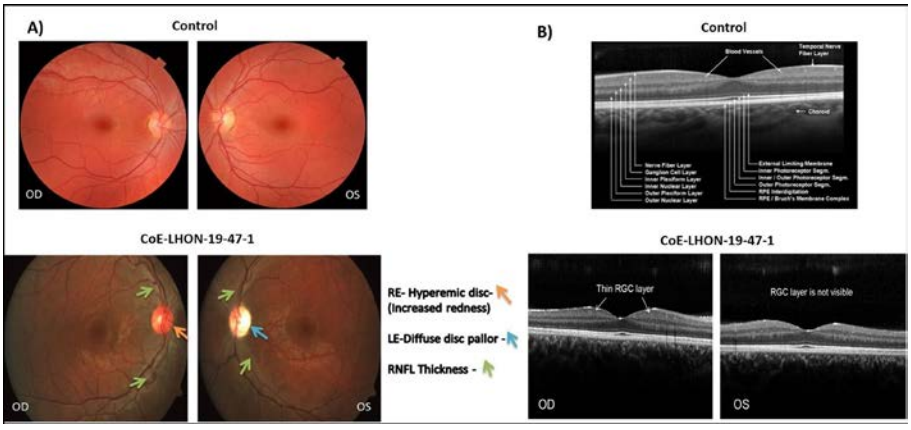

Figure 3: Fundus and OCT examination of control and LHON proband. A) Right eye (OD) showed RNFL thickness and hyperemic disc. Left eye (OS) was observed with RNFL thickness as well as temporal diffuse disc pallor. B) Right eye (OD) was observed with thin ganglion cell layer and it was not visible in the left eye (OS).

Phylotree17. Present study showed M haplogroup (67%) to be most prevalent one followed by R (14%), U (12%) and N (7%) haplogroup (Figure 5). This is consistent with earlier reports which also showed M haplogroup to be most prevalent in Indian population. Subgroup analysis showed frequency of M2 subgroup was higher followed by M5 among M haplogroup.

Whole-Exome sequencing for LHON probands

Through whole exome sequencing of two LHON probands, a novel heterozygous (c.C2671T) missense mutation in *LRPPRC* gene was identified. Mutations in this gene have been associated with the French-Canadian type of Leigh syndrome. *LRPPRC* is a Leucine rich pentatricopeptide repeats which plays a role in cytoskeletal organization, vesicular transport, or in transcriptional regulation of both nuclear and mitochondrial genes. Herein, another heterozygous mutation has been identified in *DHODH* gene (c.A19C) (Dihydroorotate Dehydrogenase (Quinone), reported elsewhere. It affects de-novo pyrimidine bio synthesis and mutations in this gene are associated with postaxial acrofacial dysostosis. Functional network analysis using String revealed *LRPPRC* and *DHODH* genes showed strong association with mitochondrial genome (Figure 6).

Studying the mitochondrial mutations using the cybrids model developed from patients platelets

Mitochondrial functions are controlled by both mitochondrial DNA (mtDNA) and nuclear DNA. Hence, it is difficult to identify whether mitochondrial or nuclear genome is responsible for a particular mitochondrial defect. Present study employs cybrids as an alternative model system, where we can compare mitochondria from different sources in a defined nuclear background. It is constructed by fusing enucleated cells harboring wild type or

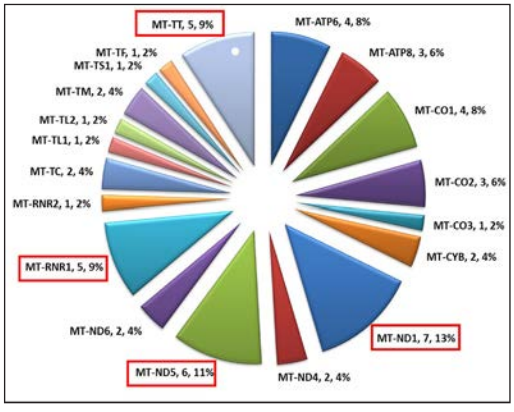

Figure 4: Mutational analysis of LHON probands through mtDNA Sequencing

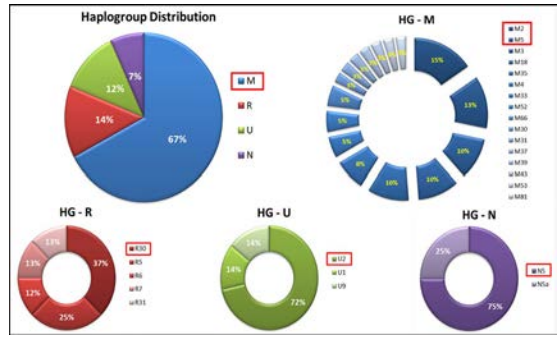

Figure 5: Haplogroup distribution among LHON probands

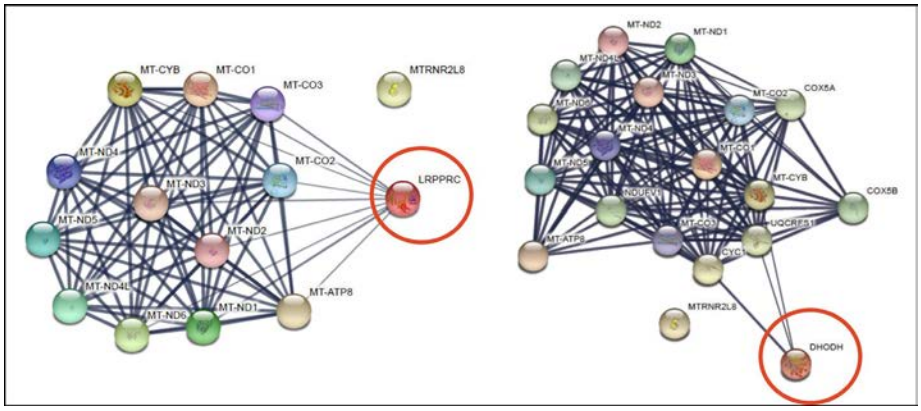

Figure 6: Functional network analysis for LRPPRC and DHODH genes using String

altered mtDNA of interest with ρ(0) cells (cells lacking mtDNA) in which the endogenous mtDNA has been depleted. Here in this study, work is in progress to produce Rho-0 phenotype using 143B TK- cell line (Figure 7) by treating with EtBr. Overall, this study will provide insights of the factors underlying the pathogenesis involved in mitochondrial diseases for further therapeutic developments.

Epigenetic mechanisms underlying tumor progression in retinoblastoma

RB1 bi-allelic loss was associated with promoter hypermethylation, which is one of the epigenetic factors responsible for gene-silencing. The samples with no *RB1* variations or deletions were analysed for promoter methylation by MS-MLPA and Bisulfite sequencing. In addition to *RB1* inactivation, other genetic and epigenetic events are essential for the retinoblastoma (RB) progression. This study aims to reveal the epigenetic events involved in the RB progression.

RB1 promoter methylation analysis by MS MLPA

Methylation specific-Multiplex Ligation dependent Probe Amplification is a modification of the MLPA technique. MS-MLPA allows the detection of both copy number changes and unusual methylation levels of different sequences in one simple reaction. MLPA probes for methylation quantification are similar to normal MLPA probes, except that the sequence detected by the MS-MLPA probe contains the sequence recognized by the methylation-sensitive restriction enzyme *HhaI*. Using this technique, promoter methylation was identified in 4 samples with one allele methylated (Figure 8).

Bisulfite sequencing for methylated promoters

Bisulfite modification of DNA is the most commonly used, "gold standard" method for DNA methylation studies at single nucleotide resolution. Bisulfite conversion was carried out using Zymo-EZ DNA methylation kit followed by bisulife PCR and direct sequencing. Primers were designed using MethPrimer tool for 11 genes – *CDKN2A, VHL, RASSF1A, TP53, APC-2, MLH1, MGMT, MSH6,*

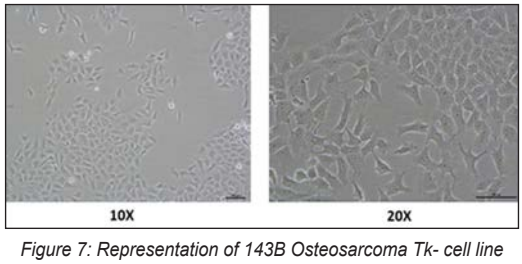

Figure 7: Representation of 143B Osteosarcoma Tk- cell line

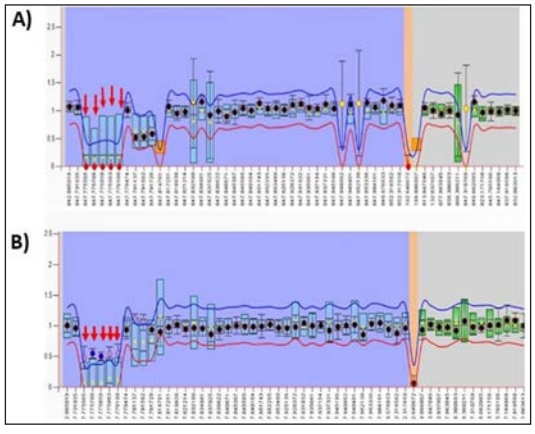

Figure 8: RB1 Promoter methylation analysis using MS-MLPA.
A. The ratio chart of the tumor sample which is unmethylated, where the red arrows pointing out the 5 probes were at ratio 0. (means of no amplification because of the action of HhaI enzyme in the CpG sequence).
B. The ratio chart of the tumor sample in which one allele is Methylated, where the red arrows point out the probe were at ratio 0.5

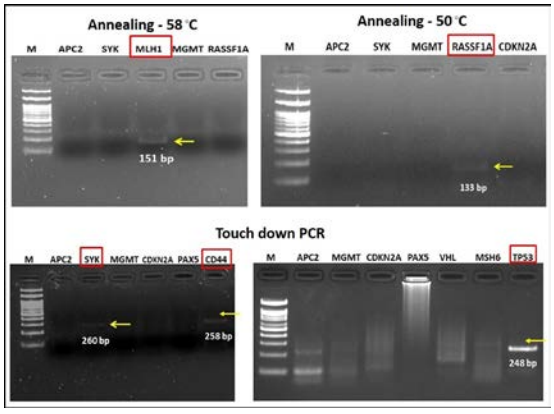

Figure 9: Optimization of Bisulfite PCR for 5 genes. Gel showing the amplification of MLH1, RASSF1A, SYK, CD44 and TP53 in the bisulfite converted DNA.

PAX5, CD44, SYK. Further, optimization was done for 5 genes with neural retina at different annealing temperatures (Figure 9). Further, the transcriptomic analysis could be correlated with the differential methylated regions to decipher the candidate genes involved in the pathogenesis of tumor progression.

Development of in-house bioinformatics pipelines for whole exome/genome, transcriptome sequencing data from paediatric eye disease patients

Previously, the team has established human whole exome data analysis pipeline based on the bench-marking results of GiaB (NA12878, NA24385 and NA24632) using five different aligners and four variant callers were executed in all pairwise combinations (20 pipelines). Recently, the performance of pipelines was compared with new updated version of tools. The recently automated pipeline provides accurate identification of genomic variants from exome datasets as mentioned previously. Here, we provide modular pipeline for whole genome data sets and variant prioritization methods for eye diseases. In tandem, we also benchmarked tools for transcriptomic data for the development of best performing pipeline.

Results

A modular pipeline (Figure 10) for benchmarking the updated tools for the genome data sets was developed. The datasets were FASTQ files of human exome HapMap/1000 CEU female NA12878 (accession No.: SRR622457) downloaded from NCBI-Sequence Read Archive (SRA- http://www.ncbi.nlm.nih.gov/sra). This was sequenced using HiSeq Illumina 2000 platform. The human reference genomes GRCh38 were downloaded from the

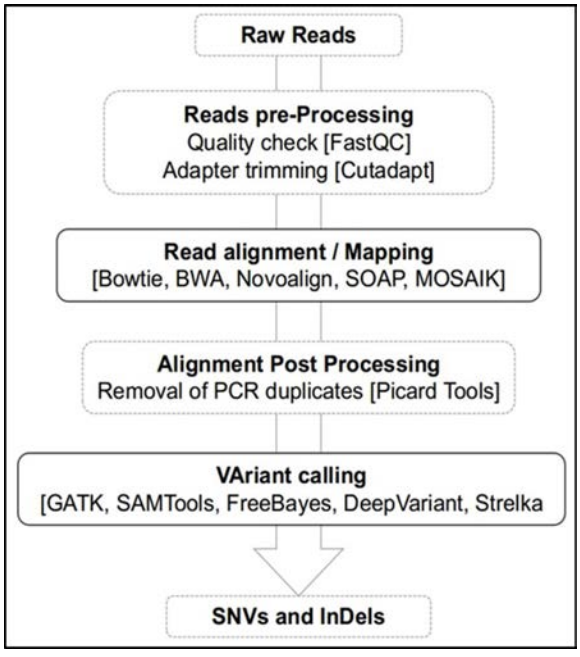

Figure 10. Schematic of the NGS data analysis pipeline

Ensembl. GiaB high confidence callset version 2.19 along with a BED file was downloaded from NCBI, which was further filtered to highly accurate call set using the BED file. NA12878 in GiaB is the only 'gold standard' variant genotype dataset publically available for systematic comparison of variant callers. The list of variants provided in that was created by integrating 14 different datasets from five different sequencers and was used to validate the variants detected by pipelines.

In all the datasets, BWA_DeepVariant, Novoalign_DeepVariant, BWA_Strelka, Novoalign_Strelka were the top four best performing pipelines for the SNVs and InDels with the similar F-score 0.985 and 0.943.

The detected SNVs and InDels will be subjected to variant filtering heuristically as below.

Functional Variants (Exonic Region)>Allelic frequency (MAF) 1000g, ExAC < 0.01> GREPP > 4.4 (Conservation)>CADD > 20 >QD (Quality/Depth) value > 2.5>nsSNVs – three Deleterious prediction among Polyphen2, SWIFT, LRT, FATHMM, MutationTaster, MetaSVM.

Once the variants were filtered, the knowledge based-gene model for eye diseases were applied to prioritize the known pathogenic variants. The model was developed using random forest (RF) method with the total of 221 eye disease genes, containing 23,438 nonpathogenic variants (dbSNP & 1000 Genome) and 14,762 pathogenic variants (HGMD) total number of variants. The RF method showed highest

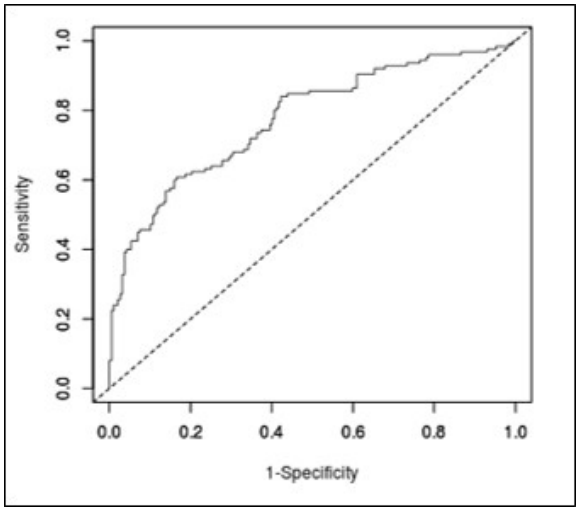

Figure 11. ROC curve for Random Forest model

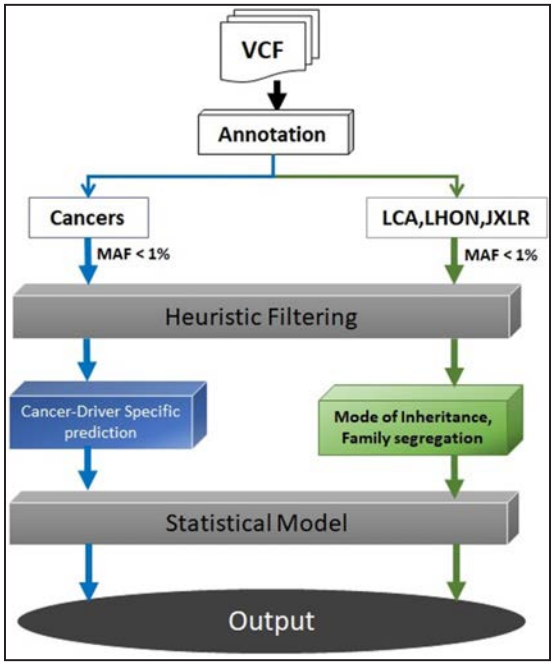

Figure 12. Variant filtering and prioritization for eye disease gene panel including retinoblastoma, LCA, LHON and JXLR

sensitivity and specificity compared to other machine learning model such as Support vector machine (SVM) as shown in Table 1.

Currently, the team following the variant filtering and prioritization for the exome data sets as shown in the Figure 12. Further improvement in the variant prioritization specific to eye disease for novel variants will be established using machine learning methods.

Automated pipeline for whole transcriptome data

The team developed 16 pipelines with combinations of aligners and quantifiers. We evaluated the performance of quantification in both gene and transcript level by comparing truth count from simulated reads using Spearman rank correlation. Also we used ocular cancer datasets for the benchmarking. Overall, STAR aligner performed well in reading and base level alignment whereas hisat2 performed well in aligning reads at the junction. Star might perform well in differential gene expression analysis and for alternative splicing, for structure variants analysis hisat2 might perform well.

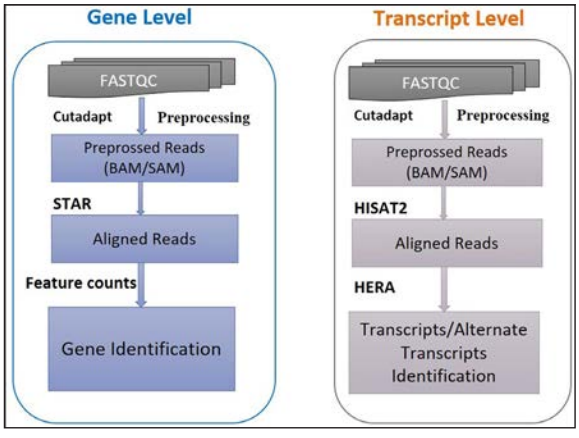

Figure 13. Best performing whole transcriptomic data analysis pipelines for gene and transcript level quantification.

Both Feature count and mmquant performed well in gene-level quantification, whereas Hera-EM outperformed RSEM in transcript-level quantification. Based on the evaluation of tools we developed a automated pipelines for gene level and transcript level analysis using RNA-Seq data (Figure 13).

STEM CELL BIOLOGY

The focus of research in this department is to understand the basic biology of adult tissue resident stem cells in the human eye – identification, role in the maintenance of tissue homeostasis, their status with ageing and in diseased condition. This basic research is significant for the development of better stem cell based therapies at an affordable cost. Studies on the human limbal epithelial stem cells are being carried out from early 2000. A combination of two parameters – high expression of p63/ABCG2 in cells with high nucleus to cytoplasmic ratio was established as a specific method for the identification and quantification of the limbal epithelial stem cells. In continuation, a two-step protocol was developed to enrich these stem cells from 3-5% to 80%. Using such an enriched population, the current focus of research is to understand the molecular regulation of these tissue resident stem cells, specifically the miRNAs. Recently, research on other stem cells of the human eye - trabecular meshwork, lens epithelium and retinal pigment epithelium has been initiated.

Limbal miRNAs and their potential targets associated with the maintenance of stemness

Investigators : Dr. Gowri Priya Chidambaranathan
Co-Investigators : Dr. Bharanidharan Devarajan
Prof. VR. Muthukkaruppan
Dr. N. Venkatesh Prajna
Collaborator : Prof. Julie T Daniels, University College London, UK
Research Scholar : Ms. Lavanya Kalaimani
Funding : Department of Biotechnology, New Delhi; Commonwealth Scholarship Commission, UK (INCN-2018-72)

Introduction

Human corneal epithelial stem cells (CESCs) reside in the basal layer of the limbal epithelium and they maintain the corneal epithelial homeostasis. The objective of the work is to understand the molecular regulation of these stem cells by microRNAs (miRNAs). Small RNA sequencing identified six miRNAs (hsa-miR-3168, hsa-miR-21-5p, hsa-miR-143-3p, hsa-miR-150-5p, hsa-miR-1910-5p and hsa-miR-10a-5p) to be highly expressed in enriched CESCs compared to central corneal epithelial cells (CCECs) which was validated by quantitative real time PCR (Q-PCR) and locked nucleic acid *in-situ* hybridization (LNA-ISH). The functional role of hsa-miR 143-3p and hsa-miR-150-5p on the maintenance of stemness were analysed by miRNA transfection studies. Transfection with the miRNA mimics independently increased colony forming potential and supported holoclone formation. In addition, higher expression of these miRNAs increased the expression of stem cell markers (ABCG2, ΔNP63, NANOG, OCT4 and KLF4) and reduced the expression of differentiation marker (CX-43) as well as the Wnt signaling regulators (β-catenin and AXIN2) at transcriptional level. Further studies were carried out using hsa-miR-150-5p to confirm this regulation at protein level.

Results

The functional role of hsa-miR-150-5p at translational level was evaluated in the primary limbal epithelial cells transfected with hsa-miR-150-5p mimics and inhibitors by Western blotting and immunostaining.

The hsa-miR-150-5p mimic transfected cells had reduced expression of Wnt regulators β-catenin (also a target of hsa-miRNA 150-5p), active β-catenin and AXIN2 compared to control cells.

In hsa-miR-150-5p inhibitor transfected group, 90% and 37% cells had nuclear positivity indicating the nuclear localization of active β-catenin and β-catenin respectively. Nuclear translocation of active β-catenin represents the activation of Wnt signaling in them. In hsa-miR-150-5p mimic transfected group the expression of AXIN2 was significantly reduced indicating the downregulation of the Wnt signaling in this group.

Western blot analysis of hsa-miR-150-5p mimic transfected cells further confirmed the reduced expression of Wnt signaling regulators (β-catenin, active β-catenin and Axin2), differentiation marker (Cx-43) and increased expression of stem cell markers (ABCG2 and p63α).

Thus, higher expression of hsa-miR-150-5p prevented the activation of Wnt signaling by reducing the expression of its targets (i) β-catenin – Wnt signaling activator, (ii) AKT3 – inhibitor of GSK3β and (iii) JARID2 – repressor of Wnt antagonist eg. secreted frizzled-related protein-1 (Sfrp1), thereby increased stemness and prevented differentiation.

Conclusion

A regulatory role for hsa-miR-150-5p in maintenance of stemness by inhibiting Wnt signaling pathway was thus indicated.

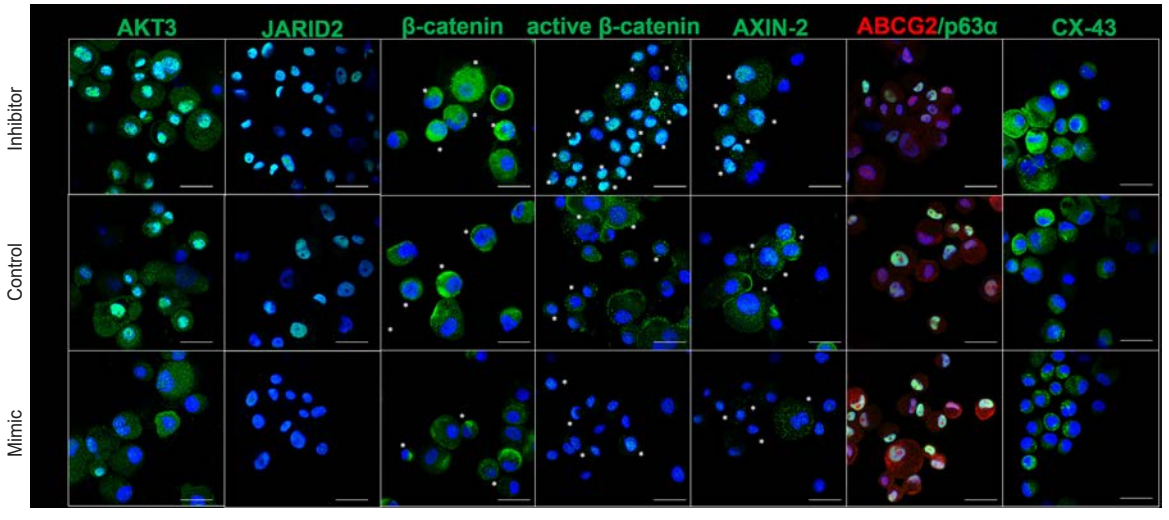

Representative confocal images of transfected limbal primary culture cells immunostained for AKT3, JARID2, β-catenin, active β-catenin, Axin2, ABCG2, p63α and Connexin-43 (CX-43). Nuclei were stained with DAPI (blue) and the protein expression with FITC (green except for ABCG2 in red). Scale bar 25 µm. The cells with nuclear positivity were marked with asterisks in Wnt signaling regulators (β-catenin, active β-catenin and Axin2). Nuclear localization of active β-catenin is the indication of active Wnt signaling.

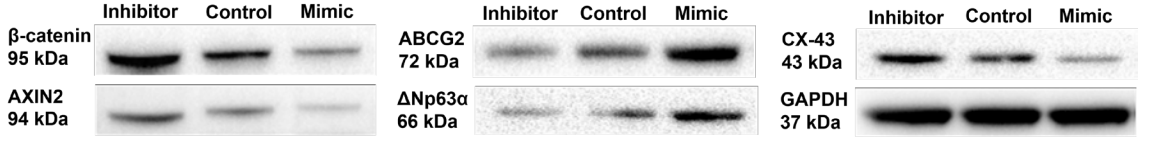

Representative Western blots of β-catenin, Axin2, ABCG2, ΔNp63α and Cx-43 in three groups miR-150-5p mimic, inhibitor and control. The experiment was carried out in triplicates and GAPDH was used as normalising reference and loading control.

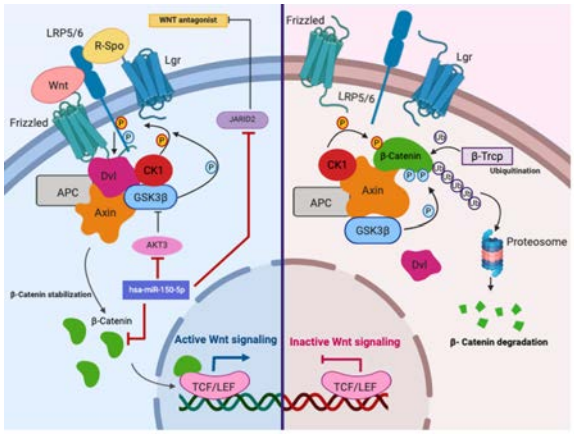

In the absence of Wnt signals, the β-catenin is degraded by destruction complex composed of Axin, glycogen synthase kinase 3 (GSK3β), adenomatosis polyposis coli (APC), casein kinase I (CK1) through phosphorylation of β-catenin followed by ubiquitination by β-TRCP E3 ubiquitin ligase and proteosomal degradation. However, in the presence of Wnt signals (binding of Wnt ligands and Wnt agonists like R-Spo), the active destruction complex is titrated thus leading to β-catenin stabilization and accumulation followed by activation of Wnt signaling through nuclear translocalization of β-catenin

Characterization and functional evaluation of trabecular meshwork stem cells in glaucoma pathogenesis

Investigator : Dr. Gowri Priya Chidambaranathan
Co-Investigators : Dr. VR. Muthukkaruppan
Dr. S. Senthilkumari
Dr. Neethu Mohan
Dr. SR. Krishnadas
Research Scholars: S. Yogapriya, R. Iswarya
Funding : Science and Engineering Research Board (SERB)

Introduction

Human Trabecular meshwork (TM) is the porous triangular tissue encircling the chamber angle of the eye. This sieve natured tissue maintains the intraocular pressure (IOP) of the eye by regulating the aqueous humor (AH) outflow. Blockage of the outflow pathway elevates the IOP which in turn leads to the development of primary open angle glaucoma (POAG). A significant reduction in the total TM cellularity was evident with ageing. This reduction was more prominent in donor eyes with POAG. The status of trabecular meshwork stem cells (TMSC) with ageing and in glaucoma pathogenesis remained explored. Hence, this study aimed at identifying, quantifying and characterizing the TMSCs with ageing, and in donor eyes with POAG.

The human TMSCs were identified based on two parameters: high expression of ABCG2 and high nucleus to cytoplasmic ratio. This method of identification was confirmed by the expression of neural crest derived stem cell marker p75 and transition zone maker AnkyrinG. The TMSCs expressing high ABCG2 and p75 were restricted to the Schwalbe's line region of human TM. Quantification of TMSCs revealed a significant reduction with ageing. This reduction correlated significantly with the age related total TM cell loss. A reduction in TMSC content was also identified in glaucomatous TM compared to age-matched controls, which might be associated with the drastic loss in TM cells and hence in disease pathogenesis. In continuation, TMSCs in cultured TM cells were functionally characterized to evaluate its role in TM regeneration.

Results

TMSCs establishes TM primary cell culture

The TM cells were isolated by collagenase A treatment from corneoscleral rims obtained from Rotary Aravind International Eye Bank, Madurai. The total TM cell count following isolation was 3.17 ±0.76 x 10^4 cells/ml in younger age group (<30 years), 2.00±0.87 x 10^4 cells/ml and 1.33±0.29 x 10^4 cells/ml in middle (30-60 years) and older age group (>60 years) respectively. Following 48 hours, the proportion of cells that adhered to the dish was calculated to be 0.96± 0.21% in younger age group which significantly reduced to 0.32±0.23% in middle age group and 0.35±0.04% in the older age group (p=0.03). In addition, all the cells (100%) attached to the dish expressed the stem cells markers ABCG2 and p75. Two-parameter analysis of cultured TM cells (after 7-days) revealed the TMSC content to be 6.5± 2.12%, indicating differentiation and proliferation

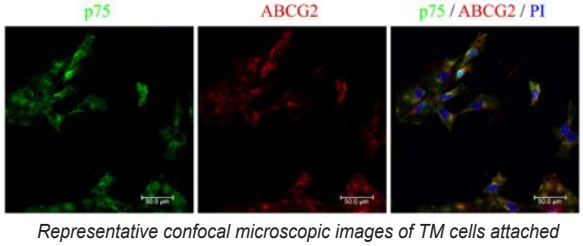

Representative confocal microscopic images of TM cells attached to the culture dish expressing the putative stem cell markers ABCG2 and p75.

Further, BrdU pulse labelling of the cultured cells revealed all cells to express BrdU indicating high proliferative potential.

Functional characterization of TMSCs in cultured cells

Slow cycling property

In order to determine the slow cycling/label retaining property of the TMSCs identified earlier by two-

parameter analysis, the TM cells were pulsed for five days and the BrdU label was chased for ten days. All the cells in the UR quadrant of the scatter plot (3.33 ±0.57%) expressing the marker p75 retained BrdU.

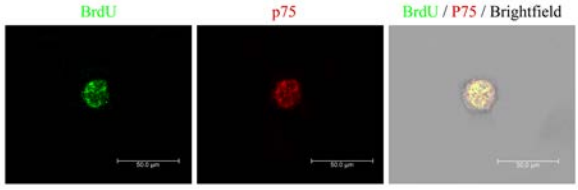

Representative confocal microscopic image of an UR cell (with high N/C ratio expressing p75), having label retaining cell property (BrdU positive).

Sphere formation

Additionally, the primary TM cells had the ability to generate neurospheres indicating the presence of adult stem cells. Immunostaining of the neurospheres for various putative stem cells such as ABCG2, p75, CD90 and CD105 indicated their higher expression in the centre of the sphere than the cells at the periphery.

Ability of the TMSCs to differentiate into TM cells

The TM spheres containing TMSCs were cultured in TM media containing serum. The sphere derived TM cells expressed increased myocilin when treated with dexamethasone, a characteristic feature of TM cell. Further, the sphere derived TM cells were also assessed for the phagocytic potential using FITC-zymosan particles. The phagocytic potential of the primary TM cells was calculated to be 16.33 ± 4.04% and the number of particles phagocytosed by these cells was 26.67±4.16. Confocal microscopic images revealed that 13.28±3.30% of sphere derived TM cells phagocytosed zymosan particles and 22.67±7.23 particles were internalized. These results indicate that the phagocytic property of sphere derived TM cells were equivalent to primary TM cells.

Conclusion

In vitro functional characterization revealed that

(i) the TM primary cultures were established by the TMSCs,

(ii) the cultured TMSCs identified by two-parameter analysis had the label retaining cell property of adult stem cells and

(iii) the spheres from cultured TM cells had the ability to differentiate into TM cells expressing myocilin upon dexamethasone induction and phagocytic potential, thus confirming the presence of adult stem cells in culture and their role in the maintenance of tissue homeostasis.

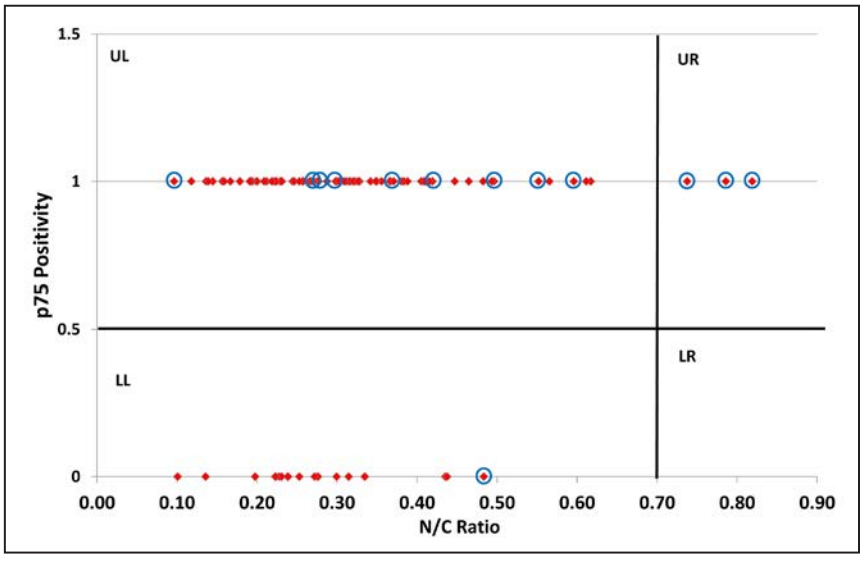

Representative scatter plot with two parameters (p75 positivity versus N/C ratio) of TM cytosmears from 10-day chase culture indicating that UR quadrant had the cells with label retention property. Each red diamond represents the p75 expression in a cell. Blue circle denotes that the cell was BrdU positive. Cells with no circle were negative for BrdU. UR: upper right UL: upper left, LL: lower left; LR: lower right

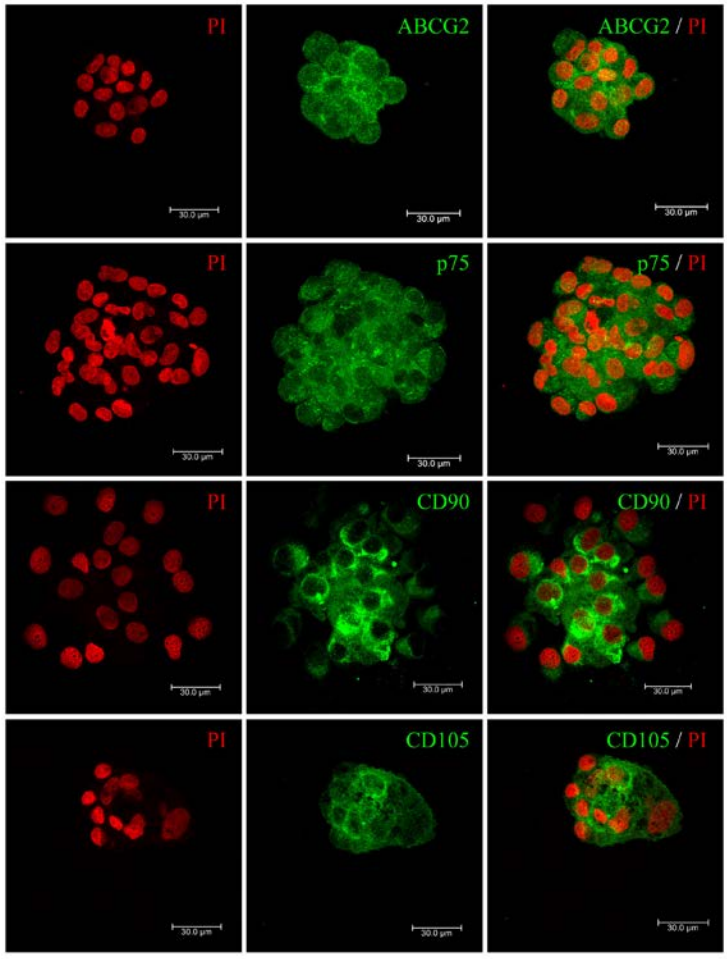

Representative confocal microscopic images of TM spheres immunostained for putative stem cell markers. Higher expression of the stem cell markers was observed at the centre of the sphere than at the periphery.

Characterization of adult human lens epithelial stem cells in the maintenance of tissue homeostasis throughout life and their functional status in cataractous lens

Investigators : Dr. Madhu Shekhar
Co-Investigators : Dr. Gowri Priya Chidambaranathan
Dr. Haripriya Aravind
Prof. VR. Muthukkaruppan
Research Scholar : P. Saranya
Funding : Science and Engineering Research Board (SERB)

Introduction

The crystalline lens is a transparent biconvex structure in the eye that is essential for focusing of light to the retina and for accommodation of vision. The lens is composed of capsule, anterior lens epithelium, cortex and nucleus. It consists of two main cell types- a monolayer of cuboidal epithelial cells and the inner material composed of elongated fibres. Based on the proliferation and differentiation, the epithelial cells can be divided into central, germinative, transition and equatorial zones. Earlier reports demonstrated the presence of stem cells in the central region of the lens epithelium in mice, on the basis of their slow cycling or label retaining property (LRC). However, in a recent review, equatorial zone in the human lens was described to contain lens epithelial stem cells. Hence this study aims to identify the location of adult lens epithelial stem cells and characterize the nature of cells in different zones of human anterior lens.

Results

Identification of adult tissue resident stem cells in human anterior lens epithelium

In order to identify the location of stem cells in human anterior lens epithelium, the lens epithelial whole mounts from donor tissues (received after removal of cornea for transplantation) were immunostained for

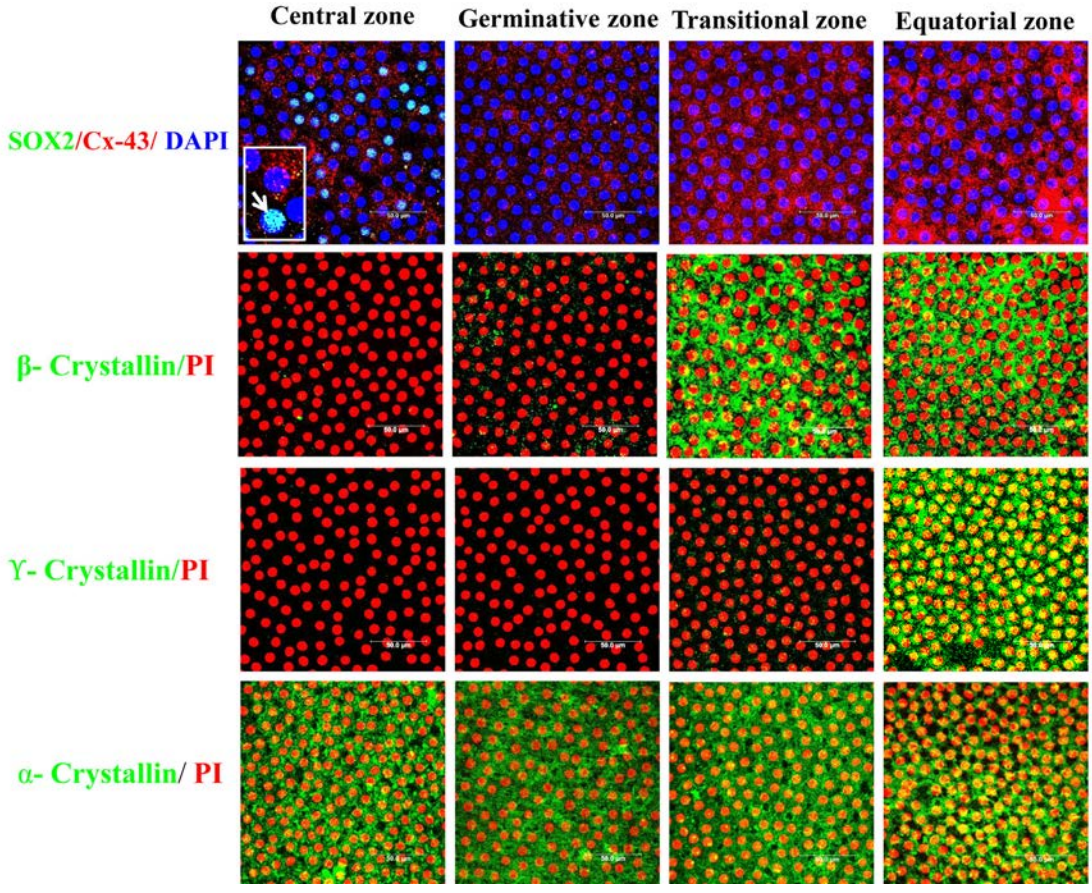

Representative confocal microscopic images of the whole mount of human lens capsule revealed the expression of zone specific markers: The central zone was defined based on the presence of SOX2 positive but Cx-43 negative stem cells.

SOX2, Connexin-43(Cx-43) and α, β, γ crystallins. Confocal analysis of the immunostained whole mount identified that the central zone measuring about 1.363mm in diameter consists of 15.8% of cells positive for stem cell marker SOX2, but negative for the differentiation marker connexin-43 (Cx-43). The epithelial cells in the germinative, transitional and equatorial zones were negative for SOX2 but positive for Cx-43.

A distinct pattern of expression of crystallin markers was observed: α-expressed throughout the anterior lens epithelium including stem cells while the transitional and equatorial zones were positive for β-crystallin. Equatorial zone was characterized by the presence of late elongation marker ϒ-crystallin.

Based on the expression of SOX2, Cx-43 and crystallins, the human anterior lens epithelium was demarcated into different zones using Leica software – LAS AF 3.3.0.10134.

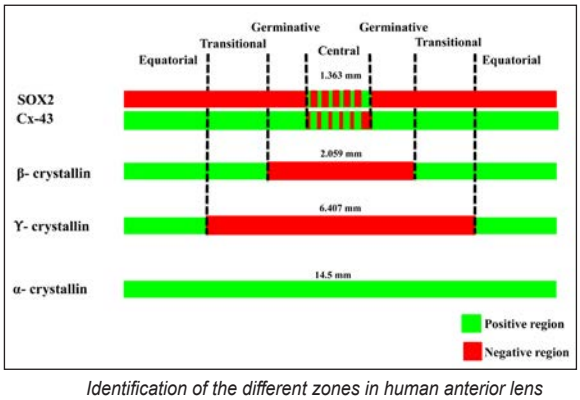

Identification of the different zones in human anterior lens epithelium: The central zone measuring about 1.363mm in diameter consists of 15.8% of stem cells that were positive for SOX2 a putative stem cell marker but negative for Cx-43 a differentiated cell marker.

Conclusion

The lens epithelial stem cells were defined as cells with SOX2+, Cx-43-, β-crystallin-, γ- crystallin- expression. The presence of adult tissue resident stem cells has been confirmed to be located in the

central zone of the human anterior lens epithelium. Further studies are essential to understand the functional role of these stem cells in maintaining tissue homeostasis throughout life.

Identification and characterization of adult human retinal pigment epithelial stem cells

Investigators : Dr. Gowri Priya Chidambaranathan
Co-Investigators : Prof. VR. Muthukkaruppan
Dr. K. Naresh Babu, Dr. R. Kim
Research Scholar : A. Waseema

Introduction

Retinal Pigment Epithelium (RPE) is a monolayer of pigmented polarized cells in human eye with a cobblestone configuration under the neural retina. Key functions of the RPE layer are to support overlying photoreceptor cells by phagocytosis of spent outer segments and transport of metabolites, nutrients and fluids to neural retina. Its degeneration is associated with diseases like age-related macular degeneration, retinitis pigmentosa and Stargart's disease. The number of individuals with such RPE-related blinding diseases is expected to be over 200 million worldwide by 2020. Clinical trials are being carried out using differentiated RPE cells derived from embryonic/ induced pluripotent stem cells (ESCs/iPSCs) for retinal regeneration. However the long term survival of such differentiated cells after transplantation and their role in regeneration is not known. Therefore, it is required to generate tissue specific adult stem cells with self-renewing capacity for long term survival and tissue homeostasis. Hence a basic understanding on the biology of human RPE stem cells (RPE-SCs) is essential in developing a method of generating such adult tissue specific stem cells from ESCs/iPSCs for transplantation.

Results

Cell size and density in the different regions of RPE

The three regions of RPE - peripheral, equatorial and central regions were demarcated as defined by Chen et al., (2016) in retina of eight donor eyes using the excised globes received after removal of cornea for transplantation from Rotary Aravind International Eye Bank, Madurai. Bright field images of RPE flat mounts (n=8) were taken and using ImageJ, the cell size and density were calculated (Table). As cited in the literature, there was a decreasing trend in the cell density from central region towards the peripheral RPE. The cell size showed an inverse correlation with cell density with peripheral RPE cells being larger than the other cells.

Expression of embryonic stem cell markers

Real time PCR analysis for embryonic stem cell markers was performed with cells isolated from different regions of RPE to identify the region encompassing the stem cells. RPE cells were isolated and subjected to RNA isolation by a two step protocol – (i) TRIzol method to isolate crude RNA with melanin pigments followed by (ii) a purification step using RNeasy mini kit to remove the pigments. Since RNA yield from the three regions of a single donor globe was not sufficient to perform Q-PCR analysis, cells from central and equatorial region were pooled together and compared with the peripheral cells obtained from four different donors.

The expression of embryonic stem cell marker Oct4 was 2.14 fold higher in peripheral RPE while the expression of other markers were similar compared to the central and equatorial RPE. Since adult tissue resident stem cells account to only 0.1 to 10%, further studies are being carried out to localize the RPE-SCs by immunostaining.

	Peripheral	Equatorial	Central
Cell Density (cells/mm^2; mean ± SD)	1700 ± 282	2815 ± 442	3597 ± 826
Cell Size (μm; mean ± SD)	23.6 ± 2.7	16.5 ± 0.9	13.9 ± 0.6

Cellular characterization of different regions of human RPE

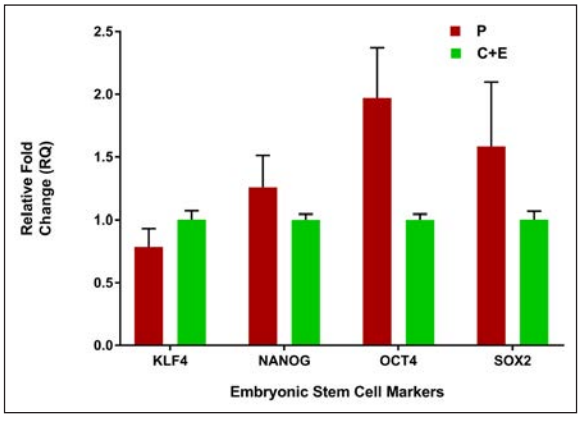

Expression of embryonic stem cell markers in the central and peripheral regions of human RPE

Conclusion

The stem cells for the human RPE might be located in the peripheral region which required further confirmation.

Proteome profiling of serum microparticles in diabetes and Diabetic Retinopathy patients: Towards identification and validation of predictive biomarkers

Investigators : Dr. J. Jeya Maheshwari
Prof. K. Dharmalingam
Clinician Scientist : Dr. R. Kim
Team Member : P. Vignesh
Funding : Department of Health Research Govt. of India

Introduction

Diabetic retinopathy (DR) is the most common and serious microvascular complication of diabetes mellitus. An early diagnosis of DR is important to prevent blindness among diabetes patients. Microparticles are known to be involved in the development of diabetic complications (Tsimerman *et al*., 2011; Zhang *et al*., 2018). An increase in microparticle release have been reported under different stimuli that can lead to diabetic complications (Ogata *et al*., 2005; Ogata *et al*., 2006; Chahed *et al*., 2010). Hence, analysis of the microparticle proteome is important to identify proteins that might be involved in development and progression of DR. And, these proteins have the potential to serve as diagnostic or predictive biomarkers.

Objectives

Profiling and comparative analysis of serum microparticle proteome from non-diabetic, type 2 diabetics (DM) and different stages of diabetic retinopathy (DR) to identify DM-specific and DR-specific protein changes

Results

Profiling of serum microparticle proteome

Circulating microparticles form a small fraction of the total serum. A high speed centrifugation method was used to enrich the microparticles in serum, followed

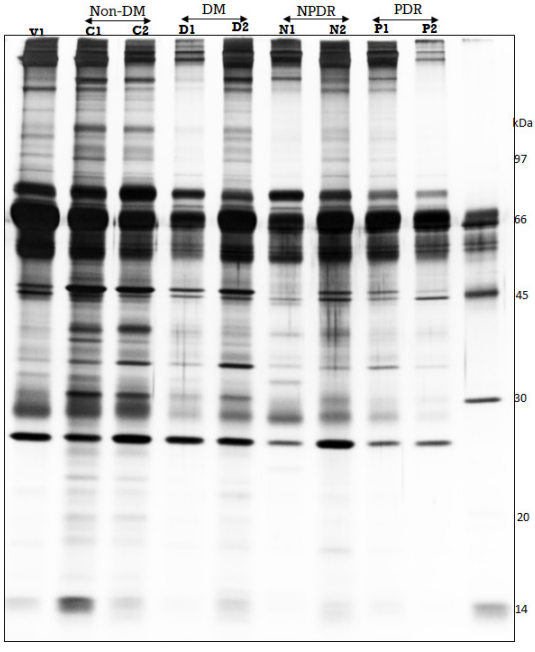

Figure 1.1. Comparison of the microparticle protein profile across different sample categories.

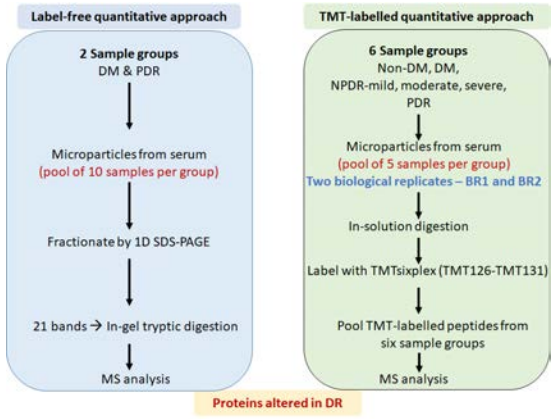

Figure 1.2. Quantitative MS-based approach to identify the microparticle proteins altered during DR

by repeated washes with PBS (3 washes) to minimize the carryover of serum proteins. The enrichment of microparticles by this method was confirmed by the mass-spectrometry based identification of microparticle-specific proteins as well as by western blot analysis using anti-integrin 6 antibody.

Microparticles were isolated from the serum of patients representing different stages of DR and the protein profile of the microparticles were compared (Figure 1.1). This comparison showed that although the major proteins were observed in all stages of DR, many proteins, particularly the less abundant ones were present at varying levels across the sample categories. A mass spectrometry approach was used to identify these difference in the microparticle proteome across the DM and DR groups.

Quantitative comparative analysis of the microparticle proteome

A comprehensive approach (Figure 1.2) using label-free quantitation and TMT-labelled quantitation methods were used to identify the microparticle proteins that were altered during DR.

The label-free quantitative method used to compare the serum microparticle proteome of DM and PDR patients identified 47 proteins that exhibited atleast two-fold change in abundance in PDR. Of these, 14 proteins were at lower abundance while 34

Table 1.1. Microparticle proteins that were significantly altered in DR using DM as the reference

Label-free quantitation Proteins altered in PDR	TMT6plex-BR1 Proteins altered in all four DR groups	TMT6plex-BR2 Proteins altered in all four DR groups
Actin, alpha cardiac muscle 1	Actin, cytoplasmic 1	Alpha-2-macroglobulin
Actin-related protein 2	Actin-related protein 3	Apolipoprotein C-I (Fragment)
Apolipoprotein A-V	APOC4-APOC2 readthrough (NMD candidate)	Band 3 anion transport protein
Apolipoprotein C-III	Apolipoprotein C-III variant 1	CD5 antigen-like
Apolipoprotein C-IV	Fermitin family homolog 3	Galectin-3-binding protein
Cofilin-1	Fibronectin	Hemoglobin subunit alpha
Complement C1r subcomponent	Ficolin-2	Hemoglobin subunit beta
Complement C3	Hemoglobin subunit beta	Immunoglobulin heavy constant mu
Desmoplakin	Histone H2A	Immunoglobulin heavy variable 3-7
Dihydropyrimidinase-related protein 2	Integrin alpha-IIb	Immunoglobulin kappa variable 4-1
Endoplasmic reticulum chaperone BiP	Integrin beta (Fragment)	Integrin alpha-6
FH1/FH2 domain-containing protein 1	Mannan-binding lectin serine protease 1	L-lactate dehydrogenase (Fragment)
Fibrinogen beta chain	Platelet glycoprotein 4 (Fragment)	Peroxiredoxin-2
Fibrinogen-like protein 1	Platelet glycoprotein Ib beta chain	Platelet factor 4
Glyceraldehyde-3-phosphate dehydrogenase	Ras-related protein Rap-1b	Vitronectin
Guanine nucleotide-binding protein G(i) subunit alpha-2	Tetraspanin	
Heat shock cognate 71 kDa protein	Tubulin beta chain	
Hemoglobin subunit alpha		

Hemoglobin subunit beta		
Isoform 2 of Fibrinogen alpha chain		
Isoform 2 of Filamin-A		
Isoform 2 of Mannan-binding lectin serine protease 1		
Isoform 2 of Proto-oncogene tyrosine-protein kinase Src		
Isoform H14 of Myeloperoxidase		
Isoform Long of Glucose-6-phosphate 1-dehydrogenase		
Junction plakoglobin		
Keratin, type I cytoskeletal 10		
Keratin, type I cytoskeletal 9		
Keratin, type II cytoskeletal 1		
Keratin, type II cytoskeletal 2 epidermal		
Lactadherin		
Plastin-2		
Profilin-1		
Pyruvate kinase PKM		
Ras-related protein Rap-1b		
Serine/threonine-protein kinase 24		
Serotransferrin		
Serum albumin		
Transthyretin		
Tubulin beta-1 chain		
von Willebrand factor		
WD repeat-containing protein 1		

proteins were identified at higher abundance in PDR microparticle proteome (Table 1.1).

As the above analysis was carried out by comparing the two end stages of DR, it was important to validate these findings as well as to identify the proteins that are altered during the course of DR. Towards this, a TMT-labelled quantitative method was used to compare the microparticle proteome across six different groups – Non-DM, DM, NPDR-mild, NPDR-moderate, NPDR-severe and PDR. The TMT-labelled analysis across these six groups was done for two independent biological replicates (BR1 and BR2). Table 1.1 lists the proteins that were altered significantly across all the four DR groups in BR1 and BR2.

Examining the functional relevance of the significantly altered proteins indicated that the proteins involved in the actin reorganization and integrin-related signalling were particularly altered and many of these proteins were also abundant platelet proteins. As more than 80% of the serum microparticles are from platelets, the changes observed might reflect the alterations in the platelet proteins and their physiology during DR. It is already established that type 2 diabetes is a pro-thrombotic disease. As platelets are involved in hemostasis with potential role in angiogenesis, the alterations observed in the platelet microparticle proteins might be relevant in explaining the changes in platelets in DM and DR. Further, acute phase proteins, proteins involved in the regulation of hemostasis and inflammation were also altered significantly.

Work in progress

Proteins that show significant variation in microparticles have been shortlisted and their alteration in microparticles across the different stages of DR will be validated using a larger sample cohort.

Functional analysis of circulating microRNAs and their regulatory role in Diabetic Retinopathy

Investigators : Dr. O.G. Ramprasad
Prof. K. Dharmalingam
Dr. D. Bharanidharan
Dr. Kim Ramasamy

Project fellows : R. Karthikeyan (July 2018 - April 2019) and T.M. Nasrin Banu (May 2019 - Dec 2019)

Funding : SERB-Early career research award.

Introduction including background

The role of serum microRNAs in the progression of Type II Diabetes mellitus (DM) to Non-proliferative diabetic retinopathy (NPDR) and NPDR to Proliferative DR (PDR) in Indian population is unexplored. The rationale of this study is to identify the microRNAs differentially expressed in the above disease conditions in our population and understand their regulatory role in the progression of microvascular complications among diabetic patients. We also aimed to validate the differentially expressed miRNAs as predictive biomarkers. Towards realising these objectives, we had previously reported the differential regulation of miRNAs 320a, 27b, 181a and 451a in the disease conditions through miRNA profiling using next generation sequencing. In this report, the results of validation of differential expression of miRNAs in a large cohort of serum samples and in primary retinal microvascular cells exposed to different levels of glucose are discussed.

Results and Conclusion

Earlier sequencing analysis with serum samples revealed miRNAs like miR-320a, miR-27b and miR-181a differentially expressed in DM, NPDR and PDR conditions. Apart from these differentially expressed miRNAs, miRNAs like miR 451a, hsa-let 7f-5p, miR 3656, miR 4497, mR 338, miR 7704, miR 4508 were differentially expressed. Among these the role of miR 451a is characterized as a regulator of ATF2 transcription factor during proliferative diabetic retinopathy. The functions of other miRNAs are not defined in literature and hence are uniquely expressed in our population with NPDR and PDR.

Name of miRNA	Gene targets	Function
miR181a	*ADCY1* (*adenylyl cyclase*), VEGF	Neoangiogenesis regulation
miR 320a	*TSP-*1(thrombospondin1)	Angiogenesis inhibitor
miR 27b	*TSP-1*	Angiogenesis inhibitor
miR451a	*ATF2*	Transcription

Table 1: Gene target prediction for the differentially expressed miRNAs

Validation of differentially expressed microRNAs through quantitative Real-time PCR

The differentially expressed miRNAs obtained through next generation sequencing in the serum samples were validated using Real-time PCR using 16-18 different sets of serum samples for each disease condition. The results are shown in Figs. 1 and 2.

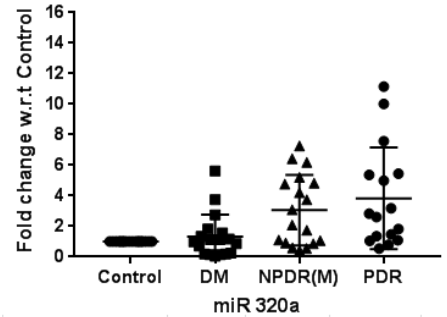

	Control	DM	NPDR(M)	PDR
Mean	1	1.32	3.06	4.83
Std. Deviation	0	1.448	2.308	3.329
Std. Error of Mean	0	0.34	0.52	0.83

p< 0.05
Control Vs PDR
DM Vs NPDR
DM Vs PDR

Figure 1a: Fold change in expression of miR320a with respect to control as validated by qPCR

In both NGS and validation experiments, the relative expression of miR 320a increased to a great extent in PDR (Fig 1A). Q-PCR validation of miR-320a has shown that its expression in PDR condition is more than 5 folds compared to control ($p<0.05$). Its expression increases to more than 2-folds in NPDR condition also suggesting that the patient with a non-proliferative diabetic retinopathy might progress to PDR depending on the miR320a expression levels in serum in these stages.

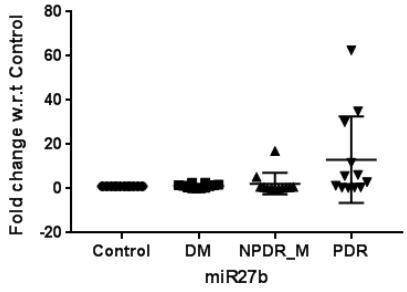

	Control	DM	NPDR_M	PDR
Mean	1	1.168	2.23	13.08
Std. Deviation	0	0.9088	4.876	19.53
Std. Error of Mean	0	0.2623	1.408	5.638

p>0.05 in DM Vs NPDR
p>0.05 in DM Vs PDR

Figure 1b: Fold change in expression of miR27b with respect to control as validated by qPCR

miR-27b expression increases to around 13 folds in PDR condition (Fig. 1b) in comparison to control with basal level expression in DM and NPDR condition.

miR320a and miR27b target thrombospondin-1 (TSP-1) which is a well-known inhibitor of angiogenesis. Higher expression of these two miRNAs means they downregulate TSP-1 protein which leads to the progression of angiogenesis conditions in PDR.

miR181a targets ADCY1 mRNA that is known to regulate neoangiogenesis process. Specifically miR181a represses VEGF pathway in retinal endothelial cells. The validation of miR181a in serum samples through q-PCR has shown that miR181a is highly expressed in DM with very less expression in PDR serum (Figure 2). Since miR181a negatively regulates VEGF, less of miR181a in PDR correlates with more of VEGF in PDR leading to angiogenesis.

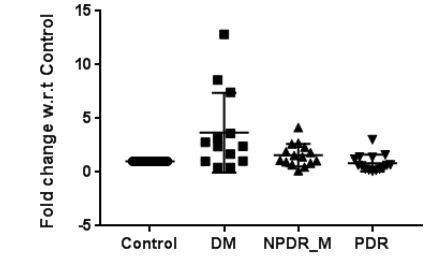

	Control	DM	NPDR_M	PDR
Mean	1	3.676	1.588	0.8344
Std. Deviation	0	3.713	1.045	0.7825
Std. Error of Mean	0	1.03	0.2698	0.202

p<0.05 in DM Vs PDR

Figure 2: Fold change in expression of miR181a with respect to control as validated by qPCR

Analysis of VEGF and TSP-1 protein levels in serum

To decipher the functional role of differentially regulated miRNAs in serum, we analyzed the serum protein levels of VEGF and TSP-1 in control, DM, NPDR and PDR conditions. The microRNAs mentioned above are differentially regulated in the study and the hypothesis is that they affect the secreted VEGF and TSP-1 levels in serum.

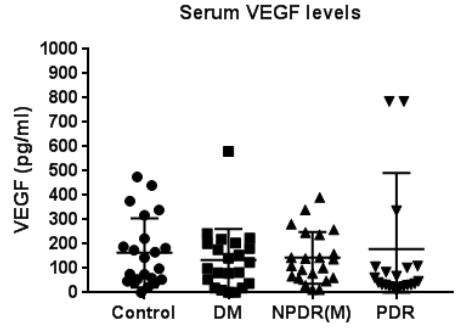

Fig. 3: Levels of secreted VEGF in serum samples of different conditions of DR, DM and control subjects

VEGF levels were measured in serum using a specific sandwich ELISA kit which recognizes hVEGF165, hVEGF121, and hVEGF165b . Accordingly, in a set of around 20 samples, the mean levels of VEGF in control was 163.4 ± 30.7 pg/ml, in DM was 133.6 ± 27.2 pg/ml, in NPDR was 143.6 ± 15.6 pg/ml and in PDR was 179.5 ± 41.24 pg/ml (Fig.:3). The above results were not significantly different between different conditions. This might be due to the fact that the ELISA measured only particular isoforms mentioned above and that these isoforms in serum samples might become equalized by the secretions from the other tissues. Only 3 samples revealed a clear trend of increased VEGF levels in PDR serum in the analysed samples.

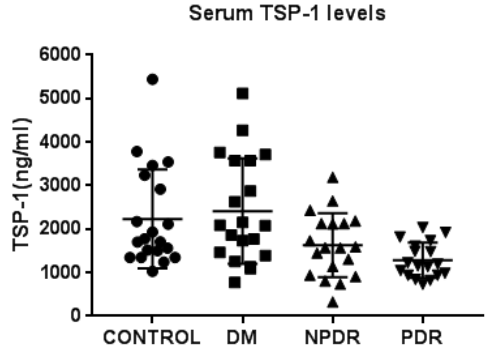

Fig. 4: Levels of secreted TSP-1 in serum samples of different conditions of DR, DM and control subjects

Thrombospondin-1 is a well-known inhibitor of angiogenesis. TSP-1 level in serum was measured by an ELISA kit. Serum TSP-1 levels progressively decreased from Control to PDR conditions (Fig. 4). In control and DM conditions mean TSP-1 levels were 2.23 μg/ml and 2.3 μg/ml respectively. In NPDR and PDR conditions mean TSP-1 levels were 1.6 μg/ml and 1.2 μg/ml respectively. ($p<0.05$ by Wilcoxon test in Con Vs. NPDR, Con Vs. PDR, DM Vs. NPDR and DM Vs PDR). The lower levels of serum TSP-1 in PDR conditions correspond to higher levels of miRNAs 27b and 320a, since miRNAs are negative regulators of their target proteins. Low levels of anti-angiogenic TSP-1 in PDR might promote angiogenesis in those conditions.

Functional analysis of differentially expressed miRNAs in human retinal microvascular endothelial cells exposed to different levels of glucose

Primary human retinal microvascular endothelial cells were isolated from cadaver retina following established procedures. They were grown either in normal endothelial cell growth medium (containing 5.5 mM Glucose) or high glucose containing medium (25 mM Glucose) or Mannitol containing medium (25 mM mannitol; osmotic control). The isolated retinal microvascular endothelial cells were checked for their specific endothelial phenotype by immunostaining using Von-willebrand factor (vWF) antibody (Fig. 5). The cells were grown in different glucose containing medium till 5 days and were passaged for a maximum of 5 times.

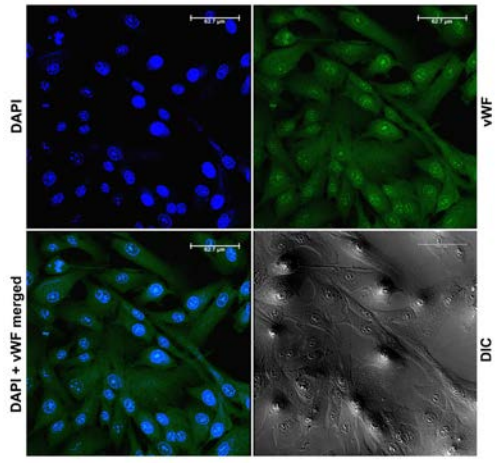

Fig.5: Isolated primary retinal microvascular endothelial cells expressing the specific endothelial marker vWF (green).

We extracted microRNAs from the primary retinal microvascular endothelial cells grown under normal conditions and in high glucose conditions. There was a > 2-fold upregulation of miR-320a in endothelial cells after treatment with high concentration of glucose after 24 hrs. In contrast, there was no significant change in the secreted TSP-1 in the cell culture medium of glucose treated cells.

Conclusions

Next generation sequencing analysis identified a set of microRNAs miR181a-5p, miR 27b and miR320a differentially regulated in the serum of DM, NPDR and PDR patients arising from Type 2 diabetes conditions. The sequencing results have been validated by q-PCR with similar levels of fold changes. The target of miRNAs 320a and 27b, TSP-1 protien, was expressed at lower levels in DR conditions which directly correlated with the higher expression of miR320a in serum in DR. The differentially regulated miRNAs in DR conditions are unique to our population with Type2 DM background. A direct validation of findings from serum was done in microvascular retinal endothelial cells which are the most proximal cells getting affected in the eye in Diabetic retinopathy.

1.3. Human corneal epithelium and immune response against ocular fungal pathogens

Investigators : Prof. K. Dharmalingam, Dr. J. Jeya Maheshwari
Clinician Scientists: Dr. N. Venkatesh Prajna, Dr. Lalitha Prajna
Team Member : A. Divya

1.3.1 Background

Aspergillus flavus, a saprophytic fungus is an opportunistic pathogen with broad host range which includes humans, animals and plants. Corneal ulcer due to fungi leading to fungal keratitis, is one of the primary causes of vision impairment and blindness worldwide. *Fusarium* and *Aspergillus* are the predominant causative agents in South India. It has been shown previously that Human Corneal Epithelial Cells has innate immune function towards bacterial and fungal infection through expression and secretion of cytokines, chemokines, antimicrobial peptides and modulation of other immune cells. We have demonstrated earlier that HCE cells engulf *A.flavus* spores by formation of actin ring surrounding the spores and subsequent trafficking of the conidia from early endosomes to late endosomes. We also confirmed the recruitment of endosomal proteins by enriching the phagosomes containing conidia and identification of phagosome specific proteins from the same using mass spectrometry.

Gene expression analysis of immunology panel using NanoString

In order to confirm and extend the previous observation we have initiated transcriptome profiling of the corneal epithelial cells after fungal infection using NanoString anlaysis. The immunology panel consisting of 589 genes (Immune response genes-574; Housekeeping genes-15) was selected for analyzing gene expression using nCounter analysis. HCE cell line and primary HCE cells were used for expression profiling. We used two clinical isolates of *A.flavus* : CI1698, an isolate from a fungal keratitis patient who responded to antifungal therapy and CI1123, an isolate from a patient who failed to respond to antifungal therapy and hence underwent surgery. We infected HCE cells with 10^7 spores and total RNA was isolated from infected cells using Qiagen RNeasy mini kit. 100ng of total RNA was further taken for nCounter analysis after quality checking. The RAW data were normalized with the housekeeping genes using GeNorm software and the resulting data were analyzed using R package and KEGG software.

Infection of HCE cells with *A.flavus* CI1698

Twenty five mRNA transcripts were found to be differentially expressed after six hrs of exposure to *A.flavus* CI1698 of which 16 mRNA were found to be up regulated and nine mRNA were down regulated compared to control ($p<0.05$) (Table 1) and the gene expression pattern was represented as MA plot (Figure 1).

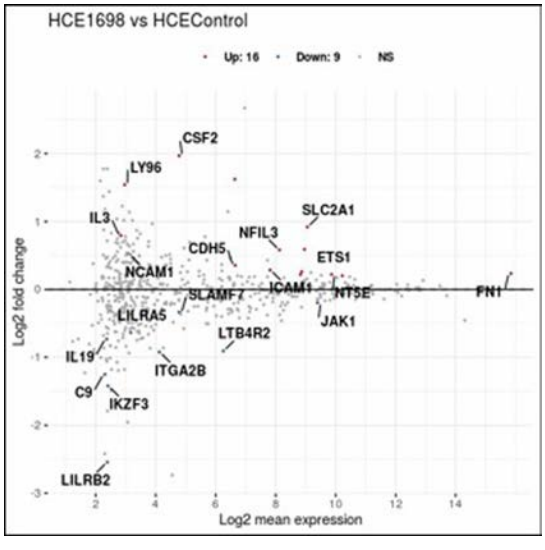

Figure 1: MA plot of mRNA transcripts from HCE cell line infected with A. flavus CI1698. Red dots-Up regulation; blue dots-down regulation; grey dots-no change.

To determine the major biological pathways associated with the differentially expressed genes, KEGG pathway analysis was done. The upregulated genes were involved in Th17 cell differentiation, NF-kB signaling and TNF signaling while the downregulated genes were related to B cell receptor signaling and JAK-STAT signaling (Figure 2).

S.No	HCE-CI1698		Primary HCE-CI1698	
	Gene	Log2 ratio	Gene	Log2 ratio
1	CSF2	1.9681	CD6	3.1751
2	TNFAIP3	1.6228	CD5	2.1740
3	LY96	1.5414	IL23R	0.7777
4	SLC2A1	0.9197	PLAUR	0.5552
5	IL3	0.7921	ETS1	0.4657
6	ETS1	0.5896	HLA-DMA	0.3909
7	NFIL3	0.5810	TICAM1	0.3236
8	NCAM1	0.5205	LGALS3	0.0466
9	CDH5	0.3546	XCR1	-0.5621
10	ICAM1	0.2850	LILRA4	-0.7656
11	RUNX1	0.2612	KLRC3	-0.9674
12	FN1	0.2360	JAK3	-1.0351
13	NT5E	0.2210		
14	PLAUR	0.2182		
15	NOTCH2	0.2014		
16	CD3EAP	0.1774		
17	JAK1	-0.1967		
18	SLAMF7	-0.3343		
19	LILRA5	-0.6356		
20	IL19	-0.7323		
21	LTB4R2	-0.9056		
22	ITGA2B	-0.9215		
23	C9	-1.2485		
24	IKZF3	-1.4196		
25	LILRB2	-2.5436		

αTable 1: Differentially expressed genes of HCE cell line and primary HCE cells infected with CI1698

Further the gene expression profile was checked in primary HCE cells in response to CI1698 in order to compare with the data generated using the cell line. 12 mRNA were found to be altered in which eight genes were upregulated and four genes were downregulated (Table 1).Upregulated genes are involved in Th17 differentiation, cell adhesion and NF-

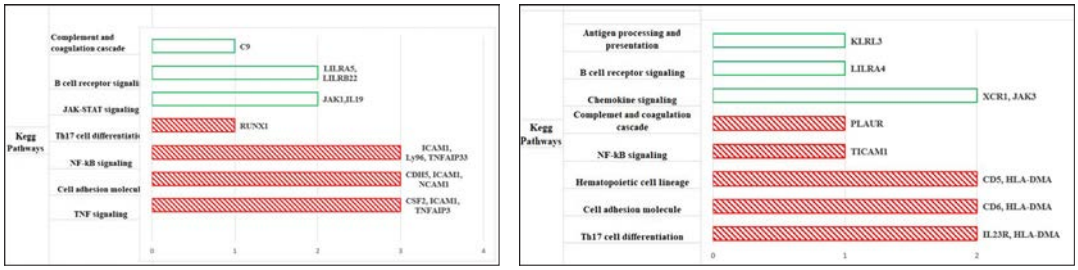

Figure 2: Kegg pathway analysis of differentially expressed genes of HCE cells infected with A. flavus CI1698. A) HCE cell line b) Primary HCE cells. Red bar-Up regulation; green bar-down regulation. Th17 cell differentiation, cell adhesion, NF-kB signaling were found to be associated with upregulation and B cell receptor signaling was downregulated.

kB signaling whereas the down regulated genes were in chemokine signaling and B cell receptor signaling, based on KEGG pathway analysis (Figure 2).

The number of genes differentially expressed were found to be two-fold more in cell line compared to primary HCE cells. The comparison between cell line and primary cells infected with CI1698 showed that only two genes (PLAUR and ETS1) were common.

Infection of HCE cells with *A.flavus* CI1123

The gene expression in response to CI1123 was checked in HCE cells and found 22 genes are differentially expressed after six hrs of exposure. Among 22 genes, mRNA of fourteen genes were found to be up regulated and mRNA of eight genes were down regulated compared to control ($p<0.05$) (table 2). KEGG pathway analysis showed that genes involved in Th17 signaling and TNF signaling were found to be up regulated while the downregulated genes were related NF-kB signaling (Figure 3).

The analysis was carried out in primary HCE cells infected with *A.flavus* CI1123 and found 11 differentially expressed mRNA transcripts (Table 2). More than half of them were downregulated and the remaining were upregulated in contrast to the rest of the data where more than half of differentially expressed genes were upregulated. Kegg pathway reveals that the genes involved in cytokine-cytokine receptor interaction and Fox o signaling were upregulated and genes in chemokine signaling and B cell receptor signaling were down regulated (figure 3).

The comparison between cell line and primary data revealed that no single gene was common. The genes involved in Th 17 signaling were not increased in primary HCE cells infected with CI1123 in contrast to the previous results.

S.No	HCE- CI1123		Primary HCE-CI1123	
	Gene	Log2 ratio	Gene	Log2 ratio
1	IL8	1.9350	CLEC4A	14.97
2	TNFAIP3	1.4408	IL1RL1	128.83
3	IL23A	0.5600	BCL6	259.40
4	IL6	0.5166	LGALS3	8278.9
5	ETS1	0.4533	MAPK1	1840.72
6	NFKBIA	0.4479	LTB4R	136.83
7	DUSP4	0.3525	CCL19	15.84
8	SLC2A1	0.3489	IRGM	9.11
9	RUNX1	0.3372	KIR_ Activating _Sub group_1	
	39.43			
10	CD14	0.3226	IL20	55.37
11	ICAM1	0.2960	LILRB2	10.49
12	IL4R	0.2852		
13	CTSS	0.1204		
14	PSMD7	0.1012		
15	MALT1	-0.129		
16	KIR_ Activating _Sub group_1	-0.267		
17	HAVCR2	-0.346		
18	TIRAP	-0.628		
19	IL1RN	-0.691		
20	AIRE	-0.715		
21	IKZF3	-0.723		
22	CD45R0	-0.760		

Table 2: Differentially expressed genes of HCE cell line and primary HCE cells infected with CI1698

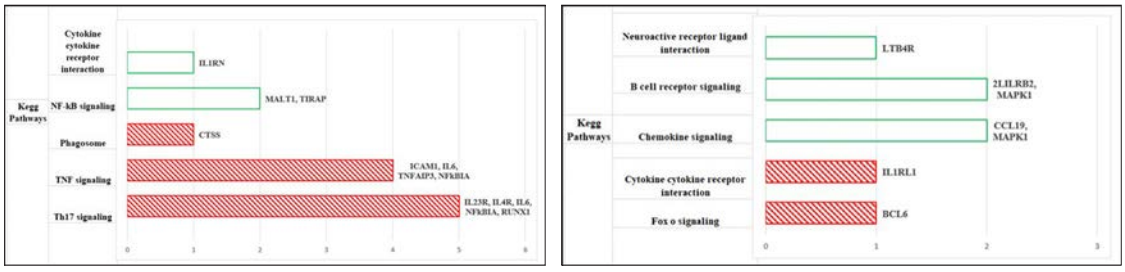

Figure 3: Kegg pathway analysis of differentially expressed genes of HCE cells infected A. flavus CI1123. A) HCE cell line b) Primary HCE cells. Red bar-Up regulation; green bar-down regulation.

Conclusion

NanoString analysis in HCE cells showed that the response against fungus between cell line and primary cells differ. The analysis revealed the activation of TH17 signaling and TNF signaling and inhibition of B cell receptor signaling during fungal infection.

2. Interaction of the *Aspergillus* spores with tear proteins

Investigators : Dr. J. Jeya Maheshwari
Prof. K. Dharmalingam
Clinician Scientist : Dr. Lalitha Prajna
Team Member : Irene Daniel
Funding : Centre for the Promotion of Advanced Research

Introduction

In fungal keratitis, neutrophils are the predominant innate immune cells that infiltrate the cornea to contain the fungus. However, in the initial stages of establishment of infection, both the corneal epithelial cells as well as the tear fluid bathing the cornea might have important roles to play even before the neutrophils reach the cornea.

Objectives

Tear has numerous proteins that are known to confer protection against bacterial and fungal infections. Further, fungal pathogens are known to exploit the host system to protect themselves from recognition and/or clearance by the host immune response. The objectives of this study was to identify the tear proteins that interact with the surface of the pathogenic Aspergilli that might aid in the host defense against fungal pathogens and/or those that might offer survival advantage to the fungal pathogens.

Results

A.flavus or *A.fumigatus* dormant spores (10^9 spores) were incubated with 100 µg of tear proteins, tear from normal individual or tear from keratitis patients (*A.flavus* or *A.fumigatus* infection). After removing the unbound tear proteins by multiple PBS washes, proteins bound non-covalently were extracted using 3M sodium thiocyanate followed by a sequential extraction with 1M hydroxylamine to recover the covalently-bound proteins. The details of the MS identification of the spore surface bound proteins are given in Table 2.1.

Spores	Tear sample details	Number of proteins identified	
		Non-covalently bound protein fraction	Covalently bound protein fraction
A.flavus	Control tear	69	53
	A.flavus keratitis tear	86	53
A.fumigatus	Control tear	60	48
	A.fumigatus keratitis tear	79	46

Table 2.1: Summary of the identification of tear proteins bound to Aspergillus spore surface

Table 2.2 A and B lists the proteins bound non-covalently and covalently to the *Aspergillus* spore surface, respectively. The abundance of these proteins in the tear samples - control, *A.flavus* keratitis and *A.fumigatus* keratitis tear is also given for comparison.

Table 2.2 A: Tear proteins non-covalently bound to Aspergillus spore surface.
Numbers represent the peptide spectral matches for the identification of the particular protein.

		A.flavus spores-tear interaction		*A.fumigatus* spores-tear interaction		Tear proteome		
Protein Description	Acc. No	CT	AFL KT	CT	AFUMI KT	CT	AFL KT	AFUMI KT
Predominant non-covalently bound proteins								
Lactotransferrin	P02788	1188	863	521	814	3915	2258	2202
Lysozyme C	P61626	693	615	727	681	1579	1431	1496
Keratin, type II cytoskeletal 1	P04264	326	484	561	420	795	557	314
Keratin, type I cytoskeletal 10	P13645	158	183	352	226	531	382	174
Keratin, type I cytoskeletal 9	P35527	145	149	323	208	328	233	137
Serum albumin	P02768	14	69	18	41	143	1209	1604
Immunoglobulin heavy constant alpha 1 (Fragment)	A0A286YEY1	58	51	37	36	255	162	192
Lipocalin-1	P31025	46	38	21	31	2488	1663	1836
Prolactin-inducible protein	P12273	40	121	14	23	1614	2072	2358
Exclusively found in the non-covalently bound protein fraction								
Antileukoproteinase	P03973	34	24	34	26	21	6	13
Pyruvate kinase PKM	P14618	8	33	5	20	16	24	10
Immunoglobulin heavy constant mu	P01871	17	29	9	19	65	86	58
Phospholipase A2, membrane associated	P14555	25	12	12	15	92	26	85
Complement C3	P01024	0	24	0	14	151	301	292
Ceruloplasmin	P00450	45	24	8	11	163	156	180
Secreted frizzled-related protein 1	Q8N474	42	15	37	11	27	2	4
Azurocidin	P20160	0	12	2	11	1	11	8
Polymeric immunoglobulin receptor	P01833	23	20	15	11	175	227	139
Mammaglobin-B	O75556	22	23	21	9	106	84	74

CT, control tear; AFL KT, A. flavus keratitis tear; AFUMI KT, A. fumigatus keratitis tear;

Table 2.2 B: Tear proteins covalently bound to Aspergillus spore surface.
Numbers represent the peptide spectral matches for the identification of the particular protein.

		A.flavus spores-tear interaction		*A.fumigatus* spores-tear interaction		Tear proteome		
Protein Description	Acc. No	CT	AFL KT	CT	AFUMI KT	CT	AFL KT	AFUMI KT
Predominant covalently bound proteins								
Keratin, type II cytoskeletal 1	P04264	1033	1014	907	709	795	557	314
Keratin, type I cytoskeletal 9	P35527	558	682	773	250	328	233	137
Keratin, type I cytoskeletal 10	P13645	536	548	414	265	531	382	174
Lactotransferrin	P02788	212	295	128	211	3915	2258	2202
Lysozyme C	P61626	225	73	53	135	1579	1431	1496
Lipocalin-1	P31025	51	66	40	71	2488	1663	1836
Alpha-1-antitrypsin	P01009	5	62	5	27	7	97	126
Desmoplakin	P15924	39	58	47	13	4	5	2
Desmoglein-1	Q02413	41	39	37	61	1	1	8
Serum albumin	P02768	159	37	173	250	143	1209	1604
Junction plakoglobin	P14923	27	24	21	16			
Prolactin-inducible protein	P12273	16	20	10	45	1614	2072	2358
Arginase-1	P05089	9	10	11	21			
Dermcidin	P81605	18	9	12	45	21	18	11
Peroxiredoxin-2	P32119	9	9	6	5	5	7	2
Exclusively found in the covalently bound protein fraction								
Fibronectin	P02751	100	3	195	491	1	72	45
Desmoglein-1	Q02413	41	39	37	61	1	1	8
Dermcidin	P81605	18	9	12	45	21	18	11
Alpha-1-antitrypsin	P01009	5	62	5	27	7	97	126
Cystatin-A	P01040	10	5	5	24	7	1	12
Arginase-1	P05089	9	10	11	21			
Keratin, type II cytoskeletal 80	Q6KB66	3	2	4	20			
Immunoglobulin heavy constant gamma 1 (Fragment)	A0A0A0 MS08	28	5	10	19	13	196	223
Junction plakoglobin	P14923	27	24	21	16			
CDSN	G8JLG2	12	8	8	13			
Serpin B3	P29508	5	11	9	13	7	2	1
Catalase	P04040	5	3	5	11	1	4	2
Fatty acid-binding protein 5	Q01469	6	2	2	11	7	11	25

CT, control tear; AFL KT, A. flavus keratitis tear; AFUMI KT, A. fumigatus keratitis tear

An enrichment analysis of the non-covalently and covalently bound proteins (Figure 2.1) showed that many of the proteins that bind to the spore surface were enzyme modulators and hydrolases. Further, some of them were also involved in cell adhesion, cell junction etc.

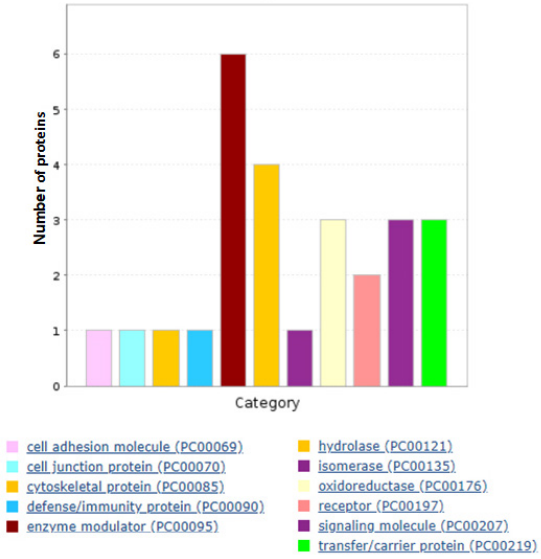

Figure 2.1. Enrichment analysis using Panther to examine the distribution of the spore surface bound proteins across different protein classes

Eight tear proteins were identified in both the non-covalently bound and covalently bound protein fractions and are

1. Lactotransferrin
2. Lysozyme C
3. Keratin, type II cytoskeletal 1
4. Keratin, type I cytoskeletal 10
5. Keratin, type I cytoskeletal 9
6. Lipocalin-1
7. Serum albumin
8. Prolactin inducible protein

Lactotransferin, lysozyme C, lipocalin-1, prolactin-inducible protein are the most abundant tear proteins in tear. Although all these four proteins were present in tear in more or less similar abundance, lactotransferrin appeared to bind the spore surface preferentially. Lactotransferrin is a multifunctional protein that is known to have immunomodulatory properties. Lactoferrin and its major naturally cleaved peptide lactoferricin have proven anti-fungal activity. The binding of lactotransferrin might provide a protective effect against the fungal infection and act as the first line of defense.

Proteins such as complement C3 and azurocidin were identified as surface bound protein primarily when incubated with tear from keratitis patients. These proteins that play important role in host immune defense were upregulated in tear during fungal infection and found at higher levels in keratitis tear when compared to the control tear. Proteins involved in cytoskeletal functions such as desmoglein-1 and junction plakoglobin were identified with good confidence in the covalently bound protein fraction even though these proteins were not identified in control or keratitis tear.

Work in progress

The functional relevance of these tear proteins binding to the spore surface will be examined by challenging the neutrophils with the tear protein coated spores and examining the cytokine response.

3. Role of iris in the pathogenesis of pseudoexfoliation syndrome

Investigators : Dr. J. Jeya Maheshwari
Prof. K. Dharmalingam
Dr. Shanthi
Clinician Scientists: Dr. R. Krishnadas
Dr. Vijaylakshmi Senthil
Dr. Shalini
Team Member : Irene Daniel

Introduction

Pseudoexfoliation syndrome (PEXS) is an age-related systemic microfibrillopathy, caused by progressive accumulation and gradual deposition of extracellular grey and white material over various tissues. In the eye, pseudoexfoliation material (PEXM) is observed throughout the anterior segment of the eye as white, fluffy deposits on the zonules, anterior lens capsule, pupillary margin of the iris, corneal endothelium and the irido-corneal angle (Nazarali *et al*., 2018). The obstruction of the aqueous humor outflow pathways due to the deposition of PEX material is considered to increase the intraocular pressure and subsequent glaucomatous optic nerve damage. Currently, there is no treatment for PEXS and the patients are treated only after the onset of glaucoma. However, as PEXG has a severe clinical course with poor prognosis, it is important to develop a method to determine the prognosis of PEXS. Therefore, understanding the source of PEX material and the pathogenesis of the tissues involved is essential. Among other structures, iris undergoes profound degenerative changes in PEXS as confirmed through histopathological analysis. However, the role of iris tissue in the PEXS pathogenesis has not been examined so far.

Objectives

To understand the proteome-wide changes in the iris during PEXS progression and identify factors that could serve as markers for PEXS diagnosis and/or progression.

Results

A gel based proteomics approach (both 1D and 2D) was used to address the objectives of this project.

Reference map of iris proteome

Two groups have reported the mass spectrometry based iris proteome (Zhang *et al*., 2016; Murthy *et al*., 2016) and a total of 4232 proteins were identified in iris. To complement this information, a 2D reference map for iris proteome was genereated. One hundred and four individual protein spots were taken for MS analysis and the proteins identified were subjected to filtering based on stringent criteria to include only confident identifications. As many as 13-80 proteins were identified per spot that resulted in the identification of 1297 proteins across 104 protein spots. Figure 3.1 shows the iris proteome reference map and the protein identified with the highest PSM is indicated for each spot.

Iris proteins (300 µg) were separated using a 18 cm IEF strip (non-linear, 3-10 pH) followed by a 12.5% SDS-PAGE. The proteins were visualized after staining with colloidal coomassie stain. The spots were excised and processed for identification by mass spectrometry.

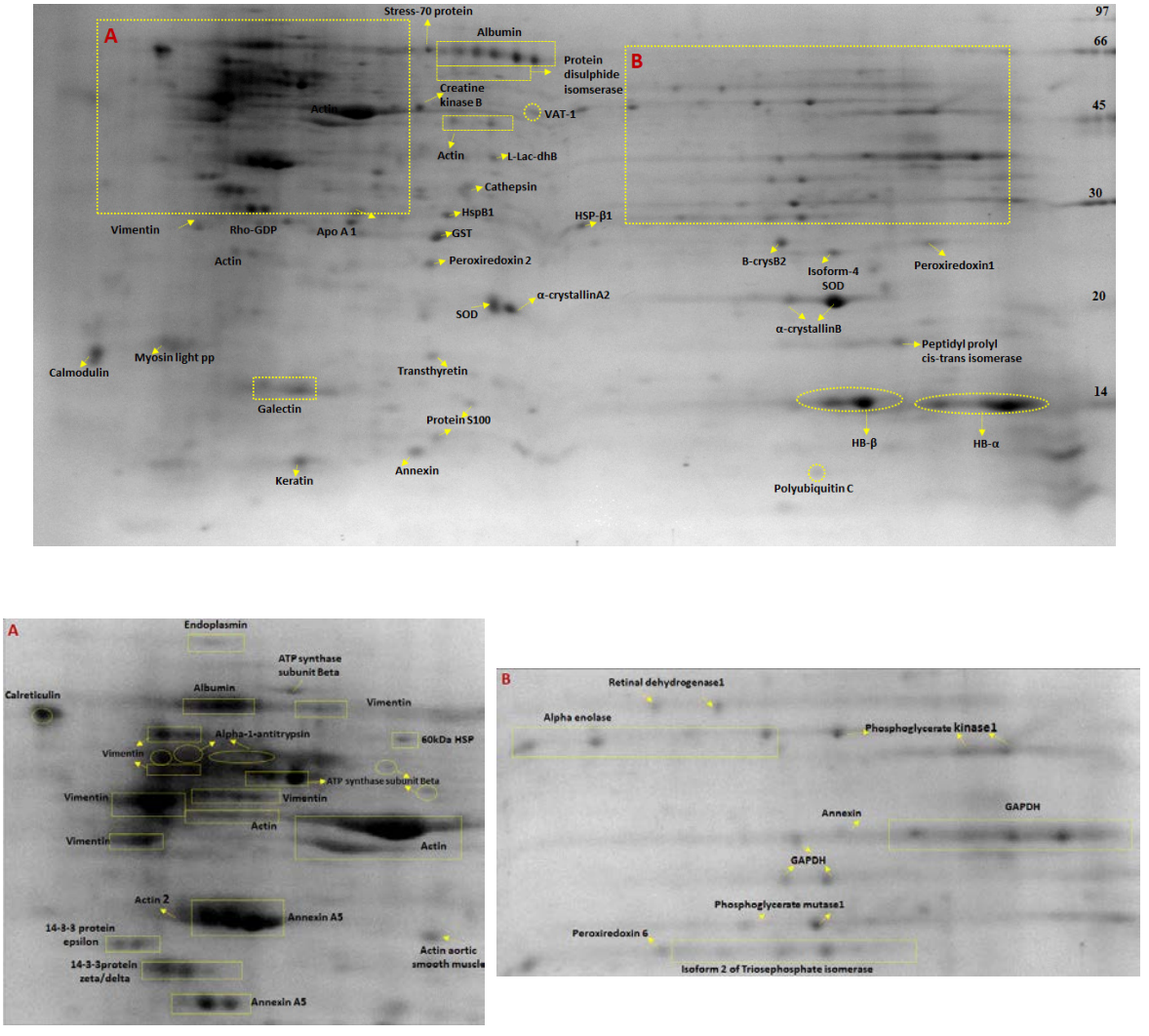

Figure 3.1. 2D reference map of iris proteome

Changes in iris proteome during pseudoexfolation syndrome (PEXS)

To understand the proteome wide changes in iris at different stages of PEXS, iris from donor eyes were used. The iris tissue was categorized into four groups as follows

- C, Control iris: no PEX deposits in iris from both eyes
- PX1: unilateral PEXS donor
  - PX1-I: Iris from one eye of the unilateral PEXS donor without PEX deposits
  - PX1-P: Iris from the other eye of the uniliateral PEX donor that has PEX deposits
- PX2: bilateral PEXS donor - Iris from both eyes has PEX deposits

Proteins were extracted from a pool of two iris tissue per sample category and fractionated on a 1D-SDS-polyacrylamide gel (Figure 3.2 A). Proteins in each lane were identified by in-gel tryptic digestion and MS analysis. Figure 3.2 B summarizes and compares the number of proteins identified across the four sample groups.

The expression profile of all the proteins identified in the iris tissue was used for clustering analysis. Figure 3.3 shows that protein expression in the iris without PEX deposits of the unilateral PEXS donor (PX1-I) clustered with that of control (C). On the other hand, the expression profile of the iris with the PEX deposits from the unilateral PEXS donor (PX1-P) clustered with that of the bilateral PEX iris (PX2). This clustering suggest that in the unilateral PEXS, the iris without PEX deposits can be considered as an incipient eye and might be in the initial stages of PEXS.

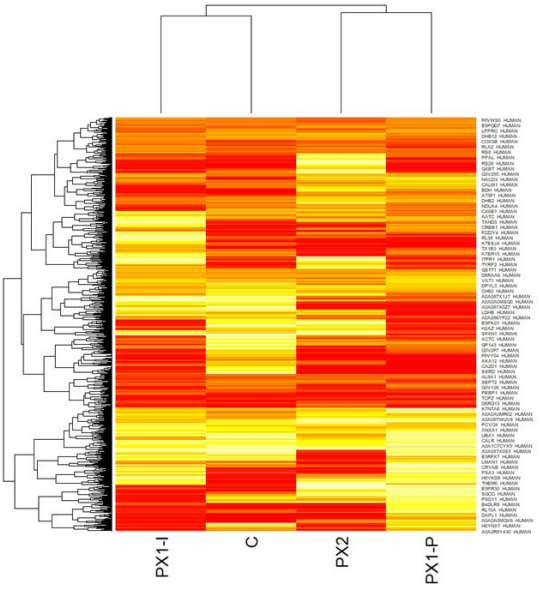

Figure 3.3. Heat map comparing the expression of iris proteins across the four sample groups

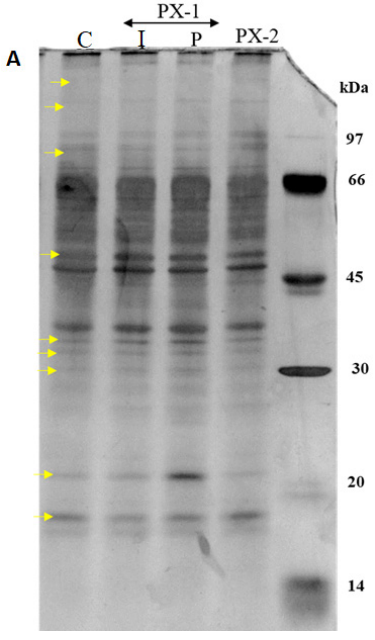

B

Sample category	Number of proteins identified
Control	921
PX1-I	864
PX1-P	933
PX2	898

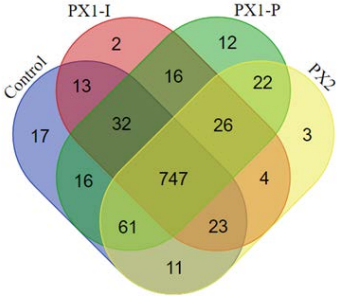

Figure 3.2. A. Comparison of the profile (A) and the MS identification (B) of the iris proteins from four different sample categories representing different stages of PEXS. Arrows indicate the proteins that show variation across the different sample groups.

Previously, many groups have identified the proteins in PEX deposits. If the iris tissue is involved in the formation of PEX deposits, the expression of these proteins would be altered in iris during PEXS. Table 3.1 lists the previously reported PEXS related proteins and its alterations across the different samples categories examined in this study. Significant upregulation was observed for emilin-1, apolipoprotein E and S100-A1.

To understand the role of iris in the pathogenesis of PEXS, the pathways that were altered with the progression of PEXS were examined. The pathway enrichment analysis (Figure 3.4) indicated that proteins involved in pathways such as axon

Table 3.1. MS identification of proteins in iris tissue that were reported to be altered in PEXS

	(1D-FRACTIONATION -> MS)				
Protein Details	**C1**	**PX1-I**	**PX1-P**	**PX2**	
Lysyl oxidase homolog 1	74	**21**	66		Cross-linking enzyme & reported to be present in PXF deposits
Emilin-1	9	**17**	**16**	**20**	Elastic fiber associated protein & reported to be present in PXF deposits
Apolipoprotein E	1		**19**	**6**	Reported earlier to be present in PXF Deposits
Clusterin	26	23	35	43	
Complement C4-B	16	9	**5**	14	
Laminin subunit beta-1		4	1	4	
Laminin subunit beta-2	43	56	**16**	58	
Laminin subunit gamma-1	53	33	**17**	49	
Metalloproteinase inhibitor 3	11	**4**	**31**	18	
Serum amyloid P-component	10	9	22	7	
Vitronectin	32	25	**20**	30	
14-3-3 protein epsilon	148	189	208	**114**	Reported earlier to be present in PXF AH
Annexin A5	441	365	441	475	
F-box only protein 50		2	9		
Flavin reductase (NADPH)	9	9	13	9	
Glucose-6-phosphate isomerase	193	156	168	145	
Glutathione S-transferase Mu 3	50	48	96	91	
L-lactate dehydrogenase B chain	148	136	206	180	
Malate dehydrogenase, cytoplasmic	40	63	43	25	
NAD(P)H dehydrogenase [quinone 1	12	**2**	7	**0**	
Phosphatidylethanolamine-binding protein 1	164	132	160	157	
Protein s100-a1	65	**2**	**122**	**159**	
Vimentin	1612	1726	1314	1682	
Superoxide dismutase [Cu-Zn]	42	27	**18**	28	

Functional Relevance	**Pathway name**	**C1**	**PX1-I**	**PX1-P**	**PX2**	**Abundance trend**
Axon guidance	Semaphorin interactions and signaling	142	138	141	173	
Cell cycle	Nuclear Envelope Reassembly	114	110	99	145	
Disease (GAG metab)	Defective B4GALT1 causes B4GALT1-CDG (CDG-2d)	114	103	103	136	
ECM organization	Laminin interactions, Non-integrin membrane-ECM interactions, ECM proteogly	46	36	24	60	
hemostasis	Thrombin signalling through proteinase activated receptors (PARs)	16	16	24	27	
Metabolism	Beta oxidation of myristoyl-CoA to lauroyl-CoA	47	26	40	76	
Metabolism of proteins	Cooperation of PDCL (PhLP1) and TRiC/CCT in G-protein beta folding	18	18	24	26	
Platelet homeostasis	Prostacyclin signalling through prostacyclin receptor	17	16	25	30	
Signal transduction	G-protein beta:gamma signalling	21	25	32	34	
Cellular response to external stimuli	Detoxification of Reactive Oxygen Species	73	68	83	60	
hemostasis	Response to elevated platelet cytosolic Ca2+ & Platelet activation, signaling and a	140	186	158	113	
Metabolism	Insulin effects increased synthesis of Xylulose-5-Phosphate	66	40	47	33	
Metabolism	Glycolysis, gluconeogenesis, glucose metabolism	218	237	312	209	
Metabolism of proteins	Post-translational protein phosphorylation	122	190	159	92	
Cell cycle	G2/M Checkpoints	68	60	118	82	
Metabolism	Pyruvate metabolism	36	31	53	44	
Metabolism of proteins	Amyloid fiber formation	132	133	208	168	
Signal transduction	Signaling by WNT	47	45	79	60	
Signal transduction	RHO GTPase Effectors	120	124	154	147	
Transcription	RUNX1 regulates transcription of genes involved in differentiation of HSCs	67	68	121	89	
Cellular response to external stimuli	Cellular responses to external stimuli	67	69	104	71	

Figure 3.4. Comparison of the enrichment of proteins involved in various pathways across the four sample categories.

guidance, cell cycle, ECM organization, hemostasis, lipid metabolism were upregulated in bilateral PEXS iris. On the other hand, cellular response to external stimuli, metabolism of carbohydrates and proteins were downregulated in bilateral PEXS iris. Interestingly, these down-regulated pathways were upregulated in the iris with PEX deposits from the unilateral PEXS donor.

Work in progress

This study enabled the identification of the proteome wide changes in iris tissue at different stages of PEXS. As this preliminary study was carried out with pooled samples, the observations made needs to be validated using individual iris samples as well as iris tissues from PEXG patients.

References

1. Murthy KR, Dammalli M, Pinto SM, *et al*. (2016). OMICS. 20:510–519.
2. Nazarali, S., Damji, F. & Damji, K. F. (2018). The British journal of ophthalmology 102, 1342-1350.
3. Zhang P, Kirby D, Dufresne C, *et al*. (2016). Proteomics. 16:1146–1153.

OCULAR PHARMACOLOGY

Glaucoma is the second leading cause of blindness in the world. The current option available for the treatment of glaucoma is to lower the intraocular pressure which is the only modifiable risk factor. Despite of continuous usage of glaucoma medications, there is still some proportion of the glaucoma patients progress to severe form of glaucoma and lose their vision. Therefore, there is always a constant search for the discovery of newer/ better drugs for glaucoma.

The main research focus of the Department of Ocular Pharmacology is to identify a newer therapeutic targets by looking at the various molecular mechanism (s) associated with the pathogenesis of glaucoma especially primary open angle glaucoma (POAG) and steroid-induced ocular hypertension (OHT)/glaucoma.

Role of microRNA in regulating glucocorticoid receptor signaling in steroid-induced ocular hypertension/glaucoma

Investigators : Dr. S. Senthilkumari
Dr. C. Gowripriya
Dr. D. Bharanidharan
Dr. R. Sharmila

International Collaborator :
Prof. Colin Willoughby,
Faculty of Life & Health Sciences, University of Ulster, Northern Ireland, UK

Mentors:
Prof. VR. Muthukkaruppan
Advisor - Research, Department of immunology and Stem Cell Biology, AMRF, Madurai

Dr. S.R. Krishnadas, Glaucoma Clinic, Aravind Eye Hospital, Madurai

Prof. K. Dharmalingam, Research-Director, Department of Proteomics, AMRF, Madurai

Research Associate : Dr. R.Haribalaganesh
Junior Research Fellow : K. Kathirvel
Funding Agency : The Wellcome Trust-DBT/India Alliance (Intermediate Fellowship)

Introduction

Glucocorticoid (GC) - induced glaucoma is a sub-type of secondary glaucoma and the usage of GC either topical or systemic administration may induce ocular hypertension in susceptible persons (Armaly et al.,1993). The clinical presentations of both GC-induced glaucoma and primary open angle glaucoma (POAG) share the clinical similarities. Like POAG, GC-induced ocular hypertension is due to increased aqueous humour outflow resistance in the anterior chamber angle of eye, at the level of the trabecular meshwork (TM) (Clark et al. 2001).

Human TM cells express GC receptors and they can respond to GC administration, thereby regulating the expression of hundreds of genes in the TM (Clark et al. 2001). Causative mechanisms for increased aqueous outflow resistance in TM include enhanced

deposition of extracellular matrix (ECM) and changes in cell cytoskeleton. Studies on differential gene expression in the TM induced by GCs have been limited to cultured TM cells neglecting the genetic predisposition to develop steroid-glaucoma.

Nuclear receptor signaling (eg GC receptor signaling) regulates microRNA expression. MicroRNAs (miRNAs) modulate gene expression at the posttranscriptional level and regulate many cellular functions (Yang and Wang 2011). Recent studies demonstrated both in vitro and in glaucomatous aqueous humor and trabecular meshwork release extracellular miRNAs which can regulate the ECM, TM contractility and senescence (Luna et al. 2009; Villarreal et al. 2011 and Tanaka et al. 2014). However, no studies have been reported related to the role of miRNAs in steroid –induced ocular hypertension/glaucoma. There is an evidence that steroid treated ocular fibroblasts demonstrate differential expression of small non-coding RNAs (miRNAs) (Liu et al. 2011). The predicted miRNA target genes include pathogenesis-relevant genes/ pathways, such as ECM remodeling, wound healing, cell cycle regulation; these however were not experimentally validated. Therefore, the key goal of this study was to understand the role of miRNAs in the regulation of glucocorticoid receptor (GR) signaling in the TM and to develop new miRNA therapeutics for the treatment of steroid – induced glaucoma

Work Plan

Human Organ-Cultured anterior segment (HOCAS), ex vivo model was used to identify the GC responsive and non-responsive eyes in response to dexamethasone (DEX) treatment based on the maximum IOP change (>5mm Hg). Since, the yield of total RNA from TM tissues after HOCAS was not sufficient for RNA-sequencing, a modified protocol was used. Using paired donor eyes, one eye was used to establish HOCAS to characterize GC responsiveness after DEX treatment and the other eye was used to establish HTM cultures. The detailed work plan is given in the following schematic representation (Figure 1).

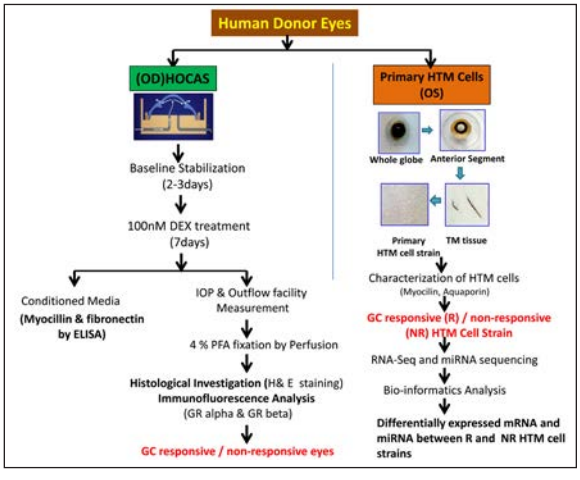

Figure 1 : Schematic Representation of Experimental work plan

Results

(A). Establishment of HOCAS characterized GC-Responsive (GC-R)and GC-Non-Responsive (GC-NR) HTM cells strains

Differential Response of Perfused Human Cadaveric Eyes to DEX Treatment

A total of 21 eyes were used for the study, out of which 11 eyes received 100nM DEX and 10 eyes received 500nM DEX treatment. The characteristics of human donor eyes used for this study is summarized in Table 1.

In 100nM DEX group, a significant elevation of IOP was seen in 4/11 eyes (mean ±SD - mΔIOP: 9.1 ± 3.5; range: 6.3-14.3 mm Hg; 36.4 % responders) whereas in 500nM group, 2/10 eyes showed a significant elevation of IOP (mean ±SD - mΔIOP: 9.3± 0.1; range: 9.25-9.46 mmHg; 20% responders) (Figure 2).

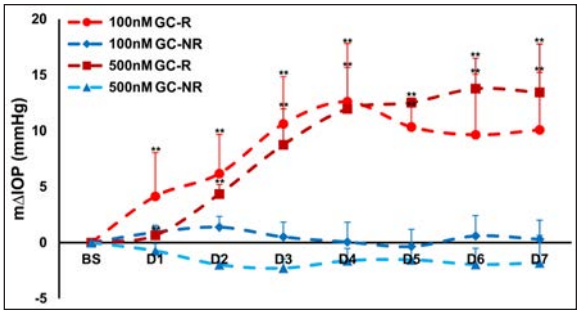

*Figure 2: A representative intraocular pressure (IOP) graph of the anterior segment receiving 100nM and 500nM DEX treatment. Out of 11 eyes received 100nM DEX treatment, 4 eyes showed elevated IOP over the period of treatment whereas in 500nM group, 2 eyes showed a significant elevation in IOP. ** p<0.001; Un-paired t-test*

Dexamethasone-induced alterations in GC-R and GC-NR Primary Human Trabecular Meshwork (HTM) Cells

Cross-linked Actin Network (CLAN) Formation

GCs are known to re-organize the actin cytoskeleton in confluent TM cells by forming CLANS (Clark et al., 2005). CLANS are three-dimensional, geodesic dome-like structures and /or “tangles” of actin filaments which are reported tin increase the

Table 1: Characteristics of Human Donor Eyes Used for this Study

DEXT	Code	Age	Sex	Cause of Death	Time B/W Death & Enu cleation (h)	Time B/W Enucleation & Culture (h)	Experiment Eye	HOCAS/ Culture	Treatment	Remarks
100nM	OCHD18-29	76	F	Natural	0.45	30.5	OD	HOCAS	DEX	Data included
							OS	Cell culture		TM Culture established
	OCHD18-38	68	M	CVA	2.50	39.83	OD	HOCAS	DEX	Data included
							OS	Cell culture		TM Culture established
	OCHD18-49	48	M	Heart Disease	2.5	30.66	OD	HOCAS	DEX	Data included
							OS	Cell culture		TM Culture established
	OCHD18-52	55	F	Vascular accident	2.75	67.91	OD	HOCAS	DEX	Data included
							OS	Cell culture		TM Culture established
	OCHD18-53	67	M	Diabetes	4.33	27	OD	HOCAS	DEX	Data included
							OS	Cell culture		TM Culture established
	OCHD18-56	82	M	CVA	4	23	OD	HOCAS	DEX	Data included
							OS	Cell culture		TM Culture established
	OCHD18-57	80	F	Respiratory disease	3	28.5	OD	HOCAS	DEX	Data included
							OS	Cell culture		TM Culture established
	OCHD19-01	73	M	Natural	4.5	30.8	OD	HOCAS	DEX	Data included
							OS	Cell culture		TM Culture established
	OCHD19-02	66	M	RTA	2.75	8.33	OD	HOCAS	DEX	Data included
							OS	Cell culture		TM Culture established
	OCHD19-03	65	F	Heart Disease	5.8	47.33	OD	HOCAS	DEX	Data included
							OS	Cell culture		TM Culture established
	OCHD19-04	72	M	Heart Disease	3.5	41	OD	HOCAS	DEX	Data included
							OS	Cell culture		TM Culture established
	OCHD19-08	67	M	Heart Disease	2.9	56.08	OD	HOCAS	DEX	Data included
							OS	Cell culture		TM Culture established
500nM	OCHD 19-15	53	M	RTA	3.5	28.5	OD	HOCAS	DEX	Data included
							OS	Cell culture		TM Culture established
	OCHD19-34	75	F	Heart Disease	2.5	52.16	OD	HOCAS	DEX	Data included
							OS	Cell culture		TM Culture established
	OCHD19-35	68	M	Heart Disease	4.5	72.75	OD	HOCAS	DEX	Data included
							OS	Cell culture		TM Culture established
	OCHD19-37	81	F	Cardiac arrest	4.66	19.5	OD	HOCAS	DEX	Data included
							OS	Cell culture		TM Culture established
	OCHD19-38	84	F	Cardiac arrest	1	47.83	OD	HOCAS	DEX	Data included
							OS	Cell culture		TM Culture established
	OCHD19-39	80	M	Respiratory disease	4.16	45.33	OD	HOCAS	DEX	Data included
							OS	Cell culture		TM Culture established
	OCHD19-40	75	F	CVA	1.83	48.6	OD	HOCAS	DEX	Data included
							OS	Cell culture		TM Culture established
	OCHD19-41	63	F	Heart Disease	1.83	33.25	OD	HOCAS	DEX	Data included
							OS	Cell culture		TM Culture established
	OCHD19-57	75	M	Respiratory disease	3.83	26	OD	HOCAS	DEX	Data included
							OS	Cell culture		TM Culture established

Mean (± SD) donor age: 70.14 ± 9.74 years; Elapsed time between death and enucleation: 3.18 ± 1.30 h; Elapsed time between enucleation and culture: 38.32 ± 15.91h. RTA- Road Traffic Accident; CVA-Cerebrovascular Accident

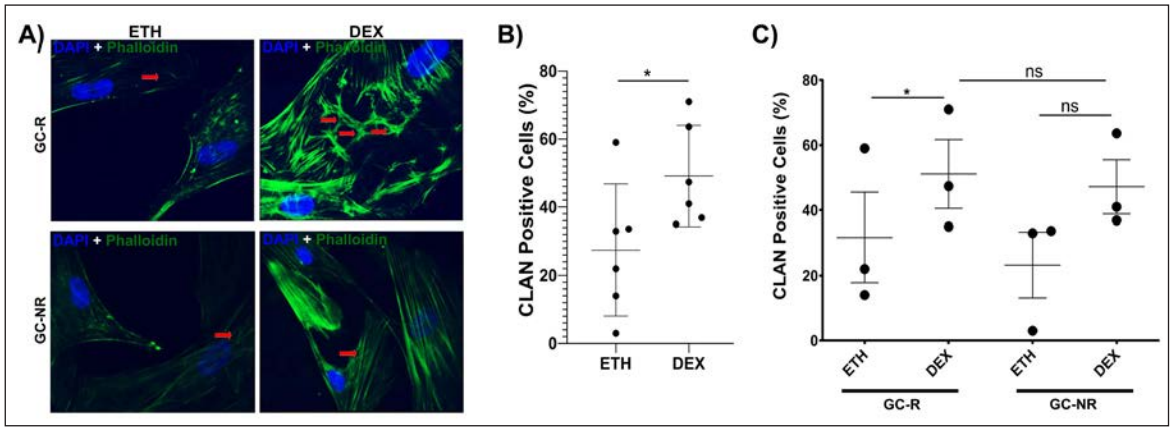

*Figure 3: Effect of DEX on CLAN Formation in GC-Responsive and non-responsive HTM cells. A) Representative image showing CLAN positive cells with respective treatments. B) Percentage of CLAN positive cells between DEX and vehicle treated group. C) Percentage of CLAN positive cells between GC-responder and non-Responder HTM cells. *p<0.05; paired-t-test; n=3. CLAN formation was significantly increased in DEX-treated GC-responder cells as compared to its vehicle treated cells whereas in GC-non-responder cells, there was an increase in CLAN positive cells in DEX-treated cells as compared to its vehicle but it was not found to be statistically significant.*

stiffness of TM and impair the functions of TM such as phagocytosis, contractility and proliferations and thus affecting the aqueous outflow pathway. However, such information is not well studied between GC-R and GC-NR HTM cells. Therefore, the effect of DEX on CLAN formation in GC-R and GC-NR cells was investigated by staining the DEX/ETH treated HTM cells with phalloidin. CLAN positive cells were defined as F-actin–containing cytoskeletal structures with at least one triangulated actin arrangement consisting of actin spokes and at least three identifiable hubs (Patel et al., 2019).An average of 100 cells were counted to calculate the percentage of CLAN positive cells.

In both GC-R HTM cells, there was a significant increase in percentage of CLAN positive cells in DEX-treated cells (51.1± 18.2 %;n=3) as compared to its vehicle control (31.7 ± 24%; p=0.04; n=3) whereas in GC-NR cells, there was an increase in the percentage of CLAN positive cells in DEX-treated cells (47.2± 14 %;n=3) as compared to its vehicle control (23.2± 17.5; n=3) but it was not found to be statistically significant (p=0.1) (Figure 3). The GC-R DEX-treated cells showed more percentage of CLAN positivity as compared to GC-non-responder cells.

Fibronectin

Fibronectin is an extracellular protein (ECM) and increased accumulation by DEX is reported previously (Clark et al., 2005). Therefore in the present study, western blot analysis of secreted fibronectin in the conditioned media after DEX

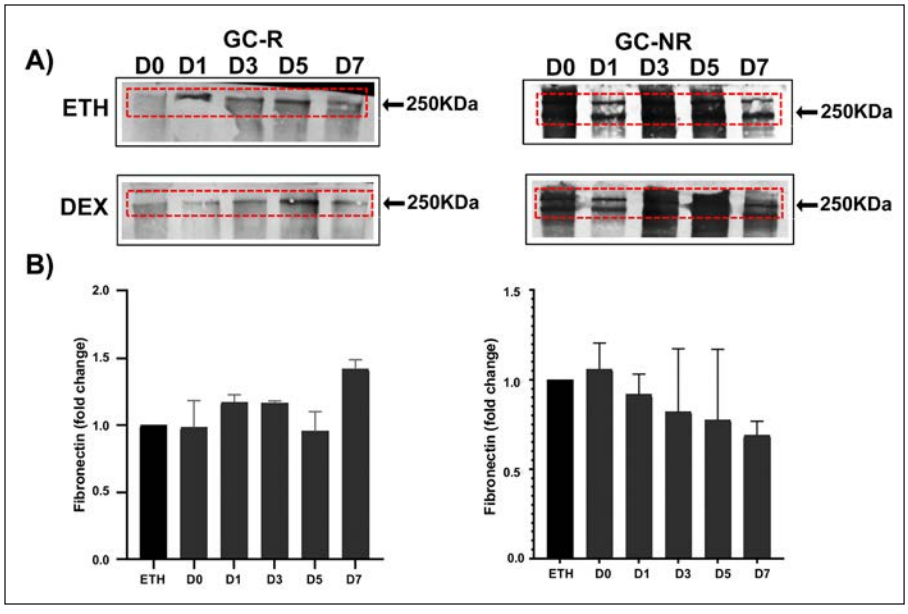

Figure 4: Effect of DEX on Secreted Fibronectin in Conditioned Media after respective treatments in GC-R and GC-NR HTM cells. A) Representative Immunoblot showing secreted fibronectin between GC-R and GC-NR groups. B) Graph showing densitometry analysis of western blot. Expression of fibronectin in the DEX- treated cells was normalized to the ETH-treated group and the mean ± SD is presented Glucocorticoid Receptor (GR) Binding and Nuclear Translocation Upon DEX Treatment in GC-R and GC-NR HTM cells

treatment between GC-R and GC-NR cells was investigated. We found a marginal increase in the levels of fibronectin in DEX-treated GC-R cells whereas in DEX-treated GC-NR group, there was a decrease in secreted levels of fibronectin over the time period but it was not found to be statistically significant (Figure 4).

Glucocorticoid Receptor (GR) Binding and Nuclear translocation upon DEX treatment in GC-R and GC-NR HTM cells

The anti-inflammatory activity of GC is mainly mediated through glucocorticoid receptor-α (GRα). The splice variant of GR gene, GR- β acts as a negative dominant transcriptional regulator to GR-α. GRα is highly expressed in the cytoplasm and GRβ is predominantly in nucleus and also in cytoplasm. Upon binding of DEX, the receptor translocate to nucleus where it supress the gene expression (trans-repression). Therefore, in the present study, the effect of DEX on GR nuclear translocation between GC-R and GC-NR HTM cells was investigated using immunofluorescence analysis.

Immunofluorescence analysis revealed that there is an increase in nuclear translocation of GRα after DEX treatment as compared to its vehicle control. GC-R group showed a distinct pattern as compared to GC-NR group but was not found to be statistically significant. The total cell fluorescent intensity also showed the similar trend (Figure 5A). In contrast, the nuclear translocation of GRβ was reduced in DEX-treated cells as compared to its vehicle treated group but it was not found to be statistically significant. However, there was a marginal increase in total cell GRβ intensity upon DEX treatment in both groups (Figure 5B).

(B) Integrated analysis of mRNA and microRNA sequencing of GC-R and GC-NR HTM cells

In this study, an integrated mRNA and miRNA analysis was carried out to identify the dys-regulated miRNA-mRNA pair which could dictate the differential response to DEX treatment in HOCAS-characterized GC-R and GR-NR HTM cells.

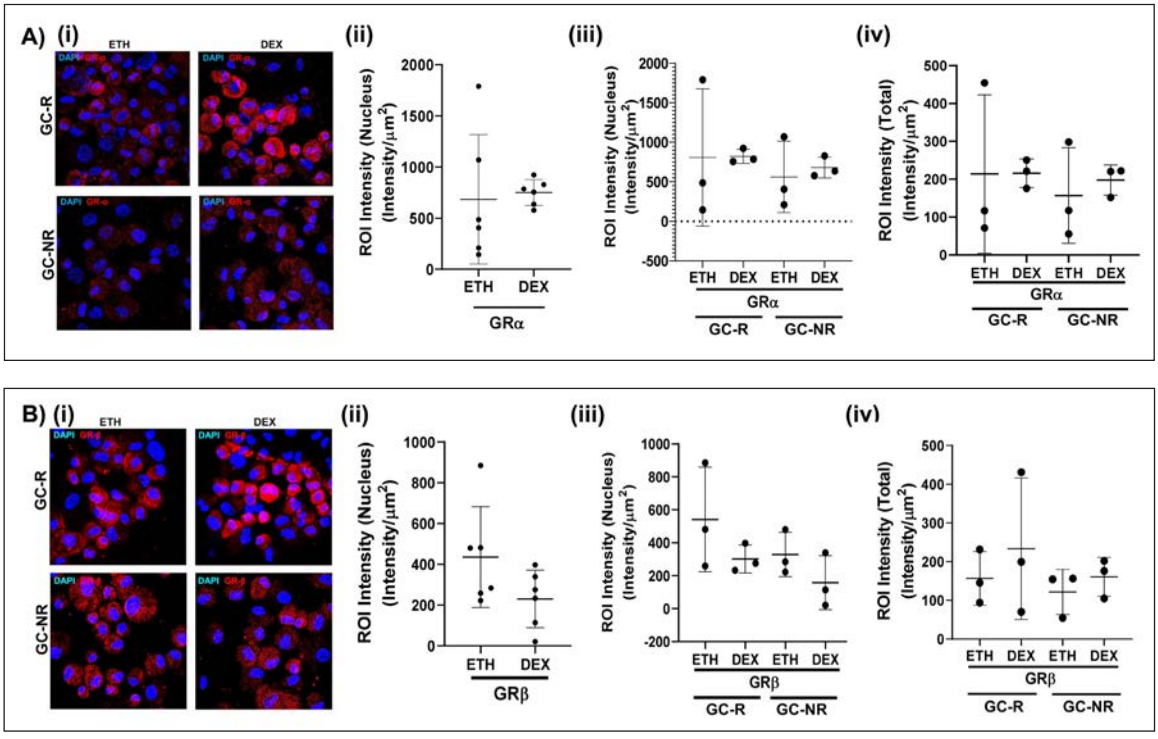

Figure 5: DEX induced differential expression and distribution of GR-α and GR-β in HTM cells with known GC responsiveness.

A. Nuclear Translocation of GRα between GC-R and GC-NR HTM cells. (i) Representative image showing the localization of GRα in HTM cells with respective treatments. (ii) 100 cells were randomly chosen, analysed and the percentage of nuclear GR calculated for DEX and vehicle –treated cells and (iii) GC-R and GC-NR cells (iv) 100 cells were randomly chosen, analyzed and the percentage of total cell GR calculated

B. Nuclear Translocation of GRβ between GC-R and GC-NR HTM cells (i) Representative image showing the localization of GRβ in HTM cells with respective treatments. (ii) 100 cells were randomly chosen, analysed and the percentage of nuclear GRβ calculated for DEX and vehicle –treated cells and (iii) GC-R and GC-NR cells (iv) 100 cells were randomly chosen, analyzed and the percentage of total cell GRβ calculated. DEX-R (GC-R); DEX-NR (GC-NR).

Cultured HTM cell strain with known GC responsiveness were treated with either 0.1%ETH (vehicle control) or 100nM DEX for 7 days. Total RNA was isolated by the TRIZol method. RNA quality and quantity were assessed by using Tape Station (Agilent) and Qubit 3.0, respectively. Additionally, the quality of RNA was observed by ratio of 28S and 18S ribosomal bands on 0.8 % agarose gel electrophoresis. The samples with RIN value more than 7 was used for NGS. The quantity and purity of RNA from each cell strain is summarized in Table.2.

In total, 21 to 36.2 million reads and 9.1 to 17.2 million reads were generated from mRNA and miRNA sequencing respectively. Pre-aligned QC reports showed the quality score (phred score) of both miRNA and mRNA reads were ≥ 30. An average of 85.6% and 97.2% reads from mRNA and miRNA-seq data were aligned with human reference genome GRCh38. The data bias from different millions of reads from each sample was eliminated using Quantile and TMM normalization strategies. The mapping rate and number genes annotated from each genome are shown in Table 3.

Table 2: RNA Quality and Quantity from HTM Cell Strains Used for this Study

Details			QUBIT Quantification Details			GC NR/R
S.No	ID		RIN	Conc. (ng/uL)	Grade	
1	18-39	ETH	8.8	830	A	R
		DEX	9.2	740	A	
2	18-53	ETH	9.2	392	A	R
		DEX	9.2	441	A	
3	19-03	ETH	9.2	1000	A	R
		DEX	9.1	890	A	
4	19-04	ETH	9.3	1000	A	R
		DEX	9.2	970	A	
5	18-49	ETH	9.3	860	A	NR
		DEX	9.4	850	A	
6	18-52	ETH	9.4	740	A	NR
		DEX	9.7	276	A	
7	18-56	ETH	9.2	520	A	NR
		DEX	8.9	600	A	
8	19-02	ETH	9.3	970	A	NR
		DEX	9.1	780	A	

The observed RIN values ranged from 8.8 to 9.7 which indicates the RNA of high purity.

Table 3: Alignment Statistics of mRNA and miRNA Sequence Data

Details			mRNA				miRNA			
S. No	ID		Total Reads (in millions)	% of Mapped Reads	% of UnMapped Reads	No. of Genes	Total Reads (in millions)	% of Mapped Reads	% of UnMapped Reads	No. of miRNAs
1	18-39	ETH	21.1	85.08	14.92	15765	17.2	98.2	1.8	892
		DEX	29.3	84.79	15.11	17079	14.6	98.2	1.8	898
2	18-53	ETH	22.5	85.76	14.24	17371	11.3	97.3	2.7	828
		DEX	36.2	82.11	17.89	16415	12.1	97.4	2.6	841
3	19-03	ETH	23.4	84.91	15.09	15353	13.2	98.3	1.7	871
		DEX	30.5	87.00	13.00	16396	-	-	-	-
4	19-04	ETH	27.5	87.40	12.60	14515	13.8	98.4	1.6	856
		DEX	30.7	85.38	14.62	16334	14.2	98.5	1.5	857
5	18-49	ETH	26.8	84.30	15.70	15439	10.8	97.1	2.9	849
		DEX	30.3	85.22	14.78	15637	9.1	97.4	2.6	837
6	18-52	ETH	23.1	84.42	15.58	14682	13.6	97.6	2.4	878
		DEX	28.4	86.27	13.73	15997	11.4	95.8	4.2	872
7	18-56	ETH	24.8	86.28	13.72	15852	12.0	98.5	1.5	857
		DEX	36.2	86.28	13.72	16654	10.7	87.3	2.7	718
8	19-02	ETH	23.4	88.60	11.40	16039	12.0	98.3	1.7	863
		DEX	32.7	85.84	14.16	16828	13.6	98.6	1.4	877

Differentially expressed genes and pathway Between GC-R and GC-NR HTM cells:

In an average, 16,022 genes were identified from all samples with read count more than 49. In GC-R group, 706 (161 up-regulated; 545 down-regulated) DE genes were identified, including the known glaucoma associated genes FRG2C (5.27), SAA4 (FC: 4.75), NTRK2 (3.39), ITGA10 (2.5) and UPK3A (-8.48), RLN1 (-8.01) (Figure 6A) which are involved in actin cytoskeleton regulation, MAPK signaling and ECM receptor interaction pathways.

In GC-NR group, totally, 284 (178 up-regulated; 106 down-regulated) DE genes were identified with absolute fold change (log2) of >2 and p value <0.05, in GC-NR cells, including STEAP4 (4.58), FAM107A (4.44), STOX1 (3.11), ABCA6 (2.8) and GRM5 (-5.03), SLC24A2 (-3.86) (Figure 6B) involved in calcium signaling, gap junction and ABC transporters pathways (Figure 7). The overlapping genes between GC-R and GC-NR groups were SAA1, ZBTB16, FKBP5 and MYOC were up-regulated and AQP1, LAMP3 were down-regulated which were reported to be known DEX-induced genes in TM cells.

The enrichment analysis from differentially expressed genes of GC-R and GC-NR was performed using GSEApreranked module in Gene Pattern with KEGG database. Pathway analysis from DE genes has revealed that, the Insulin signaling, MAPK, TLR and VEGF pathways were up-regulated in GC-R cells than GC-NR. Axon guidance, WNT signaling, P53 pathways were found to be down-regulated in both GC-NR and GC-R HTM cells. The top overlapping canonical pathways between GC-R and GC-NR group are shown in heat-map (Figure 7).

Figure 7: Heat Map of Over-lapping Pathways between GC-R and GC-NR HTM cells. R –GC-R; NR – GC-NR.

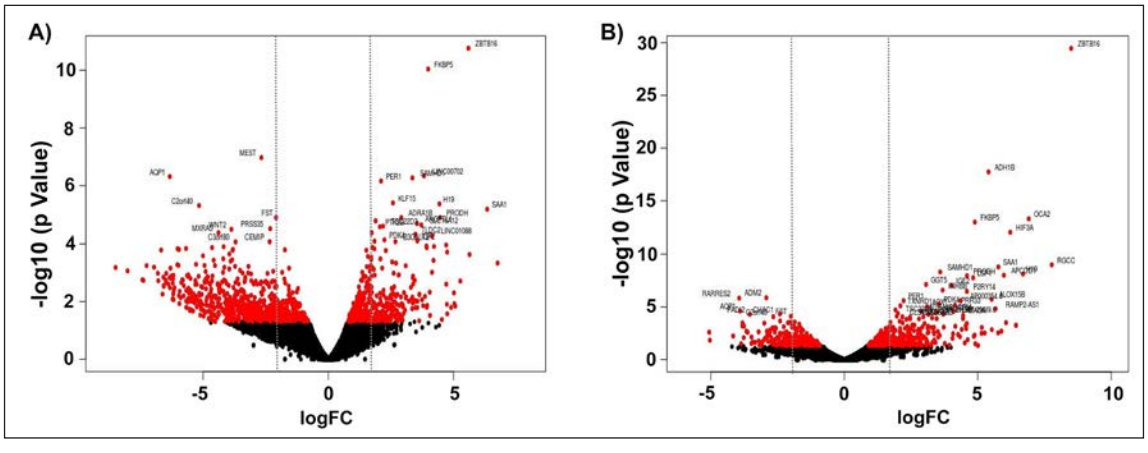

Figure 6: Volcano plot of differentially expressed genes between GC-R (A) and GC-NR (B) cells. The fold change (log2) and p value (-log10) of the dysregulated genes in GC-responder and GC-Non-responder cells are shown in volcano plot. Genes with significant FDR value <0.05, were considered (red color).

Differentially expressed miRNAs

An average, 808 miRNAs were identified from all samples with read count more than 9.In GC-R group, out of 13 significantly dysregulated miRNAs, 5 were down-regulated and 7 were up-regulated with absolute fold change (log2) of >1.5 (Figure 8A) whereas in GC-NR group, 21 miRNAs were dysregulated in DEX treated cells compared to control with significant p value <0.05. Out 21 miRNAs, 15 were down-regulated and 4 were up-regulated with absolute fold change (log2) of >1.5 (Figure 8B).

The miRNAs, hsa-miR-483-5p, hsa-miR-483-3p, hsa-miR-675-5p, hsa-miR-675-3p and hsa-miR-335-3p were identified as common miRNAs for both GC-NR and GC-R cell strains with similar expression levels. Interestingly, hsa-miR-4485-3p (FC=3.1) and hsa-miR-6842-3p (FC=1.5) was found to be up-regulated only in GC-NR and GC-R cell strains, respectively. Similarly, hsa-miR-549a-5p (FC= -2.1) and hsa-miR-335-5p (FC= - 1.7) were identified as down-regulated only in GC-R. The list of DE miRNAs are shown in table 4.

Network Analysis of Differentially Expressed miRNAs and their Target Genes

In order to determine the miRNA and mRNA functional interactions, the differentially expressed miRNAs and their predicted target genes was investigated using miRWalk 3.0 with parameters of selecting, score as > 0.95, targetscan and mirTarBase. Predicted target genes from miRWalk, were further filtered with DE genes, identified from transcriptome data of the present study. The interaction network for DE miRNAs and their binding targets are shown in Figure 9.

Table 4: List of Differentially Expressed miRNAs

GC R/NR	Up-Regulated	logFC	Down-Regulated	log FC
GC-R	hsa-miR-2114-3p	6.1	hsa-miR-335-5p	-1.7
	hsa-miR-675-3p	4.9	hsa-miR-549a-5p	-2.1
	hsa-miR-483-3p	4.6	hsa-miR-335-3p	-3.0
	hsa-miR-675-5p	4.6	hsa-miR-7151-3p	-3.1
	hsa-miR-483-5p	4.3	hsa-miR-124-3p	-6.2
	hsa-miR-5690	3.6		
	hsa-miR-2114-5p	3.2		
	hsa-miR-6842-3p	1.5		
GC-NR	hsa-miR-4485-5p	4.7	hsa-miR-6853	-1.7
	hsa-miR-483-5p	4.6	hsa-miR-335-3p	-1.9
	hsa-miR-12136	4.3	hsa-miR-550a-3p	-2.0
	hsa-miR-4328	4.1	hsa-miR-9-3p	-4.8
	hsa-miR-483-3p	4.0		
	hsa-miR-675-5p	3.6		
	hsa-miR-675-3p	3.6		
	hsa-miR-320a-5p	3.4		
	hsa-miR-4485-3p	3.0		
	hsa-miR-10396b-5p	2.6		
	hsa-miR-10396a-5p	2.6		
	hsa-miR-3195	2.4		
	hsa-miR-1246	2.2		
	hsa-miR-5690	2.1		

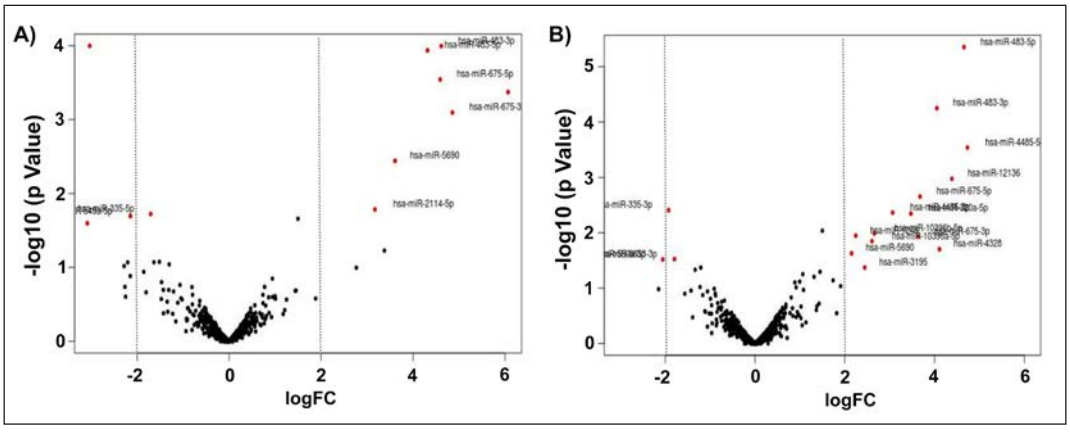

Figure 8: Volcano plot of differentially expressed miRNAs of GC-R (A) and GC-NR HTM cells (B). The fold of change (log2) and p value (-log 10) of the dysregulated genes in Dex treated cells compared to vehicle control are shown in volcano plot. p value <0.05 was considered statistically significant (red color).

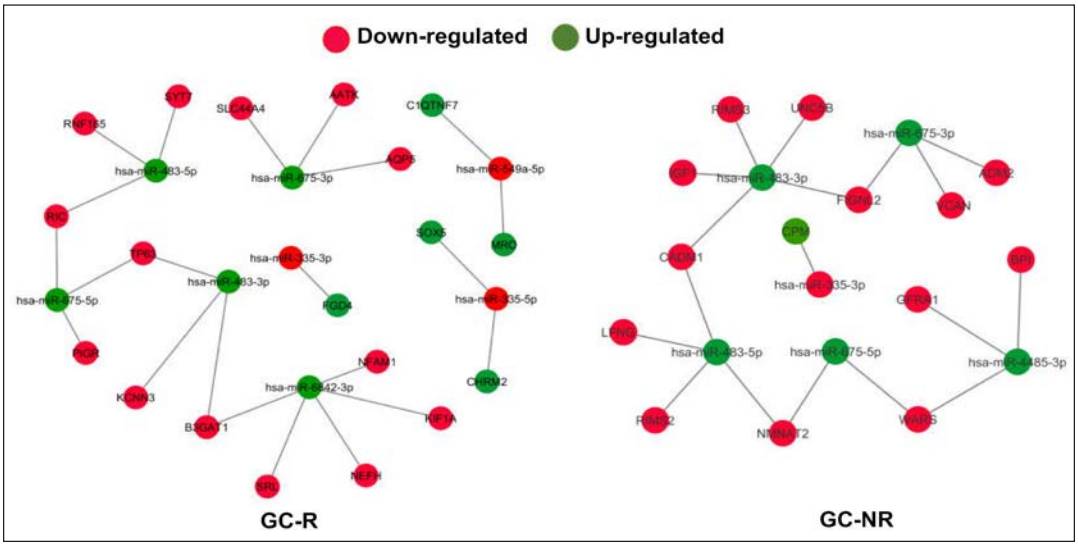

Figure 9: Network Analysis of Predicted Differentially Expressed miRNAs and their target genes for GC-R and GC-NR group.

Conclusion

- Primary HTM cells with known GC responsiveness was established successfully and the observed DEX-induced changes such as CLAN formation, fibronectin induction and GR nuclear translocation were comparable between GC-R and GC-NR.
- Using NGS, the differentially expressed miRNAs and their binding target genes from GC-non-Responder and GC-Responder HTM cells were identified. Some miRNAs and their interacting partners from this study were already reported to have a potential role in glaucoma. Further validation of miRNAs and their target genes expression is by qRT-PCR is in progress. After validation, the potential miRNA (s) will be identified and evaluated for its efficacy in alleviating GC-OHT using HOCAS model.

BIOINFORMATICS

The availability of huge omics data from genome projects and high-throughput technology (next-generation sequencing and microarray) has brought a great challenge to understand the complexity of biological processes and disease mechanisms in eye research. We seek an agile and predictive understanding of how genetic variants that results in eye diseases, including ocular cancer. We write algorithms and pipelines to get critical answers faster from NGS data. We also focus on non-coding RNA expression and its regulatory role in eye diseases by integrating data from NGS and the public. We have a reliable infrastructure and framework comprised of LINUX and Windows-based servers and desktop workstations, which allow us to integrate high throughput data and study them at the systems level. Bioinformatics centre is highly interdisciplinary, at the interface of Biology, computational biology and Informatics.

1. Clinical Exome/Genome analysis for eye diseases

Investigator	:	Dr. D. Bharanidharan
Co-investigators	:	Dr. P. Sundaresan
		Dr. A.Vanniarajan
Research Scholar	:	K. Manojkumar
Funding	:	DBT-COE, SERB

Background

Recent advances in genomic technologies, particularly next generation sequencing (NGS) methods, have brought a paradigm shift in discovering eye disease-associated genetic variants from linkage and genome-wide association studies to NGS-based genome/exome studies. Whole genome sequencing (WGS) remains prohibitively expensive for most applications and requires concurrent development of bioinformatics approaches to expeditiously analyze the large data sets, whole exome sequencing (WES) is now made as a viable approach to uncover unknown etiology with a limited number of probands with eye disease. WES, focuses on only the protein-coding sequence of human genome, is become a powerful tool with many advantages in the research setting, and moreover is now being implemented into the clinical diagnostic arena. Spurred by NGS technologies, new efficient and well-designed bioinformatics tools emerged which are addressing different tasks in the downstream analysis of NGS data. Since combining these tools into an analysis pipeline greatly facilitates the interpretation of NGS results, an exome/genome sequencing pipeline is developed in this project that connects all necessary analysis steps into a unified application in the clinical settings for eye disease panel. The pipeline will support input data generated by the NGS Illumina platforms, handles correct execution of all integrated tools. It performs quality statistics on raw and processed reads, allows users to trim and filter sequence reads, and aligns the processed reads to a reference eye disease gene panel. The pipeline will deal single nucleotide variants (SNVs) and short INDELs separately to improve the performance and to detect true positives. The integration of well-established tools and newly developed promising algorithms into a unified solution

eases the analysis of next-generation exome/genome sequencing data.

Nevertheless, the identification of pathogenic variants amongst thousands to millions of genomic variants is a major challenge, and requires new strategies for variant filtering for diseases panel. Pathogenic variant prioritization using simple heuristic filtering approaches and functional implications of variants misses the true positives. Here we aim to develop stringent filtering method and machine learning methods to prioritize pathogenic variants for eye diseases. We further wanted to focus the prioritization methods specific for Mendelian and complex eye diseases separately.

Results

Based on recent benchmarking, the team has developed an automated pipeline using unix shell scripts and GUI was written using HTML. The pipeline involves several steps to produce high-quality alignment files, and to detect definite variants. Initially, the quality of the raw reads obtained from SRA will be checked by FastQC and the low-quality reads, adapter contaminates will be trimmed by Cutadapt. Alignment of the reads with the reference genome will be performed using BWA and Novoalign. PCR duplicates will be removed using PiCard Tools with option provided by the user. The variants, single nucleotide variants (SNVs) and InDels will be identified by DeepVariant and strelka. Annovar tool performs annotation for all the variants.

The variant prioritization step will be performed on the case-by-case basis. Therefore, we provide here the github online link : https://github.com/bharani-lab/WES-pipelines/ for the details filtering option for the user. The default filtering methods as shown in figure 1.1 is better works for illumina whole exome/targeted sequencing data for Mendelian and Complex eye disorders. The stringent filtering strategy was better optimized with eye disease exome/targeted data sets, which involves heuristic filtering methods for pathogenic variant prioritization and further machine learning method for eye diseases known gene panel. The machine learning method to identify novel variants for eye diseases independent of gene-based knowledge is being developed. We provide the successful data analysis results for the following research projects on eye diseases.

Study 1: Whole Exome Sequencing to identify causative variants in patients with Leber Congenital Amaurosis (LCA)

A total of two trio south Indian family patients with LCA were sequenced using Illumina. In family 1, whole exome analysis found out 48 pathogenic variants. Among them a novel homozygous missense mutation (c.T2918A) in exon 15 of the GUCY2D gene was identified. This change substitutes the amino acid valine to glutamic acid at 973 position (p.V973E) and having direct association with LCA phenotype (VarElect score of 168.69 and pathogenic prediction

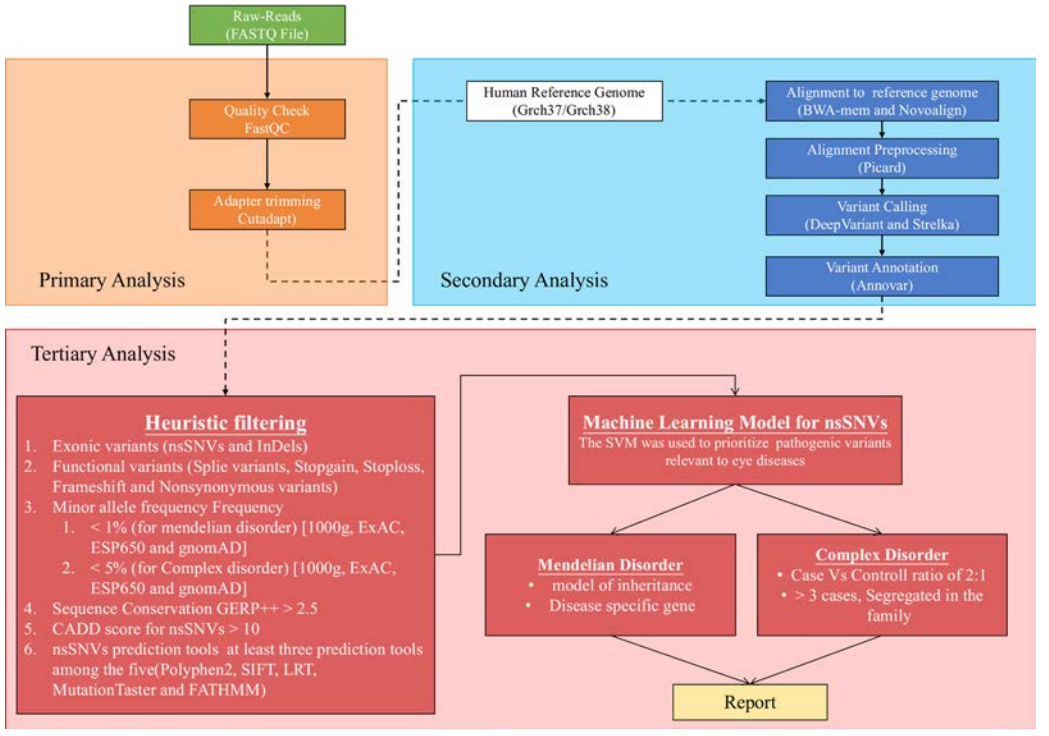

Figure 1.1. Automated Exome/Genome Data Analysis Pipeline and Variant prioritization for eye diseases.

score of 105). Consistent with an autosomal recessive mode of inheritance/transmission, c.T2918A change was observed to be in homozygous state in proband and heterozygous in both unaffected parents. In the second family, 29 pathogenic variants were detected. We prioritized a homozygous stop gain variant c.C1090T (p.R364X) in exon 11 of the IQCB1 gene, which has been previously reported elsewhere in LCA (VarElect score of 102.34 and pathogenic prediction score of 92).

Study 2: Identification of mutations in the patients with Usher syndrome using clinical exome targeted gene panel

A custom panel of Illumina platforms was designed to capture 6000 genes which were reported to be clinically relevant in OMIM and HGMD were taken for sequencing of a trio south Indian family with Usher Syndrome. Initial filtering identified 35 pathogenic variants in each family members. MYO7A (c.5880-5882del:p.F1963X) and CDH23 (c.G5411A:p.R1804Q) were prioritized for the disease.

Study 3: Identification of mutations in the patients with Stargart disease using clinical exome targeted gene panel

Illumina-based clinical exome targeted gene panel sequencing was performed on trios of family of south Indian family. Totally 29 pathogenic variants were filtered and further prioritization using machine learning method identified a novel pathogenic variants c.A217T:p.I73F in ABCA4 gene.

Study 4: Whole Exome sequencing of a large south Indian family with Primary Open Angle Glaucoma (POAG) to identify rare gene variants and pathways

We performed Whole Exome Sequencing (WES) for 16 samples of the family members (9 POAG and 7 controls). Prioritization of pathogenic variants using our approach identified multiple gene variants in each sample. Based on case-control enrichment and co- segregation, one novel variant in ARHGEF40 and four variants in RPGRIP1, OR11G2, OR4K14, RNASE13 and OR11H12 were identified. Rho guanine nucleotide exchange factors Gene Family protein (ARHGEF40) has been implicated in the risk of glaucoma by increasing intraocular pressure through RhoA/RhoA kinase pathway. The variant found in RPGR-interacting domain of RPGRIP1, distinct from variants causing photoreceptor dystrophies, may decrease the association of RPGR binding. Altogether, the data support that heterozygous non-synonymous variants of RPGRIP1 may cause or increase the susceptibility to various forms of glaucoma and that among other factors, physical impairment of the interaction of RPGRIP1with different proteins may contribute to the pathogenesis of forms of glaucoma.

2.Comparative genomics of bacterial pathogens from keratitis patients

Investigators : Dr. D. Bharanidharan, Dr. Lalitha Prajna
Research Scholar : K. Kathirvel, O. Ruthra
Funding : Aravind Eye Hospital

Background

Microbial keratitis due to either fungus or bacteria is a major cause of blindness in India. The bacterial keratitis, often caused by *Pseudomonas aeruginosa* and methicillin-resistant *staphylococcus aureus* (MRSA) at Aravind Eye hospital, Madurai, majority of times in spite of adequate medical management the ulcer does not heal and may require a corneal transplant. Pseudomonas aeruginosa can cause a most severe keratitis, carrying a wide array of virulence factors that contribute pathogenesis. Keratitis pathogenesis is a complex process, where in several virulence factors has been implicated including Cell-associated structures such as type IV pili and flagella, slime polysaccharide, proteases such as elastase B (LasB), alkaline protease, protease IV and Pasp and exotoxins. Also, clinical isolates of Pseudomonas often exhibit multiple resistances to antibiotics. On the other hand, studies have shown an increase in the pervasiveness of ocular MRSA infections. Comparative genomics through de novo assembly of next-generation sequencing and third-generation sequencing methods of ocular bacterial pathogens will show specific genetic features that can cause eye infections. Further insights would show that these strain-specific features may response to the host immune system, which may indeed affect the outcome of the disease. In the present study, we aim to investigated genetic characteristic of MRSA isolates from patients with keratitis.

Results and Conclusion

Earlier, we reported that the genome analysis of five ocular *P.aeruginosa* isolates from keratitis patients. The highlights of the study were the two strains BK4 and BK5, isolated from poor outcome patients, carries the flagellar genes fliD, fliS, flgL, fleP, flgK, fleI/flaG, pvdY, fpvI and fpvR, suggesting that they might cause more virulence to the bacteria (Figure 2.1). Specifically, the FliC protein has been reported to induce inflammasome and impairs the bacterial clearance.

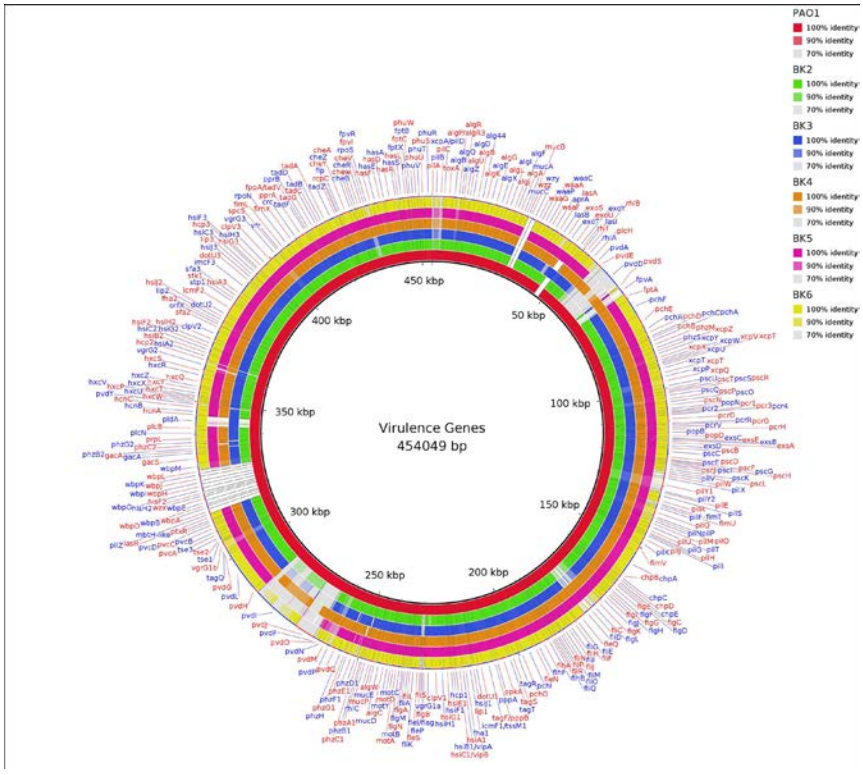

Figure 2.1: A circular representation of 395 virulence genes predicted from five ocular P.aruginosa strains named as BK2-BK6 against PA01 laboratory strain.

The present study used de novo assembly method to complete the genome sequencing of four MRSA ocular strains. Briefly, the sequencing was carried out using both the Oxford Nanopore MinION and Illumina sequencing according to the manufacturer's instructions in Genotypic technology, Bangalore. We evaluated various pipelines and identified better performing de novo assembly pipeline Canu (v1.5) (Koren et al., 2017) for the MRSA genome assembly and the resulting assembly was further followed by polishing with Illumina reads using the Pilon (v1.20) Tool (Walker et al., 2014). All four assembled MRSA contig were annotated using Rapid Annotations Subsystems Technology (RAST) server tool (Aziz RK et al., 2008). The list of four MRSA genomic features were presented in the Table 1.

All four ocular MRSA genomes were aligned with reference genome ID NC_007795.1 using Mauve aligner to determine the organization, duplication and inversion or translocation of genes. Several unique as well as common resistance and virulence genes in all four MRSA isolates were identified as shown in the Table 2 & 3.

All four MRSA strains possessed the mecA gene, known for methicillin resistance; differed significantly in their virulence and antibiotic resistance gene profile. Indeed, this MinION sequencing technology helped us to identify circular plasmid in the MRSA genomes as shown in the Table 4. Altogether, the complete genome sequences of four human ocular MRSA strains were identified first time using MinION sequencing.

Strain	No of contigs	Total length	No of Plasmid	Genome size (Mb)	Plasmid Size (bp)	Gc content	Number of coding sequence	Number of RNA	Virulence gene
AMRF - MRSA 3	1	2,846,789	1	2.8	6486	32.8	2685	81	87
AMRF - MRSA 4	1	2,888,890	1	2.8	28703	33	2783	76	66
AMRF - MRSA 5	1	2,934,806	1	2.8	6782	32.9	2852	80	67
AMRF -MRSA 6	1	2,833,283	1	2.8	59392	33	2687	79	67

Table 1: Genomics features identified in the four MRSA strains through De novo assembly

Strain	Aminoglycoside	Methicillin	Fluoro quinolone	Tetracycline	Macrolide	Diamino pyrimidine	Nucleoside	Penam	Cephalo sporin
AMRF - MRSA 3	APH(3')-IIIa, AAC(6')-Ie-APH(2")-Ia	mecA	arlS, arlR, parC	mepA, tet(38)	mphC	dfrG	SAT-4	PC1 beta-lactamase (blaZ)	mgrA
AMRF - MRSA 4	AAC(6')-Ie-APH(2")-Ia	mecA	arlS, arlR, parC	mepR, mepA, tet(38)	-	-	-	-	mgrA
AMRF - MRSA 5	APH(3')-IIIa, AAC(6')-Ie-APH(2")-Ia, aad(6)	mecA	arlS, arlR, parC	mepR, mepA, tet(38)	mphC, msrA	dfrG	SAT-4	PC1 beta-lactamase (blaZ)	mgrA
AMRF - MRSA 6	-	mecA	arlS, arlR, parC	mepR, mepA, tet(38)	-	-	-	-	mgrA

Table 2: Identification of Antibiotics Resistance Gene Profile of MRSA Genome

Sample	Type VII secretion system protein	Panton Valentine leukocidin	Gamma-hemolysin	Staphylococcal complement inhibitor	Serine protease	Enterotoxin	Aureolysin	Immuno globulin G binding protein A
AMRF-MRSA 3	essC, esaA, essB, essA, esxA, esaB	luk S-R	hlgB, hlgC, hlgA, hly/ hla	Scn	sspA, sbnA,	sec, sec3 seg,sei sem, sen seo, seu	aur	spa
AMRF-MRSA 4	essC, esaA, essB, essA, esxA, esaB, esaC	lukF-PV, lukS-PV , lukE, lukD	hlgA, hlgB, hlgC, hly/ hla	scn	splA, splB splF, splD, splE, splC, sspA	seb	aur	spa
AMRF-MRSA 5	essC, esaA, essB, essA, esxA, esaB	lukF-PV, lukS-PV	hlgA, hlgB, hlgC	scn	-	sec, sec3 seg,sei sem, sen seo, seu,sea,sel	aur	-
AMRF-MRSA 6	essC, esaA, essB, essA, esxA, esaB, esaC, esxB	lukF-PV, lukS-PV	hlgA, hlgC, hly/hla	-	splB, splF, splD, splA	Seb, Sak, Scn	-	spa

Table 3: Identification of Virulence Gene Profile of MRSA Genome

Strain	Plasmid	Gene
AMRF - MRSA 3	pkH18	cadC, cadD, Rep
AMRF - MRSA 4	pSaa6159	cadA, cadC, cadD, Rep, Tn552 transposase, Beta-lactamase, MobE, ABC transporters, Erythromycin, Penicillin, Methicillin
AMRF - MRSA 5	pKH18	cadC, cadD, Rep
AMRF MRSA 6	pSaa6159	cadA, cadC, cadD, Rep, Tn552 transposase, Beta-lactamase, MobE, ABC transporters, Erythromycin, Penicillin, Methicillin

Table 4: Plasmids identified in each of the MRSA strains

OCULAR MICROBIOLOGY

The department aims to develop rapid molecular diagnostic methods as well as understand the pathogenesis of ocular infections and host pathogen interactions. It employs various conventional microbiological methods and molecular tools such as conventional PCR, Real Time PCR, DNA barcoding and Next generation sequencing. Conventional and Real Time PCR are routinely employed for the identification and quantification of known ocular pathogens including bacteria, fungus, *Acanthamoeba* spp., *Mycobacterium* spp., Toxoplasma, Microsporidia and virus such as HSV, VZV and CMV. For identification of unknown bacterial and fungal pathogens, 16S and 28S rDNA gene barcoding by sequencing are employed respectively. Major ocular pathogens currently under study include methicillin resistant *Staphylococcus aureus* (MRSA), extended spectrum β-lactamase producers (ESBL), *Pseudomonas aeruginosa*, *Nocardia* spp., *Acanthamoeba* spp. and Trematodes. Multi locus sequence analysis is employed for the identification of the closely related pathogens such as Fusarium spp., *Nocardia* spp., and Acanthamoeba genotypes.

Clinical presentations, Genotypic diversity and Phylogenetic analysis of Acanthamoeba species, causing Keratitis

Investigators details : Dr. S. Lalitha Prajna,
Research Associate : Dr. R. Siva Ganesa Karthikeyan
Technician : A. Selva Pandiyan

Introduction

Acanthamoeba is a free-living protozoan, which can survive in diverse conditions. They have been isolated from soil, dust, fresh water, sea water and even from air samples. Acanthamoeba life cycle comprises of two stages, namely, a metabolically active trophozoite stage and an inactive, highly resistant, double-walled, cyst stage. Due to their widespread presence in the environment, humans are prone to come in contact with them easily. In the West, *Acanthamoeba* is commonly reported, as a cause of contact lens related infectious keratitis. However, in developing countries like India, trauma is a major predisposing factor for Acanthamoeba keratitis (AK), while contact lens related AK is not that frequently encountered.

Conventional microbiological methods, available for the identification of *Acanthamoeba* spp., were able to identify, only up to the genus level. Sub-generic genotypic classification can be done by exploiting the inter-strain variations in 18S ribosomal RNA (rRNA) subunit (*RNS*) sequence. *RNS* gene includes, the Acanthamoeba specific amplimer (ASA. S1) region (423 to 551 bp fragment) which has a highly variable sequence called DF3 (Diagnostic Fragment 3, ≈ 240 nucleotides long) and it is widely used for the genotyping of *Acanthamoeba* spp. Polymerase chain reaction (PCR) targeting *ASA.S1* in *RNS* gene was widely used for the genotyping and identification of *Acanthamoeba* spp. Based on the Rns gene *Acanthamoeba* spp., were classified into 20 genotypes (T1-T20). Genotyping and identification of *Acanthamoeba* spp., may help in understanding

the geographical distribution of species, and also aid in understanding the pathogenesis of AK caused by different genotypes and their clinical outcome. The following study was designed to identify genotypes and species of Acanthamoeba and understand their association to clinical outcomes of the disease.

Results and Conclusion

Thirty culture confirmed patients with Acanthamoeba keratitis, identified in Aravind Eye Hospital, Madurai, India, during the period of Dec 2017 to Dec 2018 were included in this study. Data collected from patient records included demographic details, history

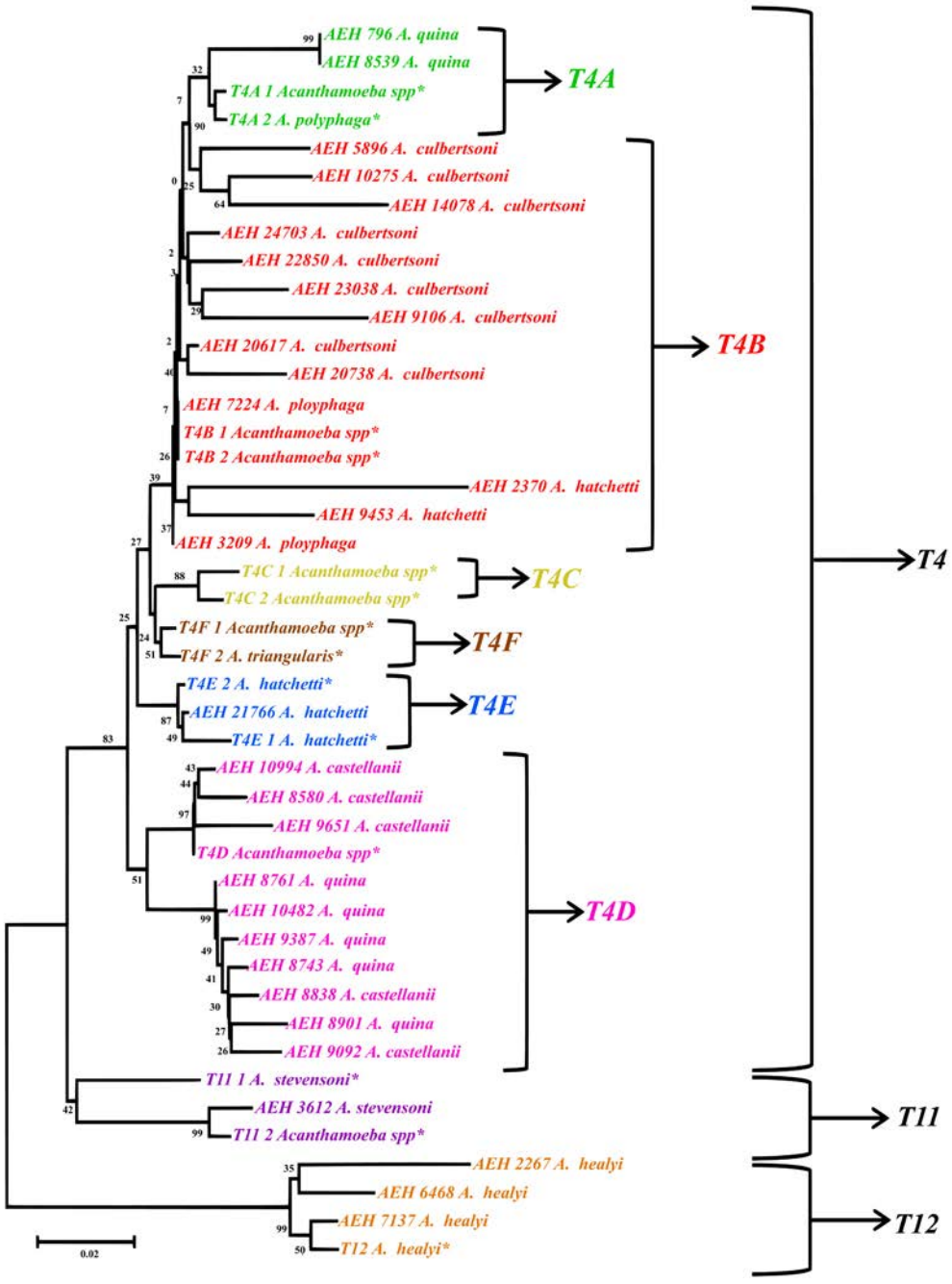

Figure: Phylogenetic tree was constructed by neighbor joining method using Kimura two algorithm with bootstrapping value of 10000 replicates. The isolates of the present study, categorizes into three major genotypic clusters with T4 as predominant genotype with 26 isolates, followed by three T12 genotypes and one T11 genotype. Twenty six T4 genotype was further subdivided into four subtypes with 13 T4B genotypes followed by ten T4D, two T4A and one T4E. (- reference genotypes)*

of illness, mode of trauma, treatment history and final follow-up status. The genotype and species of the Acanthamoeba isolates were identified based on the *RNS* region sequence and phylogenetic tree analysis. Three major Acanthamoeba genotypes were identified (T4, T11 and T12) with T4 genotype being the most predominant (n = 26). Under T4 genotype, four sub clusters belonging to T4A, T4B, T4D and T4E were identified. Seven species were identified with A.culbertsoni being most predominant, followed by *A.quina*, *A.castellanii*, *A.healyi*, *A.hatchetti*, *A.polyphaga* and *A.stevensoni*. Acanthamoeba stevensoni belonging to T11 genotype and Acanthamoeba infection by T12 genotype, is reported for the first time in this manuscript. No significant correlation was observed between clinical outcomes of corneal disease to any of the Acanthamoeba genotypes or species. Genotyping of *Acanthamoeba* spp., can be helpful for taxonomic & epidemiological purposes as well as in understanding of the pathogenesis of AK.

Molecular identification of Nocardia species causing endophthalmitis using Multi Locus Sequence Analysis (MLSA): a ten-year perspective

Investigators : Dr. S. Lalitha Prajna,
Research Associate : Dr. R. Siva Ganesa Karthikeyan
Technician : A. Selva Pandiyan

Introduction

Nocardia species are aerobic, rod-shaped, gram-positive and partially acid-fast bacteria. They are distributed globally in the environment and exist as normal soil microflora, living a saprophytic life, may also be associated with water-based habitat, decomposing plant material, dust and air. They rarely cause systemic disease in humans due toits low virulence nature. Commonly reported human infections are pulmonary nocardiosis, cutaneous nocardiosis and brain abscesses. There are numerous reports of *Nocardia* spp. causing ocular infections such as, keratitis, endophthalmitis and scleral abscess. In majority of these situations, the patients are immunocompetent, having acquired the infections through exogenous route.

Infectious endophthalmitis is an inflammatory condition of intraocular tissues due to entry of microorganisms inside the eye, either due to trauma or following intraocular surgeries or dissemination of infection via the blood stream. *Nocardia* spp., has been reported to be associated with all types of endophthalmitis, including post-operative, post-traumatic, and endogenous endophthalmitis. Endophthalmitis caused by *Nocardia* spp., are potentially sight-threatening, with generally poor visual outcome. Even though the occurrence of ocular Nocardial infection has been believed to be rare, it has been commonly reported in South India. No systematic study has been performed till date to determine the profile of *Nocardia* spp. causing human endophthalmitis and establish its prevalence in the population. The present study has been designed to fulfil this lacuna by employing the novel technique of multi-locus sequence analysis (MLSA) in place of 16S rDNA technique to identify the different Nocardial species. The clinical data were analysed to understand the disease severity in terms of the final visual outcome after treatments.

Results and Conclusion

Between January 2009 and December 2018, endophthalmitis patients who were diagnosed with Nocardia infection based on microscopic and culture characteristics were selected. Antibacterial susceptibility tests were performed and Nocardia speciation was done by MLSA and phylogenetic tree analysis of 16s rRNA gene, *gyrB*, *hsp65* and *secA1* gene. A total of 43 culture-proven patients were identified during the study period. All isolates were 100% sensitive to amikacin and 98% resistant to ceftazidime. Fluoroquinolone sensitivity was observed in the range of 58% to 72%. The year-wise analysis of antibiotic resistance patterns reveals there was a significant increase in resistance to fluoroquinolones. Twenty-two isolates were stored and six different species were identified. *N.farcinica* (n=10) was found to be the most predominant, followed by *N.cyriacigeorgica* (n = 4), *N.otitidiscaviarum* (n = 3), *N.amikacinitolerans* (n =2), *N.puris* (n = 2)and N. higoensis (n = 1). N. farcinica was the major pathogen, it is the first report to identify *N.otitidiscaviarum*, *N.amikacinitolerans* and *N.higoensis* causing endophthalmitis. Overall, visual outcomes were mostly poor even after aggressive management. The present work shows that the MLSA approach was very effective in identifying the different clinically important Nocardia species. We also found that every year, the species profile kept on changing, necessitating the idea that the prevalent species might need monitoring by genotyping.

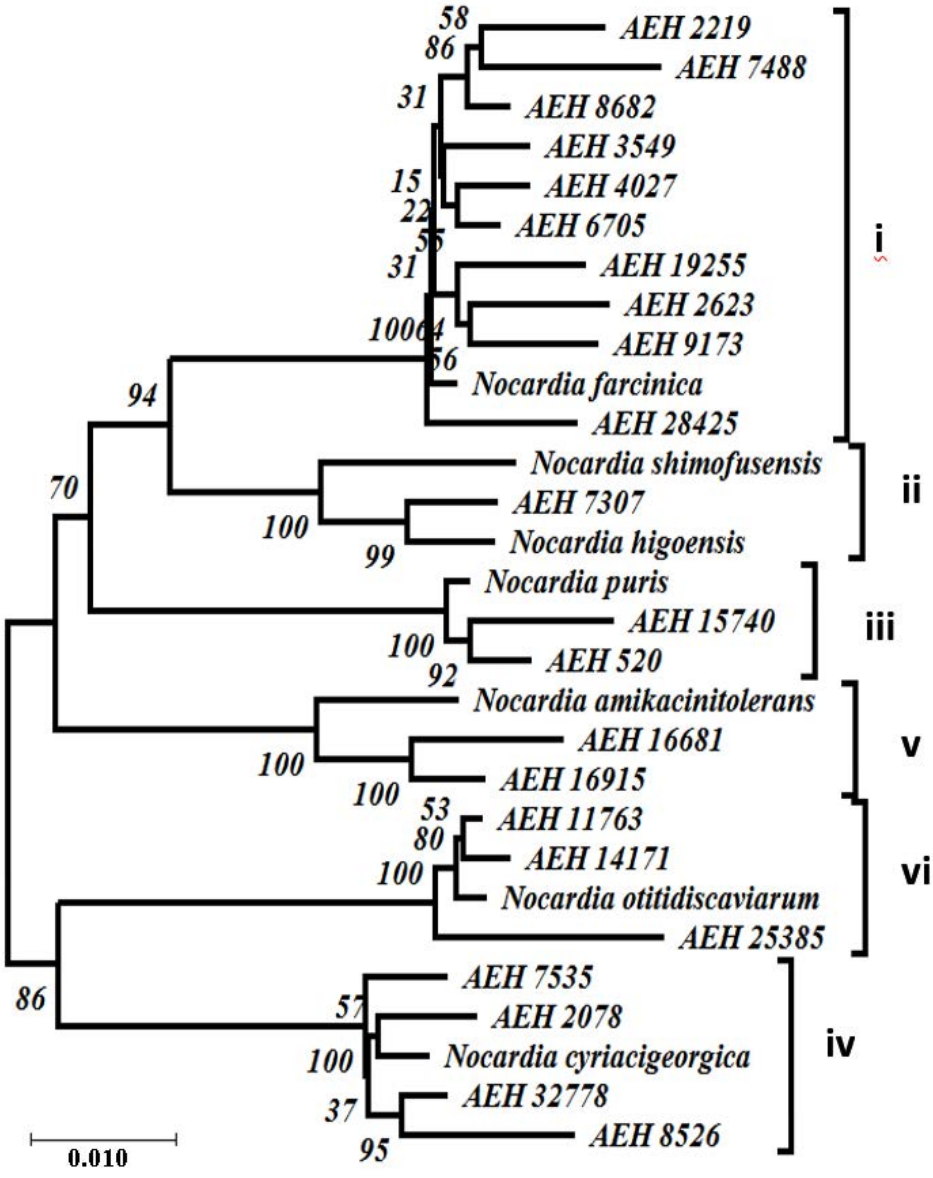

Figure: Phylogenetic tree of concatenated sequence generated in the order of 16SrDNA-gyrB-hsp65-secA1sequence by the neighbor-joining (NJ)algorithm following Kimura 2-parameter (K2P) correction with bootstrap analysis of 10,000 replicates. There are six clusters were identified belonging to i) Nocardia farcinica, ii) Nocardia higoensis, iii) Nocardia puris, iv) Nocardia cyriacigeorgica, v) Nocardia amikacinitolerans and iv) Nocardia otitidiscaviarum.

CONFERENCES ATTENDED

Annual Meeting of Association for Research in Vision and Opthalmology (ARVO) 2019

Vancouver, Canada, April 28 – May 2, 2019

Dr.P. Sundaresan

- Whole exome sequencing identifies rare gene variants and pathways in a large south Indian family with primary open angle glaucoma

Dr. Gowri Priya Chidambaranathan

- Hsa-miR143-3p regulates human corneal epithelial stem cells

Dr. S.Senthilkumari

- Steroid-induced ocular hypertension (SIOHT) model using Human Organ-Cultured Anterior Segment (HOCAS)
- Genome-wide transcriptome profiling of human trabecular meshwork cells treated with Dexamethasone

S. Yogapriya

- Quantification of human trabecular meshwork stem cells in glaucomatous donors

A. Divya

- Phagocytosis of Aspergillus flavus spores from corneal isolates by human corneal epithelial cells in vitro

Dr. P. Sundaresan also attended the signing ceremony for NEI-ICO international fellowship programme in the meeting.

26th ARVO-India: Annual Meeting of Indian Eye Research Group

Sankara Nethralaya, Chennai, July 26-28, 2019

Prof. VR. Muthukkaruppan

- Biology of the adult human ocular stem cells and their importance in health and disease of the eye

Dr. P. Sundaresan

- POAGome: Genes associated with primary open angle glaucoma

Dr. Gowri Priya Chidambaranathan

- miRNA regulating Limbal epithelial stem cells by

Dr. Senthilkumari Srinivasan

- Dexamethasone-induced ocular hypertension (DEX-OHT) in Indian donor eyes under perfusion culture

A. Divya

- Proteomic analysis of Aspergillus flavus infected human corneal epithelial cell phagosomes

C. Prakash

- Investigation of nuclear gene involvement in LHON pathogenesis

O. Ruthra

- Surface proteome and surface morphology of melanised and non-melanised conidiospores of Aspergillus flavus (Best Poster Award)

KRP. Niranjana

- Quantitative profiling of tear proteome reveals down regulation of Zinc alpha-2 glycoprotein in Aspergillus flavus keratitis patients

D. Irene

- Molecular mimicry between leptospiral antigen and human lens proteins: A possible trigger for cataract formation in leptospiral uveitis patients

P. Saranya

- Characterization of adult tissue resident stem cells in the human anterior lens epithelium

K. Saraswathi

- Clinical and genetic analysis of ocular adnexal lymphoma

A.Divya, Dr.Gowri Priya Chidambaranathan, Dr. S. Senthilkumari, S.Yogapriya, Prof.Colin Willoughby and Dr.P.Sundaresan at ARVO meeting, Vancouver, Canada

K.Jeyaprakash

- Investigation of human papillomavirus in non-familial retinoblastoma patients

P. Gowri

- Molecular genetics of mitochondrial genes associated with leber's hereditary optic neuropathy (LHON)

Anindita Rao

- Meta-analysis of Microarray Data Reveals Dysregulated Cancer Pathways in Retinoblastoma

A. S. Sriee Viswarubhiny

- Whole exome sequencing in Two family trios with Leber's Congenital Amaurosis

M. Durga

- Immunophenotypes of Macular corneal dystrophy in Indian population

R.Sivaganesa Karthikeyan

- Genotyping and Phylogenetic analysis of Ribosomal nuclear subunit (Rns) in Acanthamoeba spp. causing keratitis

A. Selva Pandiyan

- Evaluation of Direct polymerase chain reaction, conventional PCR and q-PCR methods with that of gold standard culture method for the diagnosis of infectious endophthalmitis

G. Ramesh Kumar

- Epidemiology and molecular identifi cation of Nocardia spp. causing endophthalmitis by multi locus sequence analysis (MLSA)

Prof. K. Dharmalingam chaired Dr. Venkat Reddy Oration Lecture. Travel awards were given to Durga, Irene Daniel and Sriee Viswarubhiny.

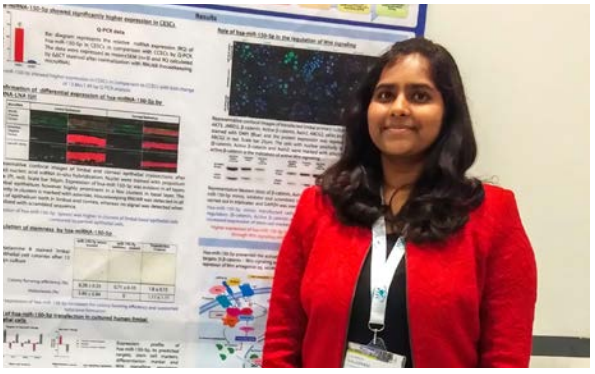

Lavanya Kalaimani at EVER 2019 congress meeting, France

Workshop on Bioimaging

Pune, August 1-14, 2019

Ms. P. Saranya, Junior Research Scholar, Department of Immunology and Stem Cell Biology, attended a Building Bharat Boston Biosciences (B4) Program - Workshop on Bioimaging at Indian Institute of Science Education and Research, Pune.

XXII European Association for Vision and Eye Research (EVER-2019) congress

Nice, France, October 17-19, 2019

Lavanya Kalaimani

- Hsa-miR-150-5p regulates human corneal epithelial stem cells through Wnt signalling (Best Poster Award). Part of this work was carried out under the guidance of Dr.JulieT. Daniels at University College London, UK during her one year Commonwealth Split-site Pre-Doctoral Fellowship.

2nd Annual Global Eye Genetics Consortium meeting

Dr. Shroff's Charity Eye Hospital, New Delhi, February 7,2020

Dr.P.Sundaresan

- Nuclear and Mitochondrial genome cross talk in diabetic retinopathy

AMRF team at IERG meeting, Chennai

CONFERENCES / WORKSHOPS CONDUCTED

17th Research Advisory Committee Meeting

March 16, 2019

During the meeting faculty members of AMRF presented their work and received feedback. Research scholars presented their findings as posters and interacted with the committee members. Best poster was selected for Prof. VR.Muthukkaruppan Endowment award..

Science in Everyday Life

September 28, 2019

As part of October Summit 2019, Aravind Medical Research Foundation organized a one day exhibition on the theme "Science in Everyday Life" in consultation with various colleges in and around Madurai and universities. Elaborate models made by AMRF teams and students from colleges/universities were kept on display. Nearly 140 students visited the exhibition.

A model displayed by AMRF students

Advances in Clinical Genomics: Hands-on- workshop on Next Generation Sequencing (NGS)

January 23-25, 2020

As a part of the DBT Centre of Excellence program project on “Translational Genomics of Paediatric Eye Diseases”, the three-day workshop was organised by Dr. P. Sundaresan, Dr. A.Vanniarajan and Dr. D. Bharanidharan.

Dr. K.Thangaraj from Centre from Cellular and Molecular Biology gave lectures on basics of NGS and its utility in clinics. Dr. G. Kumaresan from Madurai Kamaraj University elaborated the genomic approaches in cancer. Dr. P, Sundaresan gave an overview about the usefulness of NGS in eye diseases. Application scientist Mr. Jatesh Sachdeva provided the technical details of NGS. Eleven participants including faculty and research scholars from colleges and other institutions attended the workshop.

Participants of workshop on Advnances in Clinical Genomics

17th Research Advisory Committee Meeting

Awards/Fellowships

Indian National Science Academy (INSA) - Israel Academy of Sciences Bilateral Exchange Programme

November 4-17, 2019, Jerusalem, Israel.

Dr. P.Sundaresan has been awarded visiting fellowship by INSA and the Israel Academy of Sciences under the International Collaboration/ Exchange programme 2019. As part of this, he visited Department of Ophthalmology, Hadassah-Hebrew University Medical Center, Jerusalem, Israel. The main purpose of the visit was to work on molecular genetics of inherited retinal dystrophies and explore bioinformatics analysis of Next generation sequencing.. During the visit, Dr. Sundaresan delivered a lecture on "Discovery of Genes causing Blindness" and interacted with senior members and students.

Dr.P.Sundaresan at Hadassah-Hebrew University Medical Center, Israel

Commonwealth Split-site Scholarship

Lavanya Kalaimani, Senior Research Fellow, Department of Immunology and Stem cell Biology received Commonwealth Split-site Scholarship awarded by Commonwealth Scholarship Commissions UK and pursued, a part of her doctoral research with Prof. Julie T Daniels at Institute of Ophthalmology, University College London (UCL-IOO), London, United Kingdom from January 2019 to December 2019). She carried out studies to understand the molecular regulatory potential of corneal epithelial stem cells specific miRNAs in the maintenance of stemness in the limbal epithelial cells using 3D RAFT culture system.

Lavanya Kalaimani at UCL, London

Ph.D Awarded by Madurai Kamaraj University

- Mr. Mohd Hussain Shah, Department of Molecular Genetics

  Thesis: Genetics and functional approaches to understand the pathogenicity of primary open angle glaucoma.

  Guide: Dr.P.Sundaresan

- Ms. G. Prakadeeswari, Department of Molecular Genetics

  Thesis: Molecular analyses of various risk factors involved in Pseudoexfoliation Syndrome

  Guide: Dr.P.Sundaresan

- Ms. M.K. Jhansi Rani, Department of Immunology and Stem Cell Biology

  Thesis: Molecular signature of human limbal epithelial stem cells

  Guide: Dr. Gowri Priya Chidambaranathan

Mohd Hussain Shah

Prakadeeswari

Jhansi Rani

Prof. VR.Muthukkaruppan Endowment Award

Students and colleagues of Prof.VR.Muthukkaruppan, Advisor, Aravind Medical Research Foundation created an endowment in his name in 2014 out of which an award will be given to the best researcher at Dr. G. Venkataswamy Eye Research Institute every year. The award is given based on the scientific merit of abstracts and presentation by the research scholars. The award carries a certificate and cash prize of Rs.25,000/-

Prof. VR. Muthukkaruppan Endowment award 2019 was given to Divya Arunachalam, Proteomics department for her outstanding research work on "Isolation and identification of *A.flavus* conidia containing phagosomal proteins from human corneal epithelial cells".

Divya Arunachalam receiving Prof.VR.Muthukkaruppan Endowment award

GUEST LECTURES DELIVERED BY VISITING SCIENTISTS

Prof. Colin Willoughby, Professor of Ophthalmology, School of Biomedical Sciences, Ulster University, UK

Topic: Developing new therapies for corneal neovascularisation

11th July 2019

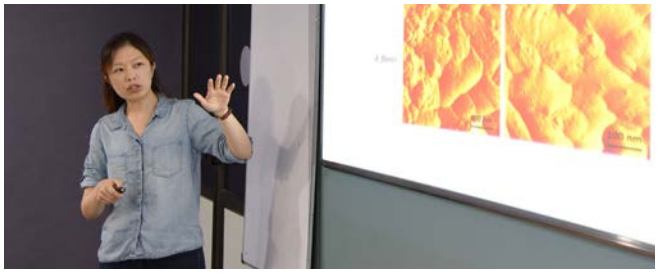

Dr. Sarah Wong, Post-doctoral Fellow, Institut Pasteur, Paris, France

Topic: Comparative study of two pathogenic Aspergillus.

15th August 2019

Dr. Ganesh Balasubramanian, Assistant Research Professor; Manager, Proteomics, Metabolomics and Mass Spectrometry Facility, Montana State University, Bozeman, Montana.

Topic: Proteomics and metabolomics: The value of temporal data in understanding biological systems.

20th June 2019

Dr. Bini Ramachandran, Postdoctoral Research Associate, Food Allergy Research and Resource Program (FARRP), Department of Food Science and Technology, University of Nebraska-Lincoln, Lincoln, NE

Topic: Finding the needle in haystack with targeted proteomics: A story about protein-rich complex matrices and sub nanogram level analytes

23rd September 2019

PUBLICATIONS 2019-2020

Bo Gong et al.,
- *"Mutant RAMP2 causes Primary Open Angle Glaucoma via the CRLR – CAMP axis"*

Genet Med 2019 Oct;21(10):2345-2354

Premanand Chandran, Prakash Chermakani, Prasanna Venkataraman, Siva rasanna Thilagar, Ganesh V Raman & Periasamy Sundaresan
- *"A novel 5 bp homozygous deletion mutation in ASPH gene associates with Traboulsi syndrome"*

Ophthalmic Genetics 2019 Apr;40(2):185-187

T Daniel Berner et al.,
- *"The protective variant rs7173049 at LOXL1 locus impacts on retinoic acid signaling 1 pathway in pseudoexfoliation syndrome"*

Human Molecular Genetics 2019

S Rajasekaran, Chitraa Tangavel, Sri Vijay Anand, Dilip Chand Raja Soundararajan, Sharon Miracle Nayagam, Monica Steffi Matchado, Raveendran Muthurajan, Ajoy Prasad Shetty, Rishi Mugesh Kanna, Dharmalingam Kuppamuthu
- *"Inflammaging determines health and disease in lumbar discs-evidence from differing proteomic signatures of healthy, aging, and degenerating discs"*

Spine J. 2020 Jan;20(1):48-59

Niranjana Parthiban, Nithya Lakshmi Sampath, Jayapal Jeya Maheshwari, Namperumalsamy Venkatesh Prajna, Prajna Lalitha, Kuppamuthu Dharmalingam
- *"Quantitative Profiling of tear proteome reveals down regulation of Zinc alpha -2 glycoprotein in Aspergillus flavus keratitis patients"*

Exp Eye Res. 2019 (Jun 21) E pub

Yogapriya Sundaresan, Ganesh Govardhan Gaikwad, Kishan Anilkumar Prajapati, N Venkatesh Prajna, Gowri Priya Chidambaranathan
- *"Comparison of structural integrity and functional status of corneal endothelium stored in Cornisol and Optisol -GS"*

Indian Journal of Ophthalmology 2019 Oct;67(10):1579-1584.

Yogapriya Sundaresan, Muthukkaruppan Veerappan, Krishnadas Subbiah Ramasamy, Gowri Priya Chidambaranathan
- *"Identification, quantification and age related changes of human trabecular meshwork stem cells"*

Eye and Vision (2019) 6:31

Sivakumar Rathinam, Irene Daniel, Dharmalingam Kuppamuthu & Jeya Maheshwari Jayapal
- *"Molecular Mimicry between Betaine Aldehyde Dehydrogenase of Leptospira and Retinal Dehydrogenase 1 of Human Lens: A Potential Trigger for Cataract Formation in Leptospiral Uveitis Patients"*

Ocular Immunology and Inflammation 2019 e pub

Rajendran Kadarkarai Raj, Pankaja Dhoble, Rupa Anjanamurthy, Prakash hermakani, Manojkumar Kumaran, Bharanidharan Devarajan, Periasamy Sundaresan
- *"Genetic characterization of stargardt clinical phenotype in South Indian patients using sanger and targeted sequencing"*

Eye Vis.2020

Roshni Prithiviraj, Swasthikka, Siva Ganesa Karthikeyan Rajapandian, Hariharan Gnanam, Rameshkumar Gunasekaran, Ponlakshmi Mariappan, Sharma Sankalp Singh, and Lalitha Prajna.
- *"Clinical Presentations, Genotypic Diversity and Phylogenetic Analysis of Acanthamoeba Species Causing Keratitis."*

Journal of Medical Microbiology.2019

Appavu, Selva Pandiyan, Lalitha Prajna, and Siva Ganesa Karthikeyan Rajapandian..
- *"Genotyping and Phylogenetic Analysis of Pythium Insidiosum Causing Human Corneal Ulcer."*

Medical Mycology, 2019

ONGOING RESEARCH PROJECTS

No	Projects	Funded by	Investigators	Research Scholar
PROTEOMICS				
1.	Pathogenic Aspergillus: Interaction with Innate Immune cells (Indo-French Collaborative project)	CEFIPRA	Dr. Lalitha Prajna Dr.J.Jeya Maheshwari Dr. K.Dharmalingam Dr. Rabbind Singh	V. Lakshmi Prabha Irene Daniel
2.	Study on “Human mycotic keratitis”	AMRF & AEH	Dr.N. Venkatesh Prajna Dr.Lalitha Prajna Dr.J. Jeya Maheshwari Dr.K.Dharmalingam Dr.O.G.Ramprasad	G. Hariharan S. Nishanti Jobin John
3.	Prospective Multicenter discovery and validation of diagnostic circulating and urinary biomarkers and development of sensor(s) to detect sight threatening diabetic retinopathy - Biomarker and Biosensor study in UK and India (Indo-UK collaborative project)	Research Councils UK	Dr. K. Dharmalingam Dr. Kim Dr. J.Jeya Maheshwari	V. Nivetha K.S. Guhan K. Ramaraj K.R. Shruthi Mahalakshmi
4.	Proteome profiling of serum microparticles in diabetes and diabetic retinopathy patients: Towards identification and validation of predictive biomarkers	Department of Health Research (DHR)	Dr. J.Jeya Maheshwari Dr. K.Dharmalingam Dr. R.Kim	P. Vignesh
5.	Functional analysis of circulating microRNAs and their regulatory role in Diabetic Retinopathy	SERB	Dr. O.G.Ramprasad Dr. K.Dharmalingam Dr. Kim Ramasamy Dr. D. Bharanidharan	R. Karthikeyan T.M.Nasrin Banu
6.	Interaction of pathogenic fungi with Human Corneal Epithelial cells	ICMR-SRF	Dr. K.Dharmalingam	A. Divya
MOLECULAR GENETICS				
7.	Molecular genetics of macular corneal dystrophy (MCD) in Indian population	DST INSPIRE Fellowship	Dr. P.Sundaresan Dr. N.Venkatesh Prajna	M. Durga
8.	Genetics of Retinal Dystrophies	Aravind Eye Care System	Dr. P.Sundaresan, Dr. Pankaja Dhoble Dr. K.C.Lavanya	R. Kadarkarai Raj
9.	Genetic and transcript analysis of RB1 gene in South Indian Retinoblastoma Patients	ICMR	Dr. A.Vanniarajan Dr. Usha Kim Dr. R.Shanthi	K.Thirumalai raj
10.	Understanding the molecular mechanisms of chemoresistance in retinoblastoma	CSIR-NET	Dr.A.Vanniarajan	T. S.Balaji
11.	Molecular characterization of tumor progression in retinoblastoma	DST INSPIRE Fellowship	Dr. A.Vanniarajan	T.Shanthini

12.	Identification and validation of deregulated cancer pathways in retinoblastoma	SERB	Dr. A. Vanniarajan Dr. Usha Kim Dr. D. Bharanidharan Dr. R. Shanthi	Anindita Rao
13.	Translational Genomics of Ocular Cancers	Aravind Eye Foundation	Dr. Usha Kim Dr. A. Vanniarajan Dr. D. Bharanidharan Dr. R. Shanthi Dr. VR. Muthukkaruppan	K.Saraswathi
14.	COE LEAD: Translational Genomics of paediatric eye diseases	DBT	Dr. P. Sundaresan Dr. A. Vanniarajan Dr. D. Bharanidharan Dr. P. Vijayalakshmi Dr. R. Kim Dr. Usha Kim	Dr. Roopam Gowri Poigaialwar A.S.Sriee Viswarubhiny
15.	COE PR-I: Molecular analysis of mitochondrial diseases with ophthalmic manifestations	DBT	Dr. P. Sundaresan Dr. A. Vanniarajan Dr. P. Vijayalakshmi	A. Aloysius Abraham
16.	COE PR-II: Epigenetic mechanisms underlying tumor progression in retinoblastoma	DBT	Dr. A. Vanniarajan Dr. D. Bharanidharan Dr. VR. Muthukkaruppan Dr. Usha Kim	K. Jeya Prakash A. Mohamed Hameed Aslam
17.	COE PR-III: Functional validation of novel candidate genes using alternate model	DBT	Dr. P. Sundaresan Dr. A. Vanniarajan	C. Prakash
18	Molecular Genetics of Juvenile X-linked Retinoschisis in South Indian Population	Lady Tata Memorial trust	Dr.P.Sundaresan	Susmita Chowdhury
IMMUNOLOGY AND STEM CELL BIOLOGY				
19.	Characterization and Functional Evaluation of Trabecular Meshwork Stem Cells in Glaucoma Pathogenesis	SERB	Dr. C. Gowri Priya Dr. S. Senthilkumari Dr. Neethu Mohan Dr. SR.Krishnadas Prof. VR. Muthukkaruppan	R. Iswarya
20.	Characterization of adult human lens epithelial stem cells in the maintenance of tissue homeostasis throughout life and their functional status in cataractous lens	SERB	Dr. Madhu Shekhar Dr. Gowri Priya Chidambaranathan Dr.Haripriya Aravind Dr. Muthukkaruppan Veerappan	Nithyapurana
21.	Understanding the Role of Trabecular Meshwork Stem Cells in The Maintenance of Tissue Homeostasis in Normal and Glaucomatous Human Eyes	Lady Tata Memorial trust	Dr. Gowri Priya Chidambaranathan	S. Yogapriya
22.	MicroRNAs specific to corneal epithelial stem cells	CSIR-SRF	Dr. Gowri Priya Chidambaranathan	K. Lavanya

23.	Characterization of adult human lens epithelial stem cells, their niche and their role in the maintenance of tissue homeostasis	Lady Tata Memorial trust	Dr. Gowri Priya Chidambaranathan	P. Saranya
OCULAR PHARMACOLOGY				
24.	Role of miRNA in the regulation of Glucocorticoid Receptor (GR) signalling and Development of New therapeutics for Steroid-induced glaucoma	Wellcome-DBT /India Alliance Intermediate Fellowship (2017-2022)	Dr. S. Senthilkumari Dr. Gowri Priya Chidambaranathan Dr. D. Bharanidharan Dr. R. Sharmila	Dr. R. Hari-balaganesh K. Kathirvel
BIOINFORMATICS				
25.	Diagnostic Markers for Ocular Tuberculosis	DBT	Dr. D.Bharanidharan Dr. SR.Rathinam Dr. Lalitha Prajna Dr. M. Vidyarani	O.Ruthra
26.	Identification of Dysregulated MicroRNAs In Ocular Fluids as Diagnostic Markers for Intraocular Tuberculosis	ICMR-SRF	Dr.D.Bharanidharan	Swathi Chadalawada
27.	Computational Methods For Whole Exome/Genome Sequencing Of Paediatric Eye Diseases	DBT-COE, R&D	Dr.D.Bharanidharan Dr.A.Vanniarajan Dr.P.Sundaresan	K.Manojkumar
28.	Comparative genomics of Methicillin-Resistant Staphylococcus aureus (MRSA) and Pseudomonas aeruginosa ocular isolates from keratitis patients with different clinical outcomes	AEH	Dr. D. Bharanidharan Dr. M. Vidyarani Dr. Lalitha Prajna	K.Kathirvel O.Ruthra
MICROBIOLOGY				
29.	Genotyping and phylogenetic analysis of Pythium insidiosum causing human corneal ulcer	AEH	Dr. Lalitha Prajna	A. Selva Pandiyan Dr. R. Siva Ganesa Karthikeyan
30.	Identification and evaluation of genetic relationship based on Multilocus Sequence Analysis in Nocardia sp causing human ocular infection	AEH	Dr. Lalitha Prajna	A. Selva Pandiyan Dr. R. Siva Ganesa Karthikeyan
31.	Genotyping and Phylogenetic analysis of Acanthamoeba sp using the 18S Ribosomal DNA region (JDP 1/2) from Acanthamoeba Keratitis patients	AEH	Dr. Lalitha Prajna	A. Selva Pandiyan Dr. R. Siva Ganesa Karthikeyan

Much has been done, but much remains to be done… we look to the future with renewed strength to continue the mission of providing quality eye care and hope that some of what we have learned will be useful to other eye care workers around the world.

G. Venkataswamy

ARAVIND MEDICAL RESEARCH FOUNDATION

DR. G. VENKATASWAMY EYE RESEARCH INSTITUTE

1, Anna Nagar, Madurai 625 020, Tamilnadu, India.
Phone: (0452) 435 6550

www.amrf.org.in

ARAVIND EYE CARE SYSTEM